REAL-TIME QUANTITATIVE PCR ANALYSIS OF DIESEL-DEGRADING GENES OF *Acinetobacter calcoaceticus* ISOLATES

by

RAKSHA TOOLSI

Submitted in fulfillment of the academic requirements for the degree of Master of Science in the School of Biochemistry, Genetics, and Microbiology, University of KwaZulu-Natal, Westville.

January 2009

As the candidate's supervisor I have approved this dissertation for submission.

Signed:_____ **Name:** Prof. Johnson Lin **Date:** _____

PREFACE

The experimental work described in this dissertation was carried out in the School of Biochemistry, Genetics, and Microbiology, University of KwaZulu-Natal, Westville, and the Doris Duke Medical Research Institute, Nelson. R. Mandela School of Medicine, University of KwaZulu-Natal, from January 2006 to December 2008, under the supervision of Professor Johnson Lin.

These studies represent original work by the author and have not otherwise been submitted in any form for any degree or diploma to any tertiary institution. Where use has been made of the work of others it is duly acknowledged in the text.

_____

Raksha Toolsi (9600022)

January 2009

DECLARATION 1 – PLAGIARISM

I, Raksha Toolsi declare that

1. The research reported in this dissertation, except where otherwise indicated is my original research.

2. This dissertation may not be submitted for any degree or examination at any other university.

3. This dissertation does not contain any other persons' data, pictures, graphs or other information, unless specifically acknowledged as being sourced from other persons.

4. This dissertation does not contain other persons' writing, unless specifically acknowledged as being sourced from other researchers. Where other written sources have been quoted, then:

    a. Their words have been re-written but the general information attributed to them has been referenced.

    b. Where their exact words have been used, then their writing has been placed in italics and inside quotation marks, and referenced.

5. This dissertation does not contain text, graphics or tables copied and pasted from the internet, unless specifically acknowledged, and the source being detailed in the dissertation and in the References section.

Signed……..

DECLARATION 2 – PUBLICATIONS

DETAILS OF CONTRIBUTION TO PUBLICATIONS that form part and/or include research presented in this dissertation (include publications in preparation, submitted, *in press* and published and give details of the contributions of each author to the experimental work and writing of each publication)

Publication 1

NOT APPLICABLE

Publication 2

Publication 3

etc.

Signed……

TABLE OF CONTENTS

PAGE

ACKNOWLEDGEMENTS i

ABSTRACT ii

LIST OF FIGURES iv

LIST OF TABLES viii

1. INTRODUCTION AND LITERATURE REVIEW 1

1.1 INTRODUCTION 1

1.2 PETROLEUM AND ITS DERIVATIVES 3

1.3 REMEDIATION STRATEGIES FOR PETROLEUM-CONTAMINATED SITES 4

1.4 BIOREMEDIATION 5

1.5 MICROBIAL DEGRADATION OF HYDROCARBONS 6

1.6 HYDROCARBON-DEGRADING BACTERIA 7

1.7 PATHWAYS OF ALKANE DEGRADATION 8

1.8 GENES AND ENZYMES INVOLVED IN *n*-ALKANE DEGRADATION 11

1.9 MONITORING OF GENE EXPRESSION 16

1.10 REAL-TIME PCR 17

1.10.1 Quality of RNA and its influence on real-time PCR 18

1.10.2 Reverse transcription and cDNA synthesis 19

1.10.3 Real-time PCR instrumentation 19

1.10.4 Detection chemistries 20

1.10.5 Quantification strategies in real-time PCR 25

1.10.6 Amplification efficiency 28

1.10.7 Data evaluation 29

1.11 MOTIVATION 30

1.11.1 Purpose 31

1.11.2 Aims 31

1.11.3 Objectives 32

2. MATERIALS AND METHODS 33

2.1 SELECTION AND IDENTIFICATION OF DIESEL DEGRADING BACTERIAL ISOLATES 33

2.2 MAINTENANCE AND PRESERVATION OF CULTURES 34

2.3 GROWTH OF BACTERIAL ISOLATES ON DIESEL 34

2.4 DETERMINATION OF BACTERIAL CARBON SOURCE UTILIZATION PATTERNS 35

2.5 RNA EXTRACTION AND VALIDATION 36

2.6 SYNTHESIS OF cDNA 37

2.7 VALIDATION OF cDNA 38

2.8 LightCycler QUANTITATIVE REAL-TIME PCR 38

2.8.1 Nucleotide sequences, primer design, and primer preparation 38

2.8.2 Optimizing the components of the LightCycler real-time PCR 39

2.8.3 LightCycler real-time PCR protocol 41

2.8.4 Confirmation of real-time PCR primer specificity 42

2.8.5 Generation of a relative standard curve 43

2.8.6 Real-time PCR data analysis and quantification of gene expression 45

3. RESULTS 46

3.1 IDENTIFICATION OF ALKANE DEGRADING BACTERIAL ISOLATES 46

3.2 GROWTH OF BACTERIAL ISOLATES ON DIESEL 46

3.3 DETERMINATION OF BACTERIAL CARBON SOURCE UTILIZATION PATTERNS 48

3.4 RNA EXTRACTION AND VALIDATION 50

3.5 SYNTHESIS AND VALIDATION OF cDNA 50

3.6 OPTIMIZING THE COMPONENTS OF THE REAL-TIME PCR MASTERMIX 53

3.7 CONFIRMATION OF PRIMER SPECIFICITY 57

3.8 GENERATION OF RELATIVE STANDARD CURVES 60

3.9 STATISTICAL ANALYSIS OF REAL-TIME PCR DATA AND RELATIVE QUANTIFICATION OF GENE EXPRESSION 62

3.9.1 Analysis of 16S rRNA gene expression 65

3.9.1.1 Expression profile of 16S rRNA gene 65

3.9.1.2 Randomization test results for 16S rRNA gene (not normalized by a reference gene) 66

3.9.1.3 Melting peak analysis of 16S rRNA gene 66

3.9.2 Analysis of *rubA* expression 67

3.9.2.1 Expression profile of *rubA* 67

3.9.2.2 Randomization test results for *rubA* (normalized by reference gene) 69

3.9.2.3 Melting peak analysis of *rubA* 71

3.9.3 Analysis of *alkM* expression 70

3.9.3.1 Expression profile of *alkM* 70

3.9.3.2 Randomization test results for *alkM* (normalized by reference gene) 71

3.9.3.3 Melting curve and melting peak analysis of *alkM* 72

3.9.3.4 Validation of *alkM1* and *alkM2* amplicons by agarose gel electrophoresis 75

3.9.3.5 Sequencing and alignment of *alkM1* and *alkM2* amplicons 77

3.9.4 Analysis of *alkR* expression 78

3.9.4.1 Expression profile of *alkR* 78

3.9.4.2 Randomization test results for *alkR* (normalized by reference gene) 79

3.9.4.3 Melting peak analysis of *alkR* 79

3.9.5 Analysis of *estB* expression 81

3.9.5.1 Expression profile of *estB* 81

3.9.5.2 Melting peak analysis of *estB* 82

3.9.6 Analysis of *lipA* expression 84

3.9.6.1 Expression profile of *lipA* 84

3.9.6.2 Melting peak analysis of *lipA* 84

3.9.7 Analysis of *lipB* expression 86

3.9.7.1 Expression profile of *lipB* 86

3.9.7.2 Randomization test results for *lipB* (normalized by reference gene) 86

3.9.7.3 Melting peak analysis of *lipB* 87

3.9.8 Analysis of *xcpR* expression 89

3.9.8.1 Expression profile of *xcpR* 89

3.9.8.2 Randomization test results for *xcpR* (normalized by reference gene) 90

3.9.8.3 Melting peak analysis of *xcpR* 90

3.8.9.4 Validation of *xcp*R amplicons by agarose gel electrophoresis 92

4. DISCUSSION 93

5. CONCLUSION 114

6. REFERENCES 115

7. APPENDICES 138

APPENDIX I 138

APPENDIX II 140

APPENDIX III 142

APPENDIX IV 144

APPENDIX V 145

APPENDIX VI 147

ACKNOWLEDGEMENTS

The author wishes to express her gratitude to:

Prof. J. Lin for his supervision, encouragement, and patience during this study.

National Research Foundation (NRF) and Department of Labour (DoL) for the much-needed financial assistance.

Saziso Ndlovu, laboratory manager of Pfizer Molecular Biology Research Facility, Nelson R. Mandela School of Medicine, for the use of laboratory facilities.

Veron Ramsuran and Duran Ramsuran of Doris Duke Medical Research Institute (DDMRI), Nelson R. Mandela School of Medicine, for their technical expertise and invaluable friendship.

Staff and post-graduate students of DDMRI for their kindness and assistance.

Punjee Naidoo, disability coordinator, Office for Students with Disabilities (OSD), for her support and encouragement throughout my academic career.

My mum Leela, and husband Prasidh, for their unconditional love and support.

ABSTRACT

The diesel-degrading capabilities of *Acinetobacter calcoaceticus* isolates LT_1, LT_1A and V_2 were established in previous studies. LT_1 and LT_1A were isolated from diesel-contaminated soil and V_2 was from soil contaminated with used engine oil. Isolates were grown in Bushnell-Haas medium supplemented with 1% sterile diesel. Determination of diesel-degradation patterns by gravimetric analysis and harvesting of cells for RNA extraction were performed at regular time intervals over a 60 day period. The involvement of genes *alkM*, *alkR*, *rubA*, *rubB*, *estB*, *lipA*, *lipB,* and *xcpR* in hydrocarbon degradation has been reported in previous studies. LT_1, LT_1A, and V_2 were compared in terms of gene expression levels by real-time quantitative PCR. Expression levels were assessed by relative quantification and normalized against the 16S rRNA reference gene using the Relative Expression Software Tool - XL (REST-XL). Amplification of all genes, except *rubB*, was achieved with a high degree of efficiency. The expression of *rubA*, *alkM*, *alkR*, *xcpR*, and *lipB* based on pair-wise randomization, was all down-regulated in LT_1A in relation to LT_1. Highest expression levels of the aforementioned genes were documented during the initial stages of incubation for LT_1 while LT_1A showed highest expression levels midway through the study period. LT_1, LT_1A, and V_2 achieved 58.6%, 51.7%, and 48.3% diesel degradation after 5 days of incubation, respectively. The higher percentage of diesel degradation achieved by LT_1 can be attributed to higher levels of overall gene expression in the initial stages of degradation. Amplification of alkane hydroxylase *alkM* of V_2 revealed a possible second hydroxylase gene that was

expressed after 20 days of incubation. Amplification of *alkR* and *xcpR* in V_2 isolates also resulted in multiple product formation. Very low *lipB* and *lipA* expression was detected in LT_1 and LT_1A and the absence of *lipA* expression in V_2 suggests that lipases were not involved in diesel degradation. In contrast, *estB* was predominantly expressed in V_2, and suspected to be involved in the release of a bioemulsifier that was only observed in V_2 samples. Although all three isolates were comparably efficient in degrading diesel, the results of this study suggest that different mechanisms may be employed in the degradation process.

LIST OF FIGURES

PAGE

Fig. 1.1 **The proposed carbon flow from *n*-alkanes to wax esters in *Acinetobacter* sp.** Dotted lines indicate alternative ways to wax ester production. **Enzymes: 1**, alkane hydroxylase complex; **2**, NAD(P)-dependent alcohol dehydrogenase; **3**, NAD(P)-dependent aldehyde dehydrogenase; 4, acyl-CoA synthetase; **5**, acyl-CoA reductase; **6**, aldehyde reductase; **7**, acyl-CoA: alcohol transacylase; **8**, acyl-CoA dehydrogenase (Ishige et al., 2002). 10

Fig. 1.2 **Electron transfer during alkane oxidation.** Schematic representation of the various compounds of an alkane hydroxylase system and its electron transfer system. A reductase protein (red) transfers electrons from NAD(P)H via a small electron transfer protein (fdx) to the hydroxylase (oxy) protein where the substrate is oxidized to an alcohol, aldehyde, carboxylic acid, or epoxide (van Beilen *et al.*, 2007). 12

Fig. 1.3 **Mechanisms of fluorescent reporters used in real-time PCR. D** - donor; **A** - acceptor; **R** - reporter; **Q** - quencher. **a).** Sequence non-specific dyes e.g. SYBR Green I, **b)** Hybridization probe, **c).** Taqman probe (Hydrolysis probe). The grey circle indicates Taq polymerase hydrolysing the TaqMan probe, **d).** Molecular beacon **e).** Sunrise primer **f).** Scorpion primer (Wilhelm and Pingoud, 2003). 24

Fig. 3.1 **Diesel degradation patterns of *A. calcoaceticus* isolates.** 49

Fig. 3.2 **Validation of cDNA by 2% (wt/vol) agarose gel electrophoresis. A**, **B**, and **C**, represent amplicons of the 16S rRNA gene of LT_1, LT_1A, and V_2, respectively. **Lanes 1**, DNA molecular weight marker VI (Roche Diagnostics); **2**, negative control (no cDNA template); **3 - 10**, day 5 to day 60, respectively. 52

Fig. 3.3 **Optimization of real-time PCR primer concentrations.** A representative melting peak analysis showing titration of 16S rRNA primers. Primer dimer formation was observed in negative control samples with higher primer concentrations. 54

Fig. 3.4 **Optimization of real-time PCR cDNA template quantity.** A representative melting peak analysis showing amplification of *lipB* resulting from varying volumes of cDNA template. 55

Fig. 3.5 **Confirmation of real-time PCR specificity for target genes.** Amplification of target genes **(A)** 16S rRNA, **(B)** *alkM*, **(C)** *alkR*, **(D)** *rubA*, **(E)** *lipA*, **(F)** *lipB*, **(G)** *xcpR*, and **(H)** *estB*, as determined by melting curve analysis. Melting peaks were determined by plotting the continuous negative derivative of fluorescence emitted by each sample as PCR products were melted. The no-cDNA template control sample for each reaction does not show fluorescence, confirming the absence of primer dimers. 58

Fig. 3.6 **Representative standard curve assay of *rubA*.** **(A)** Melting curve analysis. **(B)** Melting peak analysis. **(C)** Amplification curve. **(D)** Standard curve constructed on the basis of sample dilution factors and the corresponding C_p values. PCR efficiency was estimated through the linear regression of the dilution curve with a correlation coefficient squared (r^2) of 1.00. The error values are the mean squared errors calculated by the LightCycler Software. Gradient and efficiency were -3.578 and 1.90, respectively. 61

Fig. 3.7 **Expression profile of 16S rRNA gene of *A. calcoaceticus* isolates LT_1, LT_1A, and V_2.** 65

Fig. 3.8 **Representative melting peak analysis of 16S rRNA gene of LT_1 samples.** 67

Fig. 3.9 **Expression profile of *rub*A gene of *A. calcoaceticus* isolates LT_1, LT_1A, and V_2.** 68

Fig. 3.10 **Representative melting peak analysis of *rub*A of LT_1A samples.** 69

Fig. 3.11 **Expression profile of *alkM* of *A. calcoaceticus* isolates LT_1 and LT_1A.** 71

Fig. 3.12 Melting curve and melting peak analysis of *alkM* of LT_1 and LT_1A samples. **(A)** Melting curve analysis determined by fluorescence (F1), and **(B)**, melting peak analysis determined by plotting the negative derivative of fluorescence [-d(F1)/dT] of *alkM*. 73

Fig. 3.13 Melting curve and melting peak analysis of *alkM* of V_2 samples. **(A)** Melting curve analysis determined by fluorescence (F1), and **(B)**, melting peak analysis determined by plotting the negative derivative of fluorescence [-d(F1)/dT] of *alkM*. Formation of an additional amplification product (*alkM2*) is indicated by the red coloured arrow. 74

Fig. 3.14 Validation of *alkM* amplicons by 2 % (wt/vol) agarose gel electrophoresis. **(A)** Electrophoresed *alkM1* amplicons of LT_1A. **Lanes 1**, Molecular weight marker IV (Roche Diagnostics); **2**, negative control (no cDNA); **3**, positive control (calibrator); **4 - 10**, day 5 to day 60, respectively. **(B)** Electrophoresed *alkM1* and *alkM2* amplicons of V_2 samples. **Lanes 1**, Molecular weight marker IV (Roche Diagnostics); **2**, negative control (no cDNA); **3**, positive control (calibrator); **4 - 11**, days 5 to 60, respectively. 76

Fig. 3.15 Partial sequence alignment of *alkM1* amplicons 77

Fig. 3.16 Expression profile of *alkR* of *A. calcoaceticus* isolates LT_1 and LT_1A 78

Fig. 3.17 Melting peak analysis of *alkR*. **(A)** Melting peaks of *alkR* of LT_1 and LT_1A samples and **(B)** V_2, determined by plotting the negative derivative of fluorescence [-d(F1)/dT]. 80

Fig. 3.18 Expression profile of *estB* of *A. calcoaceticus* isolate V_2 81

Fig. 3.19 Melting peak analysis of *estB*. **(A)** Melting peak of *estB* of LT_1 and LT_1A samples and **(B)** V_2 samples, determined by plotting the negative derivative of fluorescence [-d(F1)/dT]. 83

Fig. 3.20 **Melting peak analysis of *lipA*.** **(A)** Melting peaks of *lipA* of LT_1 and LT_1A samples and **(B)** V_2 samples, determined by plotting the negative derivative of fluorescence [-d(F1)/dT]. 85

Fig. 3.21 **Expression profile of *lipB* of *A. calcoaceticus* isolates LT_1, LT_1A, and V_2.** 87

Fig. 3.22 **Melting peak analysis of *lipB*.** **(A)** Melting peaks of *lipB* of LT_1 **(B)** LT_1A and **(C)** V_2 samples. 88

Fig. 3.23 **Expression profile of *xcpR* of *A. calcoaceticus* isolates LT_1 and LT_1A.** 89

Fig. 3.24 **Melting peak analysis of *xcpR*.** **(A)** Melting peaks of *xcpR* of LT_1 and LT_1A samples, **(B)** V_2 samples and **(C)** reproduced melting peaks of V_2 samples. 91

Fig. 3.25 **Electrophoresed *xcpR* amplicons of V_2 samples** **Lanes 1** - molecular weight marker VI (Roche Diagnostics); **2** - negative control (no cDNA template); **3** - positive control (calibrator); **4 to 11** - *xcpR* amplicons of 5 days to 60 days samples, respectively. 92

Fig IIa **Partial 16S rRNA gene sequence alignment of JL11, LT_1, LT_1A and, V_2.** 140

Fig. Va **Relative standard curves**. Standard curves of **(A)** 16s rRNA, **(B)** *alkM*, **(C)** *alkR*, **(D)** *rubA*, **(E)** *lipB*, **(F),** *xcpR*, and **(G)** *estB* were generated by the LightCycler Software, Version 3.5. Correlation coefficients (r) and amplification efficiencies (*E*) are shown. 145

LIST OF TABLES

PAGE

Table 1.1 Available real-time PCR systems and formats 20

Table 2.1 Primer sequences for real-time PCR amplification of target genes 40

Table 2.2 Amplification parameters of investigated genes for real-time PCR 44

Table 3.1 Growth of bacterial isolates on diesel determined by optical density 47

Table 3.2 RNA yield and Nanodrop spectrophotometric readings 51

Table 3.3 Composition of reaction mastermix for LightCycler real-time PCR assays 56

Table 3.4 Melting temperature (T_m) of target gene amplification products 57

Table 3.5 Real-time PCR efficiencies and standard curve gradients of target genes 62

Table 3.6 Descriptive statistics and variation data output for target genes of LT_1, LT_1A, and V_2 samples 64

Table IIIa Computation of percentage diesel degradation 142

Table IVa Reaction composition for cDNA synthesis 144

Table VIa Crossing point values for 16S rRNA gene 147

Table VIb Crossing point values for *rubA* 148

Table VIc Crossing point values for *alkM* 149

Table VId Crossing point values for *alkR* 150

Table VIe Crossing point values for *xcpR* 151

Table VIf Crossing point values for *estB* 152

Table VIg Crossing point values for *lipA* 153

Table VIh Crossing point values for *lipB* 154

1. INTRODUCTION AND LITERATURE REVIEW

1.1 INTRODUCTION

Petroleum fuel and its derivatives are indispensable commodities in contemporary society. Not only does this valuable, non-renewable resource provide energy, it also serves as a source of wealth for many nations, ultimately affecting global economies. Consequently, with the colossal demand and quantity of fuel required, accidental spillage during transportation, and leakages from pipelines and storage facilities are often inevitable.

The contamination of the environment with petroleum hydrocarbons, whether inadvertent or deliberate, appears to be an escalating problem, with obvious ecological and economic ramifications (Marín *et al*., 1995). Petroleum contains a plethora of deleterious compounds such as benzene, toluene, ethylbenzene, xylenes, and naphthalene, and its consequential contamination can be detrimental to the health of plants, animals, and humans (Sarkar *et al*., 2005).

Increased societal awareness towards protecting human health as well as the conservation and preservation of the environment, demands for new remediative strategies that are both environmentally friendly and cost-effective. Various protective and remediative strategies for cleaning hydrocarbon contaminated sites have been developed. These strategies include physical, chemical, and biological processes, with each exhibiting varying degrees of success.

Many organisms including yeasts, plants, insects, and microorganisms, produce alkanes (hydrocarbons) as either moisture barriers, reserve materials, pheromones, or products of metabolic overflow (Park, 2005). As a result, many microorganisms have evolved and are now equipped with the essential metabolic machinery that enables them to utilize alkanes as a carbon and energy source and co-exist with the alkane producing organisms. Microbial communities that have also been continuously exposed to hydrocarbon pollutants have adapted, exhibiting genetic modifications resulting in augmented proportions of hydrocarbon-degrading bacteria and bacterial plasmids encoding hydrocarbon catabolic genes (Leahy and Colwell, 1990).

Microorganisms are considered to be preeminent for the degradation of hydrocarbons and exploitation of their degradative capabilities for environmental remediation has become fundamental to petroleum microbiology (Atlas, 1981). A wide array of studies have dealt with biodegradation and bioremediation of petroleum hydrocarbons, and interest in unraveling the intricacies of bacterial hydrocarbon degradation has mobilized large research communities that have generated a wealth of genetic, biochemical, and physiological knowledge.

Through the advent of molecular techniques, knowledge of the processes of hydrocarbon degradation has advanced considerably, and many novel catalytic mechanisms have been elucidated (Van Hamme *et al.,* 2003). A molecular approach has also contributed to a more comprehensive portrayal of bacterial membrane structure, cellular and physiological adaptations to the presence of hydrocarbons, and the biochemical

mechanisms involved in the accession and uptake of hydrocarbons (de Bont, 1998; Heipieper *et al*., 1994). Although momentous gains have been made in understanding the processes involved in hydrocarbon degradation, the minutiae of individual systems as well as the diversity of systems have yet to be fully articulated (Van Hamme *et al.,* 2003).

Molecular techniques such as real-time polymerase chain reaction (real-time PCR) provides a powerful instrument for gene expression studies, which is increasingly being adopted for RNA quantification and genetic analysis and is of paramount importance in a large number of scientific, medical, and diagnostic fields. Therefore, this study investigated the efficiency of *Acinetobacter calcoaceticus* isolates in the degradation of diesel, and applied LightCycler real-time PCR to quantify the levels of mRNA expression of genes whose roles have been conjectured in the diesel degrading process.

1.2 PETROLEUM AND ITS DERIVATIVES

Petroleum is a complex mixture comprising hydrocarbons, organic compounds, and organometallic components and varies in odour, colour, and viscosity, depending on its origin (Van Hamme *et al*., 2003). Diesel fuels, together with aviation fuel and kerosene, belong to a class of petroleum products known as middle distillates. Carbon chain lengths ranging from C_8 to C_{24}, and a boiling range of approximately 175°C to 375°C are characteristic of the middle distillates (Speight, 2002). Petroleum derived diesel is composed of a mixture of linear alkanes (*n*-alkanes) with traces of aromatics (< 30 ppm polycyclic aromatic hydrocarbon) and less than 1% total additives such as solvent red dye

(Speight, 2002). Diesel has a density of 0.830 g cm^{-3} at 15°C and a viscosity of 2.0 mm^2/s to 4.5 mm^2/s at 40°C (Baldi *et al.*, 1999).

Diesel contains a fraction of compounds that are comparatively lighter, mobile, water soluble, and volatile. Such compounds have a tendency to migrate into ground water, evaporate into the atmosphere, or rapidly disintegrate upon exposure to sunlight and oxygen (Irwin, 1997). The non-volatile and hydrophobic constituents of diesel and other petroleum products are recalcitrant (Abed *et al*., 2002). Such compounds persist in the environment and are detrimental to the health of plants, animals and humans due to their carcinogenicity, mutagenicity and immunotoxicity (Boonchan *et al*., 2000; Samanta *et al*., 2002)

1.3 REMEDIATION STRATEGIES FOR PETROLEUM-CONTAMINATED SITES

The incessant contamination of both marine and terrestrial environments by petroleum hydrocarbons has incited the development and refinement of remediation strategies. These strategies include the comparatively well established physical and chemical methods, and biological methods, that have been a subject of debate and extensive research in recent years (Swannell *et al*., 1996).

Currently, with mounting interest towards the preservation of the environment, biological clean-up methods have provided a valuable, efficient, and cost-effective, alternative to physical and chemical treatment (Atlas, 1991; Molina-Barahona *et al*., 2004). Biological

methods encompass an array of different procedures including, the use of plant material or straw as an absorbent for oil (Tookey and Abbott, 1991), biosurfactants to clean oil covered surfaces (Banat *et al.*, 1991), biological polymers to cover surfaces to avert the adhesion of oil, and the addition of materials to promote microbiological biodegradation of oil, known as bioremediation (U.S. Congress Office of Technology Assessment, 1991).

1.4 BIOREMEDIATION

Bioremediation is an ecologically acceptable technology (Molina-Barahona *et al*., 2004) that exploits the adaptability and metabolic diversity of microorganisms to degrade or transform a variety of organic and inorganic contaminants for the restoration of contaminated environments (Cunningham and Philp, 2000). As a treatment technology, bioremediation has been extensively applied for the degradation of petroleum hydrocarbons including jet fuel, petrol, diesel, and heating oils (Cunningham and Philp, 2000).

Bioremediation of contaminants can be achieved by two methods, bioaugmentation and/or biostimulation. The process of bioaugmentation, in its application to the remediation of petroleum hydrocarbon contamination, involves the introduction of cultured microorganisms that are capable of degrading various chain lengths of hydrocarbons, into a contaminated system (Sarkar *et al*., 2005). Hydrocarbons are metabolized under aerobic or anaerobic conditions by biochemical processes of the microorganisms (Collin, 2001).

There are various parameters such as, the type of microorganism, availability of nutrients and oxygen, pH, temperature, and moisture, which can limit hydrocarbon biodegradation (Molina-Barahona *et al*., 2004). Optimizing such parameters to improve pollutant biodegradation is termed biostimulation (Margesin *et al*., 2000). Most often, the bioremediation of oil contaminated environments has involved biostimulation, where nutrients and oxygen are supplemented to stimulate the indigenous microbial population (Cunningham and Phlip, 2000).

1.5 MICROBIAL DEGRADATION OF HYDROCARBONS

Many indigenous microorganisms present in groundwater and soil are efficient in transforming both naturally and artificially occurring hydrocarbons through direct metabolism. Biodegradation of organic constituents is achieved by enzymes produced by microorganisms. Due to their substrate specificity, several types of enzymes may be required to completely biodegrade organic compounds. Biodegradation of a compound usually occurs via a step-wise process involving a variety of different enzymes. Therefore, in the natural environment, a constituent may not be entirely degraded, but rather transformed into intermediate product/s that may be less, equally, or even more detrimental than the original compound (Ghazali *et al*., 2004).

Biodegradation of complex hydrocarbon compounds usually necessitates the collaboration of several species of microorganisms as individual microorganisms are capable of metabolizing only a limited range of hydrocarbon substrates. Diverse populations exhibit wide-ranging enzymatic capabilities that increase the rate and extent

of petroleum biodegradation (Ghazali *et al*., 2004). Microbial populations consisting of strains belonging to various genera have been detected in petroleum-contaminated soil or water (Sorkhoh *et al*., 1995).

1.6 HYDROCARBON-DEGRADING BACTERIA

The identification of organisms that are pivotal in the pollutant degrading processes is pertinent to the development of optimal *in situ* bioremediation strategies (Abed *et al*., 2002). Characterization of bacterial communities, isolation of prospective degraders, monitoring their response to pollutants, and identifying functional genes and enzymes involved in biodegradation processes have been subject to extensive research in recent years (Cerniglia, 1992; Colores *et al.*, 2000; Laurie and Lloyd-Jones, 2000).

Pioneering research focusing on microbial alkane degradation commenced nearly a century ago, when Söhngen (1913), discovered that the microbes responsible for the disappearance of oil slicks on surface waters were pseudomonads and mycobacteria. Over the years, a multitude of bacterial species capable of hydrocarbon degradation, have been readily isolated from hydrocarbon-contaminated and non-contaminated sites. Such organisms include *Sphingomonas* sp. (Bastiaens *et al*., 2000), *Bacillus* sp., *Alcaligenes* sp., *Moraxella* sp., *Streptococcus* sp., and *Acinetobacter* sp. (Bhattacharya *et al*., 2002).

The *Acinetobacter* are one of the representative genera capable of utilizing *n*-alkanes (Johnson *et al*., 1996; Rusansky *et al*., 1987; Tani *et al*., 2002; Van Hamme *et al*., 2003). *Acinetobacter* are obligate aerobes, non-motile, Gram-negative coccobacilli that are

prevalent in nature, and can be isolated from water, soil and living organisms. They are capable of utilizing various carbon sources for growth and are culturable on relatively simple media (Barbe *et al*., 2004). *Acinetobacter* species have adopted systems that are essential in the biodegradation of an array of toxic compounds but are best recognized for their capacity in biodegradation of alkanes and aromatic hydrocarbons. Subsequently, *Acinetobacter* have been attracting growing interest in both environmental and biotechnological applications for their involvement in biodegradation, and in the extra- and intracellular production of several economically important products (Abdel-El-Haleem, 2003).

1.7 PATHWAYS OF ALKANE DEGRADATION

Linear alkanes (*n*-alkanes), ranging from methane (CH_4) to compounds with chain lengths exceeding 40 carbon atoms (C_{40}), have been found to be degraded by both laboratory and environmental cultures. Even though the metabolism of *n*-alkanes ranging from C_6 to C_{12} is probable, such alkanes may act as solvents (Chakrabarty, 1973). Consequently, these alkanes are therefore toxic to many microorganisms as cells become permeable due to membrane phospholipids being partially solubilized (Sikkema *et al*., 1995).

Three pathways for the initial metabolic attack of *n*-alkanes as well as the participating enzyme reactions have been explicated: (i) the monoterminal oxidation (ii) biterminal oxidation and (iii) subterminal oxidation pathways. Monoterminal oxidation, ($RCH_3 \rightarrow RCH_2OH \rightarrow RCHO \rightarrow RCOOH$), is the most representative pathway in *Pseudomonas* sp.

(May and Katoposis, 1990). Biterminal oxidation (H_3CRCH_3 → H_3CRCH_2OH → $HOCH_2RCH_2OH$ → HOOCRCOOH) occurs when both terminal methyl groups of *n*-alkanes are sequentially hydroxylated and is evident in several types of bacteria and fungi (Rehm and Reiff, 1981). Subterminal oxidation [RCH_2CH_3 → $RCH(OH)CH_3$ → $RC(O)CH_3$], is a less common pathway and has been observed in *Nocardia* sp. (Markovetz, 1971).

In all three pathways, an *n*-alkane is initially attacked by hydroxylases (monooxygenases) to produce the resulting primary or secondary alcohol, although the enzymes that participate in the catalytic mechanism differ (Maeng *et al*., 1996). In the monoterminal and biterminal oxidation pathway, the resulting primary alcohol is sequentially oxidized to the corresponding aldehyde by alcohol dehydrogenases and then to carboxylic acid by aldehyde dehydrogenases. In the subterminal pathway, the corresponding secondary alcohol, is oxidized to a ketone, and ultimately to a carboxylic acid.

However, a fourth metabolic pathway [RCH_3 → RCH_2COOH → $RCO(O)OH$ → RCHORCOOH], known as the Finnerty pathway, was proposed for long-chain *n*-alkane oxidation in *Acinetobacter* sp. strain HO1-N (Finnerty, 1988). In this pathway, an *n*-alkane is initially oxidized by a dioxygenase to the corresponding hydroperoxide that is then transformed to the corresponding primary alcohol or to the corresponding aldehyde. The tentative bases for the Finnerty pathway to ensue are: (i) the bacterium absolutely requires molecular oxygen for *n*-alkane oxidation (Finnerty, 1977), (ii) peroxy acid [$RCO(O)OH$] oxidation should occur in a cell extract system (Finnerty, 1988), (iii) no *n*-

alkane hydroxylase activity should be detectable (Finnerty, 1990), and (iv) enzymes for long-chain fatty alcohol oxidation should exhibit much lower activities than several types of aldehyde dehydrogenase (Singer and Finnerty, 1985).

The resultant carboxylic acid that is produced in the common *n*-alkane metabolic pathway is then integrated into the β-oxidation cycle via acyl coenzyme A (acyl-CoA) formation. Acyl-CoA is then reduced to the corresponding alcohol via acyl-CoA reductase and aldehyde reductase (Fig. 1.1). *Acinetobacter* species are also known to accrue a wax ester as an energy storage material, which is synthesized from an alcohol and an acyl-CoA (Ishige *et al.,* 2002; Tani *et al.,* 2000).

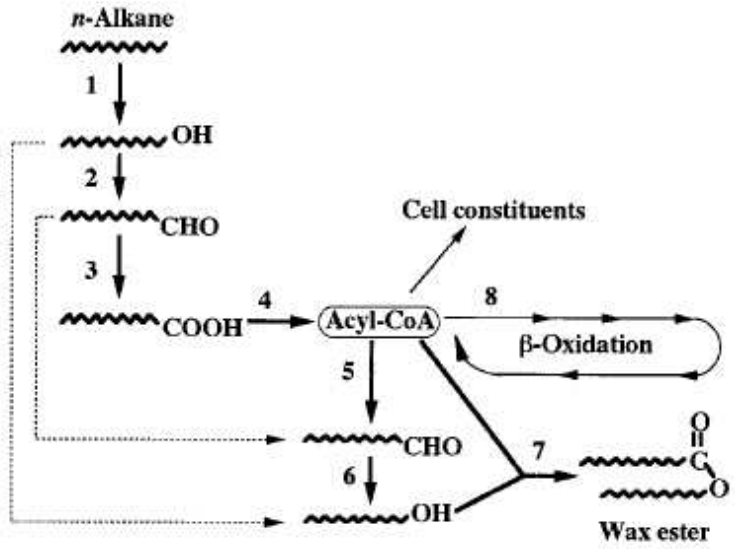

Fig. 1.1 The proposed carbon flow from *n*-alkanes to wax esters in *Acinetobacter* sp.
Dotted lines indicate alternative ways to wax ester production. **Enzymes: 1**, alkane hydroxylase complex; **2**, NAD(P)-dependent alcohol dehydrogenase; **3**, NAD(P)-dependent aldehyde dehydrogenase; 4, acyl-CoA synthetase; **5**, acyl-CoA reductase; **6**, aldehyde reductase; **7**, acyl-CoA: alcohol transacylase; **8**, acyl-CoA dehydrogenase (Ishige *et al.,* 2002).

1.8 GENES AND ENZYMES INVOLVED IN *n*-ALKANE DEGRADATION

The enzymatic facet of alkane degradation amongst microorganisms has attracted mounting interest for the remediation of oil-contaminated sites as well as for the development of conversion processes for petrochemicals. Not only do the intermediate compounds in the alkane degradation pathway boast great potential as important constituents of industrial products, but the participating enzymes can also serve as catalysts for various bioconversion reactions (van Beilen *et al*., 1994a).

Alkane hydroxylases belong to several different oxygenase classes. Degraders of short-chain length alkanes (C_2 to C_4), possess enzymes related to the soluble and particulate methane monooxygenases; while medium- to long-chain length alkane degraders were found to have integral membrane nonheme iron alkane hydroxylases (van Beilen *et al*., 2003). The genes encoding alkane hydroxylase (*alkM*), rubredoxin (*rubA*), and rubredoxin reductase (*rubB*) constitute a three-component alkane hydroxylase complex in *Acinetobacter calcoaceticus* and were found to be obligatory for *n*-alkane degradation (Tani *et al*., 2001). The *alkR* gene that encodes the alkane hydroxylase regulator, is of the AraC-XylS family, and is necessary for *alkM* transcription (Ratajczak *et al*., 1998).

The alkane hydroxylases belong to a large class of essential membrane proteins (Fox *et al*., 1994) and is of interest as a biocatalyst for the production of fatty acids, alcohols, and epoxides (Witholt *et al*., 1990). Thus far, the biochemistry and genetics of the alkane hydroxylase systems of *Pseudomonas oleovorans* and *Acinetobacter* sp. strain ADP1 has been studied extensively. This system confers growth of the organism on medium-chain

length alkanes ranging from hexane to dodecane. The *alk* genes of *P. oleovorans* encode enzymes that are involved in the conversion of alkanes to acyl coenzyme A (acyl-CoA) and are located in two different regions of the OCT plasmid (van Beilen *et al*., 1994b), whereas the organization of *alk* genes in *Acinetobacter* sp. strain ADP1 is entirely different. They are neither contained in large operons nor on a plasmid but occur in apparent disorder on the *Acinetobacter* chromosome (Gralton *et al*., 1997).

Rubredoxins are the simplest of the iron-sulfur redox active proteins and usually contain a single $Fe(S\text{-}Cys)_4$ site. Rubredoxin is an essential component of the alkane hydroxylase system as it shuttles electrons from rubredoxin reductase (Fig. 1.2), a protein which reduces its flavin adenine dinucleotide at the expense of NADH, to alkane hydroxylase (Lee *et al*., 1998).

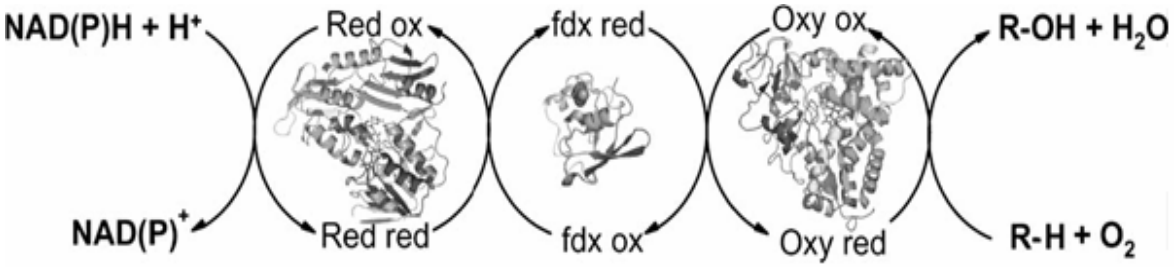

Fig. 1.2 Electron transfer during alkane oxidation. Schematic representation of the various compounds of an alkane hydroxylase system and its electron transfer system. A reductase protein (red) transfers electrons from NAD(P)H via a small electron transfer protein (fdx) to the hydroxylase (oxy) protein where the substrate is oxidized to an alcohol, aldehyde, carboxylic acid, or epoxide (van Beilen *et al*., 2007).

With the burgeoning of the enzyme industry and the continuous search for novel enzymes and applications, interest in *Acinetobacter* lipases has increased recently. Lipolytic strains have been commonly isolated from environments where they may have been incessantly exposed to petroleum pollutants (Abdel-El-Haleem, 2003). In such environments, lipase activity has been correlated with hydrocarbon degradation (Schindler *et al*., 1975). The mechanisms that regulate lipase expression in *Acinetobacter* sp. has thus far only been described in strain BD413 (ADP1) and its derivatives. The gene *lipA* encodes the extracellular lipase and the *lipB* gene encodes a chaperone-like protein LipB that has been found to be essential in the production of extracellular lipase (Kok *et al*., 1995).

In Gram-negative bacteria, secreted proteins must traverse two membranes. In the main terminal branch of the general secretory pathway, secretion occurs in a two-step process. The translocation of extracellular lipase of *A. calcoaceticus* BD413 across the cytoplasmic membrane, is mediated by the Sec system (Pugsley, 1993), and translocation through the outer membrane proceeds via a complex similar to the Xcp system in *Pseudomonas* spp. (Tommassen *et al*., 1992).

The participation of *xcpR* gene in alkane degradation was proposed in *A. calcoaceticus* ADP1 after the insertional inactivation of *xcpR* impeded the secretion of lipase and esterase that lead to the lack of growth on dodecane and slower growth on hexadecane (Parche *et al*., 1997). XcpR is a protein that is also necessary for the assembly of type IV pili in Gram-negative bacteria (Hobbs and Mattick, 1993). Type IV pili enable twitching motility, which is the mode of translocation used by bacteria to spread over the surface of

host tissue, and are therefore recognized as important virulence factors. Type IV pili are also essential for the formation of biofilms and fruiting bodies (Mattick, 2002). In addition to promoting protein secretion, it has also been suggested that type IV pilus-related systems could possibly represent a general transport system for a variety of macromolecules (Tommassen *et al*., 1992) or aid cells in overcoming membrane stress as a result of alkane utilization (Parche *et al*., 1997).

Esterases belong to a diverse class of hydrolytic enzymes. Even though widely distributed in animals, plants, and microorganisms (Okuda, 1991), the physiological role of several members belonging to this class of enzymes, remains largely unknown. Esterase and lipase production is a common occurrence amongst *Acinetobacter* species (Breuil *et al.,* 1978) and activities have been detected in cell-free supernatants of *Acinetobacter* incubated on petroleum by-products. Although the involvement of these enzymes in the degradation of hydrocarbons has been proposed, their exact function is unknown (Asperger and Kleber, 1991).

During alkane metabolism, significant changes occur in the cellular lipid composition, resulting in the formation of several lipid products therefore, the production of these enzymes could be related to the metabolism of lipids (Asperger and Kleber, 1991). In *Acinetobacter* sp. strain ADP1, the *estB* gene encodes a functional esterase and is localized in an operon with genes *rubA*, *rubB*, and *oxyR*. Given that *rubA* and *rubB* are constituents of the alkane hydroxylase complex, the involvement of *estB* in alkane degradation has been investigated (Geißdörfer *et al.*, 1999).

The solubility of alkanes in an aqueous medium is limited. The enzymes that are known to be involved in alkane oxidation are cell bound. Consequently, for alkane oxidation to occur, bacterial cells are required to be in direct contact with the alkane, or be able to pseudosolubilize it (Parche *et al*., 1997). Innovatory research conducted by Mudd in 1924 (Baldi *et al*., 1999; Paul and Jeffrey, 1985) focused on the adhesion of microbial cells to hydrocarbons. Over the last two decades, more extensive studies have been carried out (Paul and Jeffrey, 1985). Microbial adhesion to hydrocarbons has been suggested to occur mainly via proteins. In *Acinetobacter* sp. strain A3 adhesion occurs via two proteins of 26.5 kDa and 56 kDa (Hanson *et al*., 1994), and via an acidic protein, possibly a glycoprotein, of 65 kDa in *Acinetobacter* sp. strain MJT/F5/199A (Thornley *et al*., 1974). *Acinetobacter calcoaceticus* RAG-1 was found to adhere to hydrocarbons via fimbriae (Rosenberg *et al*,. 1982).

The hydrocarbon-degrading *A. calcoaceticus* RAG-1 was found to produce a potent, amphipathic, polyanionic bioemulsifier known as emulsan which stabilizes a wide variety of oil-in-water emulsions. Emulsan consists of a polysaccharide backbone comprised of *N*-acyl D-galactosamine, *N*-acyl L-galactosamine uronic acid and 2,4-diamino-6-deoxy-D-glucosamine (Rosenberg *et al*., 1979). The amphipathic properties of emulsan are attributable to the presence of fatty acids bound to the polysaccharide backbone in both ester and amide linkages (Belsky *et al*., 1979).

The genes responsible for the synthesis of the emulsan biopolymer exist within a single gene cluster, termed the *wee* regulon (Nakar and Gutnick, 2001). Emulsan initially

accumulates on the surface of cells in the exponential phase as a minicapsule, and is released into the medium as an active protein-polysaccharide complex as the cells approach the stationary phase (Goldman *et al*., 1982). It has been proposed that the release of emulsan from the cell surface is mediated by an exocellular esterase produced by *A. calcoaceticus* RAG-l (Shabtai and Gutnick, 1985).

1.9 MONITORING GENE EXPRESSION

The detection and monitoring of bacterial gene expression in the environment have become fundamental components of microbial ecology, diversity monitoring, and bioremediation (Sharkey *et al*., 2004). Estimating microbial activity and determining individual contributions of species to particular processes has presented ongoing challenges.

The advent of molecular techniques for the quantification of gene expression from complex environmental samples has engendered a greater understanding of the roles and diversity of various bacterial populations. Various methods, such as *in situ* hybridization techniques (Amann *et al*., 2001), Northern blotting (Wouters *et al*., 2003), RNase protection assays (Wilderman *et al*., 2001) and reverse transcription Polymerase Chain Reaction (PCR) (Alfreider *et al*., 2003) have been implemented for the quantification of mRNA from environmental samples. Reverse transcriptase PCR presents the most flexible and sensitive method for the detection of expression of both single and multiple genes. However, a major disadvantage of this technique is that it is inherently semi-quantitative. The coalescence of reverse transcriptase PCR, fluorescence detection

chemistries, and technology that is capable of automated detection and quantification of specific mRNAs, has led to the development of innovative technologies, such as real-time PCR, that have revolutionized gene expression analysis studies (Sharkey *et al*., 2004).

1.10 REAL-TIME PCR

The progression of conventional PCR to real-time PCR and the development of novel chemistries and instrumentation platforms have enabled the detection of PCR products on a real-time basis. This has led to the extensive implementation of real-time PCR as the method of choice for quantifying changes in gene expression.

Real-time PCR quantifies the initial amount of the template under investigation specifically, sensitively, and reproducibly. Real-time PCR requires a fluorescent reporter that binds to the product being formed and monitors fluorescence that is emitted during the exponential phase of the reaction as an indicator of amplicon production during each PCR cycle as opposed to the endpoint detection by conventional PCR methods (Sharkey *et al*., 2004). Since real-time PCR does not necessitate post-PCR sample analysis, the arduous validation techniques associated with conventional PCR are evaded (Teo *et al*., 2002). To ensure optimal, precise and reproducible real-time PCR, several factors should be ascertained. Such factors include RNA integrity, reverse transcription and complementary DNA (cDNA) quality, instrumentation, detection chemistries, quantification strategies, amplification efficiency, and data evaluation (Pfaffl, 2004).

1.10.1 Quality of RNA and its influence on real-time PCR

Prior to quantification of gene expression, it is essential to determine the quality and quantity of the total concentrations of the nucleic acid that is being investigated. The quality of RNA encompasses both its integrity and purity and is fundamental for the overall success of RNA-based analyses (Nolan *et al*., 2006). Therefore, the accuracy of gene expression evaluation is largely dependent on the suitability of the starting RNA (Fleige and Pfaffl, 2006). Starting with RNA of poor quality may notably compromise the results of downstream applications which are often laborious, protracted, and very expensive (Imbeaud *et al*., 2005).

To ensure the success of real-time PCR experiments it is imperative to use intact RNA. Extracted total RNA should be undegraded, and free of protein, genomic DNA, enzymatic inhibitors, and nucleases (Bustin and Nolan, 2004b; Pfaffl, 2005). However, studies have shown that RNA samples that are moderately degraded can still be reliably analyzed and quantified (Nolan *et al*., 2006; Schoor *et al*., 2003), provided that the amplification products are short (< 250 bp) and that expression is normalized against an internal reference (Nolan *et al*., 2006). The evaluation of RNA integrity can be achieved by various techniques such as denaturing agarose gel electrophoresis, classical gel optical density measurement, modern optical density measurement via NanoDrop spectrophotometry, or with lab-on-chip technologies (Fleige and Pfaffl, 2006).

1.10.2 Reverse transcription and cDNA synthesis

A major drawback of conventional PCR and DNA polymerase is that DNA must be used as a template. RNA, however, does not serve as a template for DNA polymerase and cannot be amplified in the same manner. This limitation can be circumvented by the use of another enzyme, reverse transcriptase, which converts RNA into cDNA. Under the appropriate reaction conditions, the relative amount of cDNA generated by reverse transcription is proportional to the relative amount of its RNA template (Valasek and Repa, 2005).

Although the conversion of RNA into a cDNA template is presumably a small step, it is a significant contributor to the inconsistency and lack of reproducibility that is commonly observed in real-time PCR experiments. This variability can be attributed to the inherent disparity in RNA due to the dynamic state of cells prepared from biological samples, the instability of RNA once extracted, template abundance, and the different priming approaches used in cDNA synthesis (Bustin *et al*., 2005).

1.10.3 Real-time PCR instrumentation

A diverse range of systems for real-time PCR analysis are available and differ in sample processing capacity, format, and dynamic range (Table 1.1). The instrumentation platform consists of a thermal cycler, computer, optics for flourescence excitation and emission collection, and software for the acquisition and analysis of data (Sharkey *et al*., 2004).

The LightCycler real-time PCR system (Roche Diagnostics) enables real-time PCR amplifications to be performed in small glass capillaries with a maximum sample holding capacity of 20 µl. Capillaries are enclosed in a rotor-like carousel that is subjected to rapid heating and cooling by a stream of air. The glass capillaries facilitate the rapid heating and cooling, thereby enables shorter cycle times (Wittwer *et al*., 1989). An unsurpassed advantage of the LightCycler system over all other real-time systems, is the alacrity of the reaction (Sharkey *et al*., 2004).

Table 1.1 Available real-time PCR systems and formats (Sharkey *et al*., 2004)

Manufacturer	Real-time system	Normal sample format	Maximum no. of samples
Applied Biosystems	ABI Prism 7000	Microplate	96
	ABI Prism 7900 HT	Microplate	384
Roche Biochemicals	LightCycler	Capillaries	32
Corbett Research	Rotor-Gene 3000	Strip tubes	72
Bio-Rad	iCycler	Microplate, strip tubes	96
	MyiQ	Microplate, strip tubes	96
Cepheid	SmartCycler	Microplate, strip tubes	96
Stratagene	Mx3000P	Microplate, strip tubes	96
	Mx4000P	Microplate, strip tubes	96
MJ Research	Opticon	Microplate, strip tubes	96
	Opticon 2	Microplate, strip tubes	96
Techne	Quantica	Microplate	96

1.10.4 Detection chemistries

The ability to detect and monitor the progress of DNA amplification in real-time is achieved by specific chemistries. Currently, fluorescence is exclusively used for amplicon detection in real-time PCR. Two general methods have been established: gene-specific fluorescent probes and specific double strand (ds) DNA binding agents (Mackay

et al., 2002). Both methods are based on fluorescence resonance energy transfer (FRET) (Winer *et al*., 1999). There are several types of detection chemistries available (Fig. 1.3), including hydrolysis probes (5´-nuclease probes), sunrise and scorpion primers, molecular beacons, peptide nucleic acid (PNA) light-up probes, hybridization probes, DNA-binding dyes such as ethidium bromide (EtBr) or SYBR green I, (Valasek and Repa, 2005).

The LightCycler system presently supports two fluorescence-based methods for the detection of amplification products: gene-specific hybridization probes and dsDNA binding agent, SYBR Green (Sharkey *et al*., 2004). The hybridization probe system is mostly employed for LightCycler experiments due to the specialized detection filters that the instrument possesses. The hybridization probe system comprises of two sequence-specific probes: a donor and an acceptor.

The donor probes are 3´- terminally labeled with a reporter dye (usually 6-carboxyfluorescein, FAM) and the acceptor probes are 5´-terminally labeled with an acceptor dye such as cyanine dyes Cy3, and Cy5; 6-carboxy-4,7,2´,7´-tetrachlorofluorescein (TET); 6-carboxyrhodamine X (ROX); 6-carboxy- N,N,N´,N´-tetramethylrhodamine, (TAMRA). The 3´-end of the acceptor probe is blocked to prevent its extension during annealing. No acceptor fluorescence is detected from probes that are free in solution as only the donor dye becomes excited. During the primer-annealing phase, the probes bind adjacent to each other on the single-stranded DNA. The excitation energy is transferred from the donor to the acceptor dye through FRET. When Taq DNA

polymerase is used, the probes can be partially hydrolysed due to the intrinsic endonucleolytic activity of the polymerase, subsequently leading to a decreased effective probe concentration during the PCR. Hence, sub-optimal signal-to-noise ratios are generated. This problem can be circumvented by using polymerases that lack endonucleolytic activities (Wilhelm and Pingoud, 2003).

SYBR Green I is the most frequently used DNA binding dye. SYBR Green presumably binds to the minor groove of dsDNA, resulting in increased fluorescence. When bound to dsDNA, SYBR Green emits a 1000-fold greater fluorescence as compared to when it is free in solution (Wittwer *et al*., 1997). During the progression of the PCR, the fluorescence signal of SYBR Green increases exponentially with the amount of dsDNA product being formed (Bengtsson *et al*., 2003). This correlation, however, is not stringently in proportion as the fluorescence of SYBR Green dye is dependent on the dye:base binding ratio, which decreases as the reaction progresses.

SYBR Green is an asymmetric cyanine and is considered a sequence non-specific reporter in real-time PCR (Jansen *et al*., 1993). Consequently, an inadequacy of the dye is the emission of a fluorescence signal in the presence of any dsDNA, including primer dimers, which are the product of nonspecific annealing and primer elongation proceedings, and results in an overestimation of the target concentration. Primer dimerisation interferes with desired product formation as a result of the two reactions competing for reagents and may lead to invalid data output. However, a specific quantity of a particular dsDNA target, in the absence of significant amounts of interfering,

undesired dsDNA products, will emanate the same level of fluorescence every time. Hence, DNA binding dyes are excellent for quantitative real-time PCR when comparing samples at the same level of fluorescence in the absence of interfering DNA (Kubista *et al*., 2006).

The advantages of SYBR Green are that it is fairly simple to use and the most economical option for detecting and quantifying real-time PCR products with reactions demonstrating a high degree of sensitivity and reproducibility. SYBR Green can work optimally for single product reactions with well designed primers, with spurious, non-specific products becoming evident during very late amplification cycles (Pfaffl and Hageleit, 2001). However, detection by SYBR Green requires extensive optimization. Since the dye cannot distinguish between specific and non-specific products accumulated during PCR, post-PCR validation assays such as melting curve analysis, and agarose gel electrophoresis, are warranted (Pfaffl and Hageleit, 2001).

An unsurpassed advantage of probe based methods as opposed to DNA binding dye systems is multiplexing. Multiplexing enables both the amplification of multiple templates within a single reaction tube as well as their detection in parallel (Wittwer *et al*., 2001). Multiplexing is currently employed in diagnostics to relate reporter genes to that of an exogenous control gene and for single nucleotide polymorphism (SNP) and mutation detection studies (Mackay, 2004).

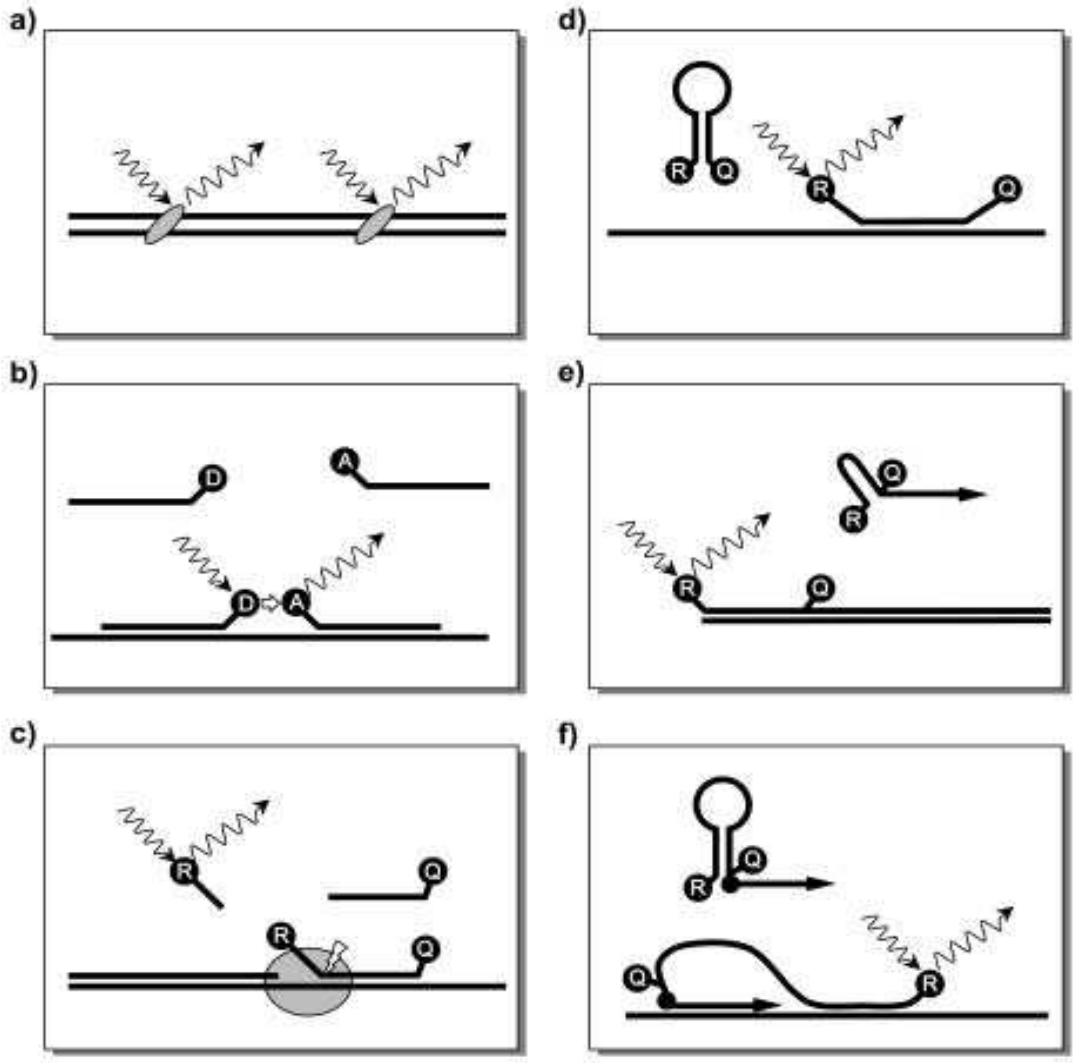

Fig. 1.3 Mechanisms of fluorescent reporters used in real-time PCR. D - donor; **A** - acceptor; **R** - reporter; **Q** - quencher. **a).** Sequence non-specific dyes e.g. SYBR Green I, **b)** Hybridization probe, **c).** Taqman probe (Hydrolysis probe). The grey circle indicates Taq polymerase hydrolysing the TaqMan probe, **d).** Molecular beacon **e).** Sunrise primer **f).** Scorpion primer (Wilhelm and Pingoud, 2003).

1.10.5 Quantification strategies in real-time PCR

The ability to accurately quantify transcription levels of specific genes has always been fundamental to investigating gene function, as many cellular decisions pertaining to survival, growth, and differentiation are reflected in varied patterns of gene expression (Zamorano *et al.*, 1996). The quantification strategy is the principal indicator in gene quantification. The level of expressed genes can be measured either absolutely or relatively. Both relative and absolute quantification strategies use crossing point (C_p) values to quantify cDNA and consequently determine gene expression. Amplification curves generated by real-time instrumentation software are used to determine the C_p value, which is the cycle number at which fluorescence reaches a threshold level. C_p values are inversely proportional to the amount of specific nucleic acid sequence in the sample. In a completely efficient PCR, the quantity of amplified product doubles with each cycle. Therefore, a difference of 2 in C_p values indicates a four-fold difference in the quantity of the amplification product (Valasek and Repa, 2005).

Absolute quantification is based on the use of a standard dilution series with known concentrations to generate a standard curve. The PCR standard can be a fragment of either double-stranded DNA (dsDNA), single-stranded DNA (ssDNA). This method of quantification assumes that all standards and samples have approximately equal amplification efficiencies (Souaze *et al.*, 1996). The standard curve produces a linear relationship between C_p values and initial amounts of total RNA or cDNA, and determines the concentration of unknowns based on their C_p values. The target concentration is expressed as an absolute value. Although this type of quantification

presents a more demanding method, it provides the exact number of nucleic acid targets present in a sample in relation to a specific unit, enabling easier data comparison from different assays and laboratories (Pfaffl *et al.*, 2002).

Relative quantification determines the changes in the steady-state mRNA levels of a gene of interest across multiple samples and expresses it relative to the levels of an internal control RNA i.e. a reference gene. A reference gene is usually a housekeeping gene that exhibits unvarying expression levels under experimental conditions. Housekeeping genes can either be co-amplified in the same reaction tube in a multiplex assay or amplified in a separate reaction tube (Valasek and Repa, 2005).

Relative quantification does not necessitate the need for standards with known concentrations and the reference can be any transcript, provided that its sequence is known (Bustin, 2002). Relative quantification is based on the expression levels of a target gene versus a reference gene and is often an adequate quantification method for investigating physiological changes in gene expression levels (Bustin, 2002).

Various mathematical models have been established to calculate the expression of a target gene in relation to an adequate reference gene. Such mathematical models can ascertain relative expression levels either without real-time PCR efficiency correction (Eq. 1.10.5.1) (Livak and Schmittgen, 2001) or with kinetic PCR efficiency correction (Eqs. 1.10.5.2 and 1.10.5.3) (Pfaffl, 2001). Present models are able to determine a single transcription difference between one control and one sample, e.g. LightCycler Relative

Quantification Software, or enable a group-wise comparison of up to one hundred samples, e.g. Relative Expression Software Tool (REST), and REST-XL. The relative expression ratio of a target gene is calculated on the basis of its actual real-time PCR efficiency (E) or on a static E of 2, and the crossing point difference (ΔC_p) of one unknown sample versus one control. The relative computation procedure, using either REST or REST-XL, is based on the mean C_p of the investigated groups (Eq. 1.10.5.3) (Pfaffl, 2004).

$$\mathbf{R = 2^{-[\Delta C_p \text{ sample} - \Delta C_p \text{ control}]}} \qquad \mathbf{R = 2^{-\Delta\Delta C_p}} \tag{1.10.5.1}$$

$$\mathbf{Ratio = \frac{(E_{target})^{\Delta C_p \text{ target (control – sample)}}}{(E_{ref})^{\Delta C_p \text{ ref (control – sample)}}}} \tag{1.10.5.2}$$

$$\mathbf{Ratio = \frac{(E_{target})^{\Delta C_p \text{ target (}MEAN\text{ control – }MEAN\text{ sample)}}}{(E_{ref})^{\Delta C_p \text{ ref (}MEAN\text{ control – }MEAN\text{ sample)}}}} \tag{1.10.5.3}$$

The most common approach in determining relative quantification is the standard curve method, where standard curves are generated for both the target and a reference gene of choice (Sharkey *et al*., 2004). The quantity of each experimental sample is primarily determined using a standard curve and then expressed relative to a calibrator (Livak, 1997).

The calibrator is reported as 1-fold, and all experimentally derived quantities are reported as an *n*-fold difference relative to the calibrator. Standard curve units are eliminated as a result of the sample quantity being divided by the calibrator quantity. Therefore, only the relative dilution factors of the standards are required for quantification. This is often a preferred method when the amplification efficiencies of the reference and target genes are disparate (Liu and Saint, 2002).

The standard curve method offers the simplest method of quantification as it does not necessitate the quantification of calibrator samples, preparation of exogenous standards, and the use of complex mathematics. However, since this method does not incorporate an endogenous control, such as a housekeeping gene, normalization of results is mandatory (Wong and Medrano, 2005).

1.10.6 Amplification efficiency

Amplification efficiency of the PCR reaction is an imperative consideration when performing relative quantification. Previous methods of calculating gene expression have been based on the assumption that the amplification efficiency of the reaction is ideal,

signifying the doubling of the PCR product concentration during every cycle within the exponential phase of the reaction (Gibson *et al*., 1996). However, many PCR reactions do not have ideal amplification efficiencies, and calculations devoid of an appropriate correction factor may significantly overestimate the starting concentration (Liu and Saint, 2002). Usually, the amplification efficiency of a reaction is calculated using data collected from a relative standard curve with equation (Eq.) 1.10.6.1 (Rasmussen, 2001).

$$\textbf{Efficiency } (\boldsymbol{E}) = [10^{(-1/\text{slope})}]-1 \qquad (1.10.6.1)$$

Real-time PCR efficiency usually varies with high linearity ($r > 0.989$) from $E = 1.60$ to $E = 2.10$ for cDNA (Pfaffl, 2004). The amplification efficiency of the reaction varies from being relatively stable in the early exponential phase and gradually declining to zero (Liu and Saint, 2002).

1.10.7 Data evaluation

The unit of data acquisition in real-time PCR is a precise and characteristic crossing point (C_p). A choice of fluorescence acquisition methodologies for C_p determination is available. The 'Fit Point Method' and 'Threshold Cycle Method' are constant threshold methods, where C_p is measured at a constant fluorescence level on the assumption that all investigated samples have equivalent cDNA concentrations at threshold fluorescence (Higuchi *et al*., 1993). Despite the robustness of these methods, automation is arduous, thereby demanding a lot of user involvement (Rasmussen, 2001). Significant variations in background flourescence during real-time PCR, has posed a challenge in measuring the

level of background flourescence. This has lead to a new acquisition model that is based on mathematic algorithms. The 'Second Derivative Maximum Method', which is exclusive to the LightCycler software, enables C_p to be identified automatically and is measured at the maximum increase or acceleration of flourescence, even if the flourescence levels differ between the curves (Rasmussen, 2001).

1.11 MOTIVATION

The fuel industry, although crucial to our sustainability, is notorious for the contamination of atmospheric, terrestrial, and marine environments. Societal and scientific interest in the fate of petroleum hydrocarbon contaminants is impelled by its harmful effects on the environment and human health.

The bacterial biodegradation of petroleum hydrocarbons has been extensively researched and has been the subject of many first-rate publications (Atlas and Bartha, 1992; Atlas and Cerniglia, 1995; Prince, 1997). Although a myriad of bacterial species have been identified as hydrocarbon degraders, there is a dearth of information regarding the genetic characteristics of their alkane-degradative systems (Whyte *et al*., 2002).

Acinetobacter calcoaceticus isolates LT_1, LT_1A and V_2 were isolated and characterized in previous studies (Singh and Lin, 2008; Mandri and Lin, 2007). LT_1, LT_1A were originally isolated from soil contaminated with unused diesel whereas V_2 was isolated from soil contaminated with used engine oil. Previous studies (Singh and Lin, 2008; Mandri and Lin, 2007) conducted preliminary degradation assays in order to determine

the efficiency of these isolates in the degradation of their respective hydrocarbon substrates with a view to developing environmental bioremediative applications. The focus of investigation was to examine the influence that various factors had on bacterial hydrocarbon degradation. Such factors included the addition of nutrients in the form of fertilizers, and changes in pH, temperature and oxygen supply.

Subsequent to the establishment of the organisms' optimal growth conditions and degradative capabilities, a natural and logical progression in research would be to investigate the mechanisms by which the bacteria degrade hydrocarbons. Therefore, the present study focused on the genetic involvement in hydrocarbon utilization.

1.11.1 Purpose

The purpose of this study was to investigate and quantify the levels of mRNA expression of genes of *Acinetobacter calcoaceticus* isolates, whose roles have been conjectured in the diesel degrading process, by evaluating, optimizing, and validating a LightCycler real-time PCR assay.

1.11.2 Aims

- The primary aim of this investigation was to use quantitative real-time PCR to analyze the expression levels of the target genes at specified sampling times during the diesel degrading process.
- An auxiliary aim was to evaluate the probable correlation between levels of hydrocarbon degradation and target gene expression.

1.11.3 Objectives

- Isolate and validate total RNA from *A. calcoaceticus* LT_1, LT_1A, and V_2 samples.
- Reverse transcribe mRNA, and synthesize cDNA.
- Design a suite of real-time PCR primers for the investigated target genes *alkM*, *alkR*, *rubA*, *rubB*, *estB*, *lipA*, *lipB*, and *xcpR*.
- Identify a suitable reference gene for normalization.
- To optimize the reaction components, conditions and cycling parameters of the real-time PCR assay.
- To quantitatively assess the diesel degradation achieved by each of the isolates.

2. MATERIALS AND METHODS

2.1 SELECTION AND IDENTIFICATION OF DIESEL-DEGRADING BACTERIAL ISOLATES

Isolates LT_1, LT_1A, and V_2, were obtained from departmental stock cultures. LT_1 and LT_1A were originally isolated from diesel-contaminated soil (Singh and Lin, 2008) while V_2 was isolated from engine oil-contaminated soil (Mandri and Lin, 2007), in previous studies. Isolates were streaked on nutrient agar and incubated at 30°C for 48 h to attain single colonies. Luria-Bertani (LB) broth (APPENDIX 1) was inoculated with each isolate and incubated 30°C with constant agitation (160 rpm). Genomic DNA was extracted using the High Pure PCR Template Preparation Kit (Roche Diagnostics) according to manufacturer's instructions. The quality of the extracted DNA was analyzed by electrophoresis on 2% (wt/vol) agarose gel.

The identities of bacterial strains were confirmed by 16S ribosomal RNA (rRNA) gene sequence analysis. The 16S rRNA gene was amplified from genomic DNA by PCR. PCR amplification was accomplished using 10 pmol forward primer 63F (5´- CAG GCC TAA CAC ATG CAA GTC- 3´) and reverse primer 1387R (5´- GGG CGG WGT GTA CAA GGC- 3´) (Marchesi *et al*., 1998), ReadyMix Taq PCR Reaction Mix with $MgCl_2$ (Sigma), and 2 µl DNA from each isolate as a template. Amplification was performed in the GeneAmp® PCR System 9700 (Perkin-Elmer, Applied Biosystems) using the following cycling parameters: 30 cycles consisting of 95°C for 1 min, 55°C for 1 min and 72°C for 1.5 min followed by a final extension step of 5 min at 72°C (Sambrook *et al*.,

1989). PCR amplification product was validated electrophoretically on a 2% (wt/vol) agarose gel, stained with ethidium bromide and visualized with Chemidoc UV Transilluminator (BIORAD). Product size was determined using DNA Molecular Weight Marker VI (Roche Diagnostics).

Amplicons were purified and sequenced by Inqaba Biotech (South Africa). The 16S rRNA gene sequences were aligned with published sequences from the GenBank database using National Center for Biotechnology Information (NCBI) BLAST (http://www.ncbi.nlm.nih.gov/BLAST) comparison software (Altschul *et al*., 1990).

2.2 MAINTENANCE AND PRESERVATION OF CULTURES

Pure cultures were streaked on nutrient agar plates and incubated overnight at 30°C to attain single colonies. Plates were stored at 4°C for short term storage. For long term preservation, bacterial colonies were inoculated into 2 ml nutrient broth and incubated overnight at 30°C. A 1 ml aliquot of overnight culture was combined with 1 ml sterile 40% glycerol stock and dispensed into sterile 2 ml microfuge tubes. Stock cultures were stored at -70°C.

2.3 GROWTH OF BACTERIAL ISOLATES ON DIESEL

Isolates were assessed for their ability to grow on diesel, using a liquid mineral medium, Bushnell-Haas (BH) medium (APPENDIX 1) (Bushnell and Haas, 1941). Un-used diesel was obtained from Engen Service Station (Shallcross, Durban). Isolates were grown in

separate 100 ml Erlenmeyer flasks, each with a total volume of 25 ml of liquid BH medium supplemented with 1% (vol/vol) sterilized diesel as the carbon and energy source. Diesel was filtered through 0.22 μm pore size membrane filters for sterilization and removal of particles. Each flask was inoculated with 250 μl of standardized overnight bacterial culture (OD_{600} of 1). Openings of flasks were bunged with sterile cotton wool and covered with aluminium foil.

Bacterial growth was monitored by visual observation of turbidity in the medium and determined by optical density at 600 nm (OD_{600}) at 5, 10, 15, 20, 30, 40, 50, and 60 days of incubation. Incubations were carried out aerobically at 30°C in a rotary shaker (160 rpm). An abiotic control flask, with 1% (vol/vol) diesel and devoid of bacterial inoculum, was incubated under the same conditions to ascertain abiotic loss of diesel.

2.4 DETERMINATION OF BACTERIAL CARBON SOURCE UTILIZATION PATTERNS

Carbon source utilization patterns were determined by gravimetric analysis (Marquez-Rocha *et al*., 2001). Screw cap glass tubes were pre-weighed, in grams, prior to gravimetric analysis. Twenty five microlitre samples were taken at 5, 10, 15, 20, 30, 40, 50, and 60 days of incubation and passed through 250 ml separatory funnels. Two fractions were obtained after separation: a culture medium phase and a hydrocarbon phase. The hydrocarbon phase encompassed an interface and upper oily phase.

The hydrocarbon phase was extracted from the separatory funnel with 10 ml organic solvent, dichloromethane. The dichloromethane extract was funneled through filter paper containing 5 g anhydrous sodium sulfate (Na_2SO_4) for the removal of cellular debris and absorption of moisture. The extract was collected in the pre-weighed glass tubes with screw caps lined with aluminium foil. Uncapped tubes were left overnight in a fume cupboard to facilitate evaporation of dichloromethane. The combined mass of the pre-weighed tube and diesel was recorded. The mass of the tube was subtracted to determine the mass of the diesel remaining (Alula *et al*., 1989). The mass of the diesel remaining was subtracted from the mass of diesel in the control sample and multiplied by 100 to determine the percentage of diesel remaining.

The culture medium phase was centrifuged at $4000 \times g$ for 20 min resulting in a pellet and a cell-free supernatant. The cell-free supernatant was decanted and stored at -70°C. The pellet was re-suspended in phosphate-buffered saline (PBS), pH 7.6 (APPENDIX 1), and subjected to further centrifugation at $4000 \times g$ for 20 min. The supernatant was discarded and the pellet was stored at -70°C until required for RNA extraction.

2.5 RNA EXTRACTION AND VALIDATION

Total RNA was extracted from each pellet using Aurum Total RNA Mini Kit (BIO-RAD) according to manufacturer's instructions, with modifications. The following amendments were made to the lysing of cells procedure during RNA isolation: 500 µl instead of 100 µl of 1000 µg/ml lysozyme in TE (10 mmol Tris, 1 mmol EDTA, pH 7.5) was added to

bacterial cells and incubated at room temperature. Incubation time was extended to 30 min. A 250 µl aliquot of this suspension was removed and transferred to a 2 ml microcentrifuge tube. To this, 700 µl instead of 350 µl lysis solution (supplemented with 1% mercaptoethanol) was added. This was followed by the addition of 700 µl instead of 250 µl of 70% isopropanol.

DNase treatment was included in the RNA extraction protocol and was performed on RNA samples in order to eradicate genomic DNA carry-over. Isolated total RNA purity and yield were determined spectrophotometrically ($OD_{260/280}$) by Nanodrop ND-1000 (BIO-RAD) using a 1 µl RNA sample. In addition, RNA quality was verified electrophoretically by ethidium bromide staining on 2% (wt/vol) agarose in 1×Tris Acetate EDTA (TAE) running buffer (APPENDIX 1) at 80 V. Extracted RNA was stored at -70°C.

2.6 SYNTHESIS OF cDNA

cDNA was synthesized by reverse transcriptase PCR with iScript cDNA Synthesis Kit (BIO-RAD) using standardized RNA of 1 µg (APPENDIX 2). PCR was performed with GeneAmp® PCR System 9700 (Perkin-Elmer, Applied Biosystems) using the following parameters: 25°C for 5 min, 42°C for 30 min, and 85°C for 5 min.

2.7 VALIDATION OF cDNA

A reliable internal quality control for cDNA synthesis is vital. Controls are usually implemented by the PCR amplification of a reference gene. PCR amplification of 16S rRNA gene was achieved using 10 pmol 63F and 1387R primers (Marchesi *et al*., 1998), ReadyMix Taq PCR Reaction Mix with $MgCl_2$ (Sigma), and 2 µl cDNA from each isolate as a template. A reaction containing no cDNA template served as a negative control. Amplification was performed in the GeneAmp PCR System 9700 (Perkin-Elmer, Applied Biosystems), using the cycling parameters outlined in section 2.1. Amplification products were separated on a 2% (wt/vol) agarose gel, stained with ethidium bromide and visualized with the Chemidoc UV Transilluminator (BIORAD).

2.8 LightCycler QUANTITATIVE REAL-TIME PCR

2.8.1 Nucleotide sequences, primer design, and primer preparation

The nucleotide sequences of the genes of interest were acquired from the NCBI GenBank nucleotide sequence databases under the following accession numbers: AF047691 (*lipA* and *lipB*), AJ233398 (*alkM* and *alk*R), EF524340 (16S rRNA), Y09102 (*xcpR*), and Z46863 (*rubA*, *rubB*, and *estB*). Primers for real-time PCR were designed with the aid of primer design software Primer3 (Kubista *et al*., 2006) and were synthesized by Inqaba Biotech. The real-time PCR primer sequences are presented in Table 2.1. Lyophilized primer stocks were reconstituted using DNase/RNase-free water (Fermentas). Stock solutions were aliquotted to avoid repeated freezing and thawing, and whole-batch

contamination. Forward and reverse primers were stored at -20°C, at a 10 pmol working concentration.

2.8.2 Optimizing the components of the LightCycler real-time PCR

In order to optimize the real-time PCR conditions and verify the specificity of the designed primer pairs, the optimal concentrations for primers, cDNA and $MgCl_2$ were determined. For optimization of primer concentration, a primer titration was performed using increasing concentrations of respective primers, ranging from 0.625 pmol/µl to 10 pmol/µl. The pooled cDNA obtained from day 10 to day 60 of isolate LT_1 was selected as the template during the optimizing phase. The pooled cDNA of V_2 isolate was used for optimization of *est*B gene. Optimal cDNA concentration was determined by amplification of increasing volumes of template ranging from 2.5 µl to 5 µl. $MgCl_2$ concentration, annealing temperature, and annealing time, for real-time PCR amplification of each target gene, were amended systematically until the melting peak analysis revealed a single peak at the anticipated melting temperature (T_m).

Table 2.1 Primer sequences for real-time PCR amplification of target genes

Primer	Sequence	Product Size (bp)
16S rRNA		169
Forward	5´-GTAGCGGGTCTGAGAGGATG-3´	
Reverse	5´-GCCTCCTCCTCGCTTAAAGT-3´	
rubA		91
Forward	5´-GATTTATGATGAAGCCGAAGG-3´	
Reverse	5´-GTCAGGGCAAGTCCAGTCAT-3´	
rubB		222
Forward	5´-GCCCACTGGGTCGTCTATTA-3´	
Reverse	5´-CGTGTTTTGCCAGATCAATG-3´	
alkM		189
Forward	5´-AAAGATGCGCGTAATCCAAC-3´	
Reverse	5´-ATTAATGGCACCCATCGAAA-3´	
alkR		161
Forward	5´-TGTAGCATGATGCGCTTTTC- 3´	
Reverse	5´-CACAAGGTGAATGGGCTTTT- 3´	
estB		150
Forward	5´-ATCCAAAATTCGCCACAAAG-3´	
Reverse	5´-TTTTTAATCCGCATCGCTTC-3´	
lipA		189
Forward	5´-CTTCCGTTTCAACGATTGGT- 3´	
Reverse	5´-TATACGCTGCACCGACAGAG- 3´	
lipB		153
Forward	5´-CCAACCCTAGCAGCATCATT- 3´	
Reverse	5´-TGCAACAAGCTCTGCTTCAG- 3´	
xcpR		192
Forward	5´-AGGGTTAATGGCGGAAGACT-3´	
Reverse	5´-CCAATCCCTTCGAGCTGATA-3´	

2.8.3 LightCycler real-time PCR protocol

PCR amplifications of *alkM*, *alkR*, *rubA*, *rubB*, *estB*, *lipA*, *lipB*, *xcpR*, and 16S rRNA genes were performed using LightCycler Instrument Version 3.5 real-time PCR system (Roche Diagnostics). LightCycler reactions were performed in 20 µl glass capillary tubes using LightCycler Faststart DNA Master SYBR Green I kit (Roche Diagnostics). Preparation of reaction mastermix and loading of glass capillary tubes were performed on an aluminium cooling block with centrifuge adapters (Roche Diagnostics) to maintain low temperatures and prevent exposure to light. The aluminium block was pre-cooled to 4°C, prior to use.

Composition of real-time PCR reaction mastermixes for the respective target genes are presented in Table 3.3. A 9 µl aliquot of reaction mastermix was transferred to each LightCycler glass capillary. A 2.5 µl aliquot of cDNA was then added as the PCR template. A negative control was set up for each run containing 2.5 µl diethyl pyrocarbonate (DEPC)-treated water (Invitrogen) as a substitute for cDNA. Capillaries were sealed securely with a stopper by a capping tool (Roche Diagnostics). Aluminium adapters, containing the capillaries, were placed in a benchtop microcentrifuge and subjected to centrifugation at $700 \times g$ for 5 s. Capillaries were removed from the adapters and transferred to the sample carousel of the LightCycler.

The evaluating parameters selected for data analysis were fluorescence (d[F1]/dT), melting temperature (T_m) and crossing point (C_p). A C_p is defined as the point at which the fluorescence rises significantly above the background fluorescence (Pfaffl *et al*.,

2002). The Second Derivative Maximum algorithm was employed for C_p determination where C_p was measured at the maximum increase of fluorescence (Rasmussen, 2001). The LightCycler experimental run protocol consisted of four cycle programs, i.e., initial denaturation of cDNA, amplification of target cDNA, melting curve analysis, and cooling. Cycling parameters for initial denaturation, melting curve analysis, and cooling remained constant for all real-time PCR runs. Initial denaturation of cDNA was programmed at 1 cycle of 95°C for 10 min. Melting curve analysis consisted of 1 cycle of denaturation at 95°C for 30 s, annealing at 65°C for 20 s, and melting at 95°C for 0 s. Cooling was at 40°C for 30 s. Amplification parameters for the respective target genes are outlined in Table 2.2.

2.8.4 Confirmation of real-time PCR primer specificity

Specificity of real-time PCR primers was determined by amplification plots, melting temperature, and melting curve analysis using LightCycler Software, Version 3.5 (Roche Diagnostics). Melting curves serve as an effectual means of providing the accurate identification of amplicons by distinguishing them from primer dimers and amplification artifacts. Melting peaks are generated by plotting the negative derivative (-dF/dT) of the melting curve. Melting peaks are comparable to the bands on an electrophoresis gel and facilitates qualitative post-PCR monitoring of amplification products (Nolan *et al*., 2006). Nevertheless, PCR products were still authenticated by agarose gel electrophoresis. A 10 µl aliquot of the PCR amplicons was combined with 5 µl of 6×gel loading dye (APPENDIX I), and loaded into a 2% (wt/vol) agarose gel containing 3 µl ethidium

bromide. Electrophoresis was performed in 1×TAE running buffer at 80 V. DNA Molecular Weight Marker VI (Roche Diagnostics) was used to determine fragment sizes.

2.8.5 Generation of a relative standard curve

The standard or calibration curves were generated by the LightCycler software (Roche Diagnostics, LightCycler Software, Version 3.5). The cDNA of isolate LT_1 was selected as the calibrator for 16S rRNA, *alkM*, *alkR*, *rubA*, *lipA*, *lipB*, and *xcpR* genes. The cDNA of isolate V_2 served as a calibrator of *est*B gene. Equal aliquots of cDNA obtained from LT_1 samples day 10 to day 60, and V_2 samples day 5 to day 60, were individually pooled and standardized to 1000 ng/µl. A 10-fold serial dilution using DEPC water (Invitrogen) was performed. To generate a standard curve, the serially diluted cDNA standard (1000 ng to 0.001 ng) was quantified in each real-time PCR run. Each dilution was amplified in duplicate. For each standard, the concentration was plotted against the cycle number at which the fluorescence signal increased above the threshold value (C_t) or crossing point (C_p). The gradient generated by each standard curve was used in the equation: Efficiency (E) = $10^{-1/\text{slope}}$ - 1 (Rasmussen, 2001), to determine the reaction efficiency.

Table 2.2 Amplification parameters of investigated genes for real-time PCR

Target gene	Amplification Parameters
16S rRNA	30 cycles of 5 s at 95°C, 10 s at 62°C, 5 s at 72°C
rubA	40 cycles of 5 s at 95°C, 15 s at 62°C, 5 s at 72°C
alkR	55 cycles of 5 s at 95°C, 8 s at 62°C, 5 s at 72°C
alkM	50 cycles of 5 s at 95°C, 15 s at 62°C, 5 s at 72°C
estB	55 cycles of 5 s at 95°C, 15 s at 60°C, 5 s at 72°C
lipA	55 cycles of 5 s at 95°C, 10 s at 62°C, 5 s at 72°C
lipB	55 cycles of 5 s at 95°C, 10 s at 62°C, 5 s at 72°C
xcpR	55 cycles of 5 s at 95°C, 15 s at 60°C, 5 s at 72°C

2.8.6 Real-time PCR data analysis and quantification of gene expression

Gene expression was quantified using the Pfaffl model which combines gene quantification and normalization and was calculated with the aid of Microsoft Excel based application, Relative Expression Software Tool - XL (REST-XL) - Version 2 (Pfaffl *et al*., 2002). For this mathematical model, it is essential to determine the crossing point (C_p) value of each transcript. Given that C_p values decrease linearly with an increasing target quantity, C_p values could be used as a quantitative measurement of the input target number (Heid *et al*., 1996). This method involved comparing the C_p values of the investigated transcripts with a control. The C_p values of both the control and the genes of interest were normalized to an appropriate housekeeping gene (16S rRNA gene).

REST-XL calculates relative expression using the statistical model Pair Wise Fixed Reallocation Randomization Test. For each sample, C_p values for the reference and target genes were randomly reallocated to the control and sample groups. Differences in gene expression levels between control and samples were evaluated in group means for statistical significance by randomization tests (Pfaffl *et al*., 2002).

Descriptive statistics such as the sample means, minimal (Min) and maximal (Max) values, standard deviation (SD), and coefficient of variance expressed as a percentage (CV%), of the derived C_p values were computed for each investigated gene to determine intra-sample variation.

3. RESULTS

3.1 IDENTIFICATION OF ALKANE DEGRADING BACTERIAL ISOLATES

The identities of bacterial isolates LT_1, LT_1A, and V_2 were verified to species level using 16S rRNA gene sequencing and alignment (APPENDIX II). In Genbank database searches using the BLAST program, LT_1, LT_1A, and V_2 were found to be homologous to *Acinetobacter calcoaceticus* JL11 (GenBank accession number EU418714) with 96%, 97%, and 99% similarity, respectively. The scores achieved were 1600, 1548, and 1371, respectively.

3.2 GROWTH OF BACTERIAL ISOLATES ON DIESEL

The growth patterns of the bacterial isolates on diesel were monitored over a period of 60 days and determined by optical density (OD_{600}) based on single determinations. The results obtained are presented in Table 1. Bacterial growth was not monitored nor recorded prior to day 5. Maximum growth was observed after 15 days of incubation. The OD_{600} increased progressively up to 15 days, and remained relatively constant until the end of the period studied. Growth patterns that were observed after 5 and 10 days of incubation may be indicative of a late exponential phase and early stationary phase, respectively.

Table 3.1 Growth of bacterial isolates on diesel determined by optical density

Isolate	OD_{600}
LT_1	
Day 5	1.238
Day 10	1.441
Day 15	1.536
Day 20	1.547
Day 30	1.556
Day 40	1.573
Day 50	1.572
Day 60	1.566
LT_1A	
Day 5	1.298
Day 10	1.361
Day 15	1.452
Day 20	1.469
Day 30	1.471
Day 40	1.449
Day 50	1.478
Day 60	1.466
V_2	
Day 5	1.326
Day 10	1.462
Day 15	1.557
Day 20	1.569
Day 30	1.581
Day 40	1.572
Day 50	1.564
Day 60	1.563

3.3 DETERMINATION OF BACTERIAL CARBON SOURCE UTILIZATION PATTERNS

Carbon source utilization was determined by gravimetric analysis. After 60 days of incubation, a 9.40% mass reduction in the diesel of the abiotic control flask was detected (APPENDIX III). All three isolates were capable of degrading diesel. LT_1, LT_1A, and V_2 achieved 58.6%, 51.7%, and 48.3% degradation after 5 days of incubation and 86.2%, 82.8%, and 89.7% degradation after 60 days of incubation, respectively (Fig. 3.1).

During the initial days of incubation, V_2 appeared to be the least competent diesel degrader in comparison to LT_1 and LT_1A. However, after a rapid increase in diesel degradation at day 15, V_2 emerged as the most efficient diesel degrader by the end of the incubation period (Fig. 3.1).

The presence of an opaque substance, possibly a bioemulsifier, was observed in the hydrocarbon and hydrocarbon - culture medium fraction of V_2 samples throughout the incubation process. After 10 days of incubation, however, the diesel of the V_2 samples no longer appeared as a confluent layer over the culture medium phase, but rather as minuscule droplets enfolded within the presumed bioemulsifier. This occurrence was not observed for LT_1 and LT_1A samples for the duration of the incubation period.

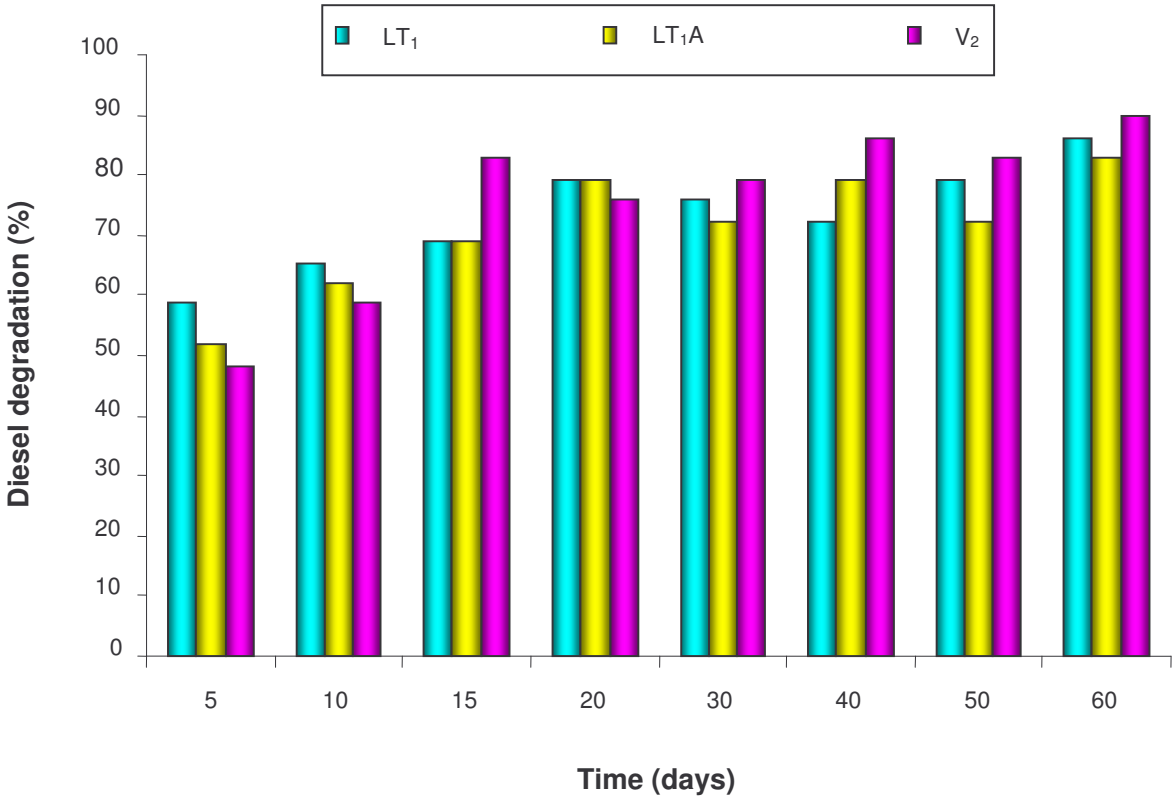

Fig. 3.1 Diesel degradation patterns of *A. calcoaceticus* isolates.

3.4 RNA EXTRACTION AND VALIDATION

RNA yield was determined spectrophotometrically using the Nanodrop ND-1000 (BIO-RAD). The $OD_{260/280}$ ratio obtained ranged from 1.30 to 2.27 (Table 3.2). A ratio greater than 1.8 is considered a suitable indicator of good RNA quality (Manchester, 1996; Sambrook *et al*., 1989). Samples LT_1 - day 5, and LT_1A - day 10, with ratios of 1.30 and 1.50, respectively, indicated poor RNA quality. The RNA extraction procedure was repeated for samples LT_1 - day 5, and LT_1A - day 10 and still yielded RNA of poor quality. In addition to spectrophotometry, RNA integrity was validated by 2% (wt/vol) agarose gel electrophoresis and ethidium bromide staining yielding intact, RNA exhibiting 23S and 16S bands.

3.5 SYNTHESIS AND VALIDATION OF cDNA

Synthesis of cDNA was accomplished by reverse transcriptase PCR. A reliable internal quality control of cDNA synthesis is essential. This was achieved by amplifying the 16S rRNA gene. Amplicons were separated on 2% (wt/vol) agarose yielding an expected product of 1380 bp (Fig. 3.2 A - C). No product was detected for LT_1 - day 5, and a poorly defined product was visible for LT_1A - day 10, as a corollary of poor RNA quality. Hence, LT_1 - day 5 and LT_1A - day 10 samples, were omitted from the study.

Table 3.2 RNA yield and Nanodrop spectrophotometric readings

Sample	Yield ng/µl	$OD_{260/280}$
LT_1		
Day 5	432.96	1.50
Day 10	421.48	2.01
Day 15	285.00	1.89
Day 20	217.67	2.06
Day 30	341.06	2.15
Day 40	447.17	1.96
Day 50	476.44	2.11
Day 60	481.90	2.27
LT_1A		
Day 5	269.71	2.05
Day 10	43.080	1.30
Day 15	179.92	2.07
Day 20	399.66	2.09
Day 30	254.49	2.10
Day 40	561.01	2.15
Day 50	439.31	2.03
Day 60	374.28	2.11
V_2		
Day 5	68.530	1.98
Day 10	161.02	2.04
Day 15	291.61	2.16
Day 20	404.87	2.19
Day 30	573.65	2.19
Day 40	531.23	2.25
Day 50	764.03	2.18
Day 60	500.61	2.22

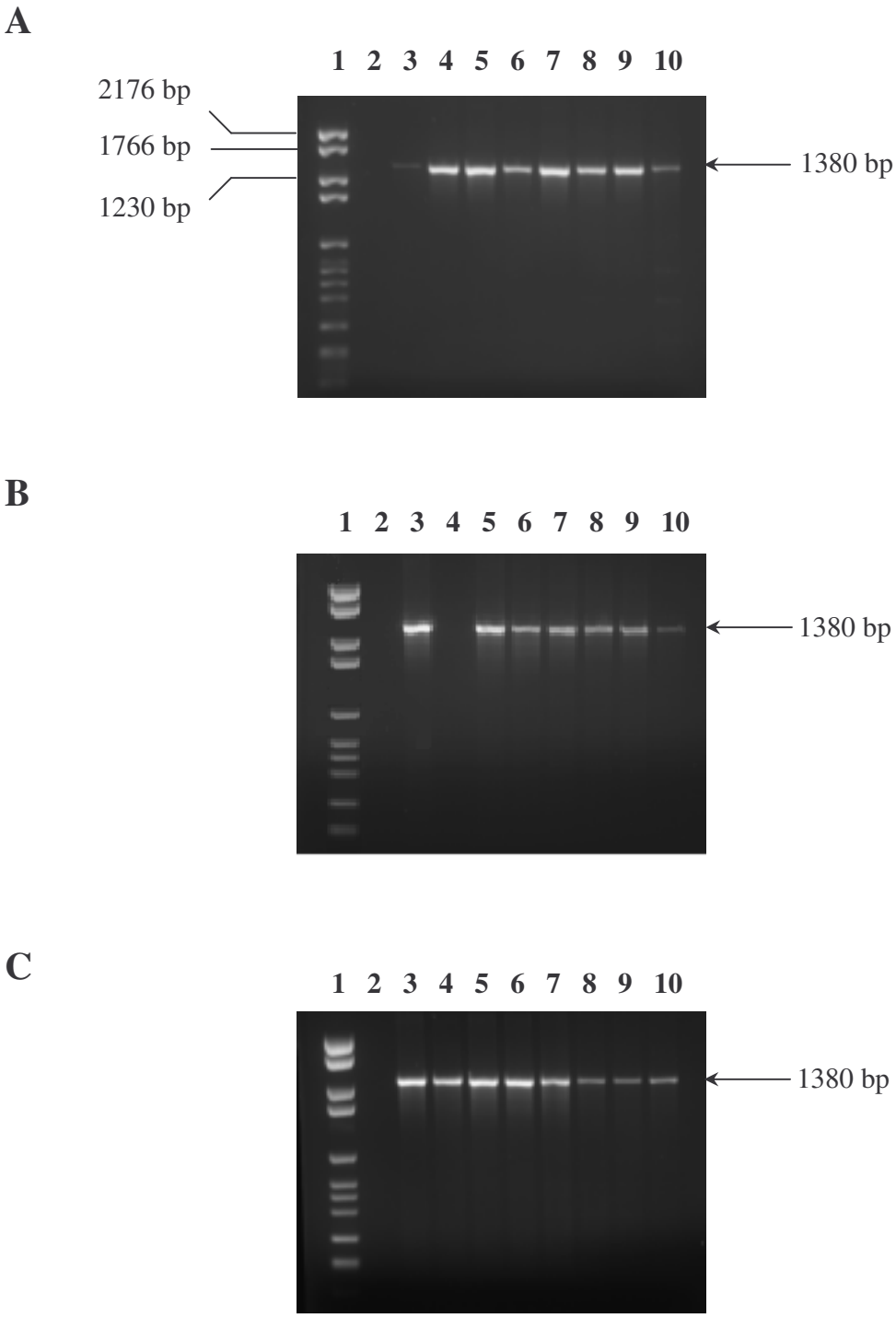

Fig. 3.2 Validation of cDNA by 2% (wt/vol) agarose gel electrophoresis. **A**, **B**, and **C**, represent amplicons of the 16S rRNA gene of LT_1, LT_1A, and V_2, respectively. **Lanes 1**, DNA molecular weight marker VI (Roche Diagnostics); **2**, negative control (no cDNA template); **3 - 10**, day 5 to day 60, respectively.

3.6. OPTIMIZING THE COMPONENTS OF THE REAL-TIME PCR MASTERMIX

Optimal primer concentration for each primer pair was determined by performing a titration using increasing concentrations of respective forward and reverse primers, ranging from 0.625 pmol/µl to 10 pmol/µl. Negative controls comprised of real-time PCR mastermix and the respective primer concentrations, but were devoid of a cDNA template.

A representative melting peak analysis of a primer titration assay using the real-time PCR 16S rRNA primers is shown in Fig. 3.3. Fluorescence observed in the negative controls was due to primer dimer formation. Primer dimer formation was evident in the negative control samples with higher primer concentrations. The negative control samples, containing only primers, exhibited peaks with lower melting temperatures (T_m), while the positive control dilution series containing the product of interest displayed peaks with higher T_m. The optimal real-time PCR primer concentrations for each of the investigated target genes are presented in Table 3.3.

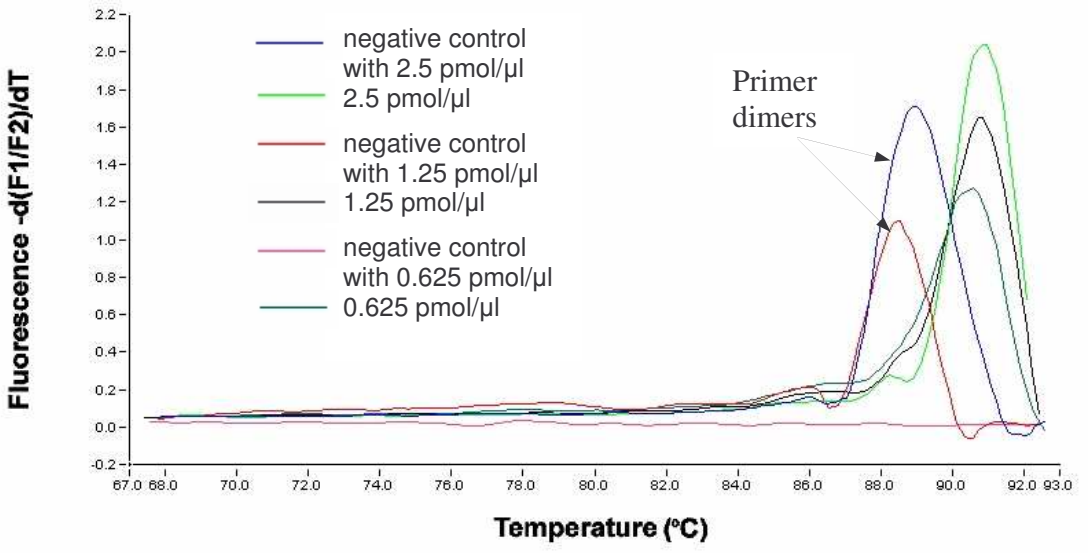

Fig. 3.3 Optimization of real-time PCR primer concentrations. A representative melting peak analysis showing titration of 16S rRNA primers. Primer dimer formation was observed in negative control samples with higher primer concentrations.

$MgCl_2$ concentration, in conjunction with annealing temperature, and annealing time, for real-time PCR amplification of each target gene, were amended systematically until the melting peak analysis revealed a single peak at the anticipated melting temperature (T_m). Diethyl pyrocarbonate (DEPC)-treated water (Invitrogen) was added accordingly to constitute a 9 µl final reaction volume. Optimal concentrations and volumes of reaction components of the PCR mastermix are presented in Table 3.3.

Optimal template cDNA quantity for was determined by amplification of increasing volumes of template ranging from 2.5 µl to 5 µl. No cDNA template was added to the negative control. A representative melting peak analysis showing amplification of *lipB*

for cDNA template determination is illustrated in Fig. 3.4. Amplification of larger volumes of cDNA resulted in duplex peak formation whereas 3 µl and 2.5 µl cDNA produced single, sharply defined peaks (Fig. 3.4). A 2.5 µl volume of cDNA was selected as the optimal template quantity for real-time PCR amplification of all investigated target genes.

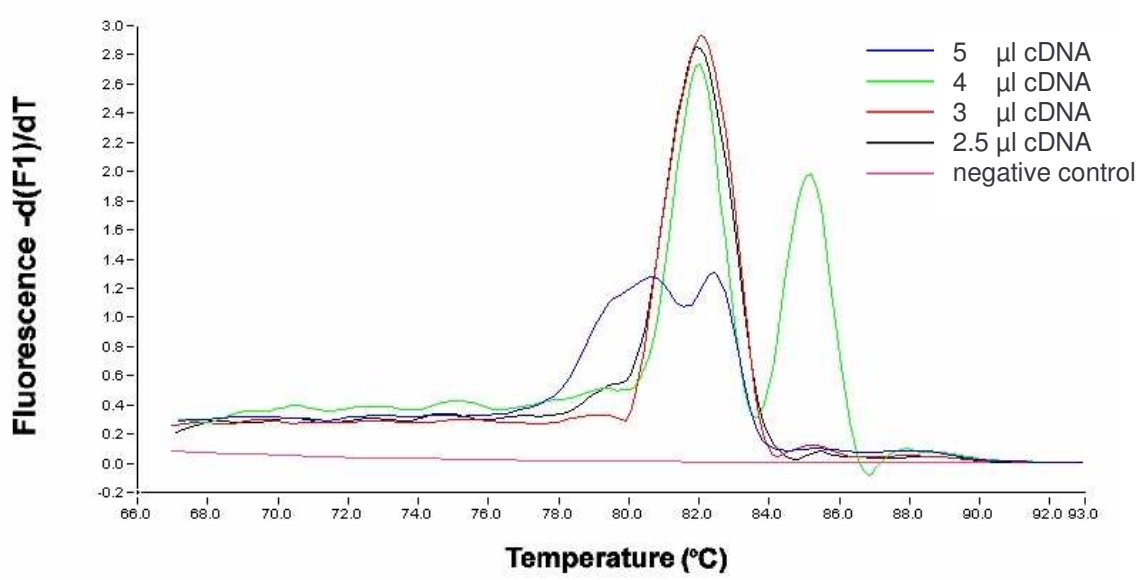

Fig. 3.4 Optimization of real-time PCR cDNA template quantity. A representative melting peak analysis showing amplification of *lipB* resulting from varying volumes of cDNA template.

Table 3.3 Composition of reaction mastermix for LightCycler real-time PCR assays

Target gene	Primer conc. (pmol/µl)	Reaction components (µl)*				
		DEPC H_2O	Forward primer	Reverse primer	$MgCl_2$ (25 mM)	SYBR green
16S rRNA	1.25	5.8	0.5	0.5	1.2	1.0
alkM	10.0	6.0	0.5	0.5	1.0	1.0
alkR	5.00	6.2	0.5	0.5	0.8	1.0
rubA	5.00	5.8	0.5	0.5	1.2	1.0
lipA	10.0	5.8	0.5	0.5	1.2	1.0
lipB	10.0	5.8	0.5	0.5	1.2	1.0
xcpR	10.0	5.8	0.5	0.5	1.2	1.0
estB	10.0	5.8	0.5	0.5	1.2	1.0

* final reaction volume of 9 µl

3.7 CONFIRMATION OF PRIMER SPECIFICITY

A LightCycler melting curve analysis was performed to determine specificity of the amplification reaction and to determine the characteristic melting temperature (Table 3.4) of the target DNA. Each amplification product for the target genes demonstrated a specific and characteristic melting curve. The melting curves were converted to melting peaks by plotting the negative derivative of the fluorescence with respect to temperature (-dF/dT) against temperature, resulting in the formation of a single, narrow peak (Fig .3.5 A - H). No primer dimerisation or nonspecific products were generated for the applied number of amplification cycles for the respective target genes. In addition, specificity of real-time PCR products were documented by agarose gel electrophoresis and resulted in a single product of anticipated length. No PCR amplification product was observed for gene *rubB*, despite rigorous optimization strategies and redesigning of primers.

Table 3.4 Melting temperature (T_m) of target gene amplification products

Primer pair	T_m (^oC)
16S rRNA	91.2129
alkM	80.3645
alkR	79.3354
rubA	85.0366
estB	82.8515
lipA	83.4089
lipB	82.3369
xcpR	84.0949

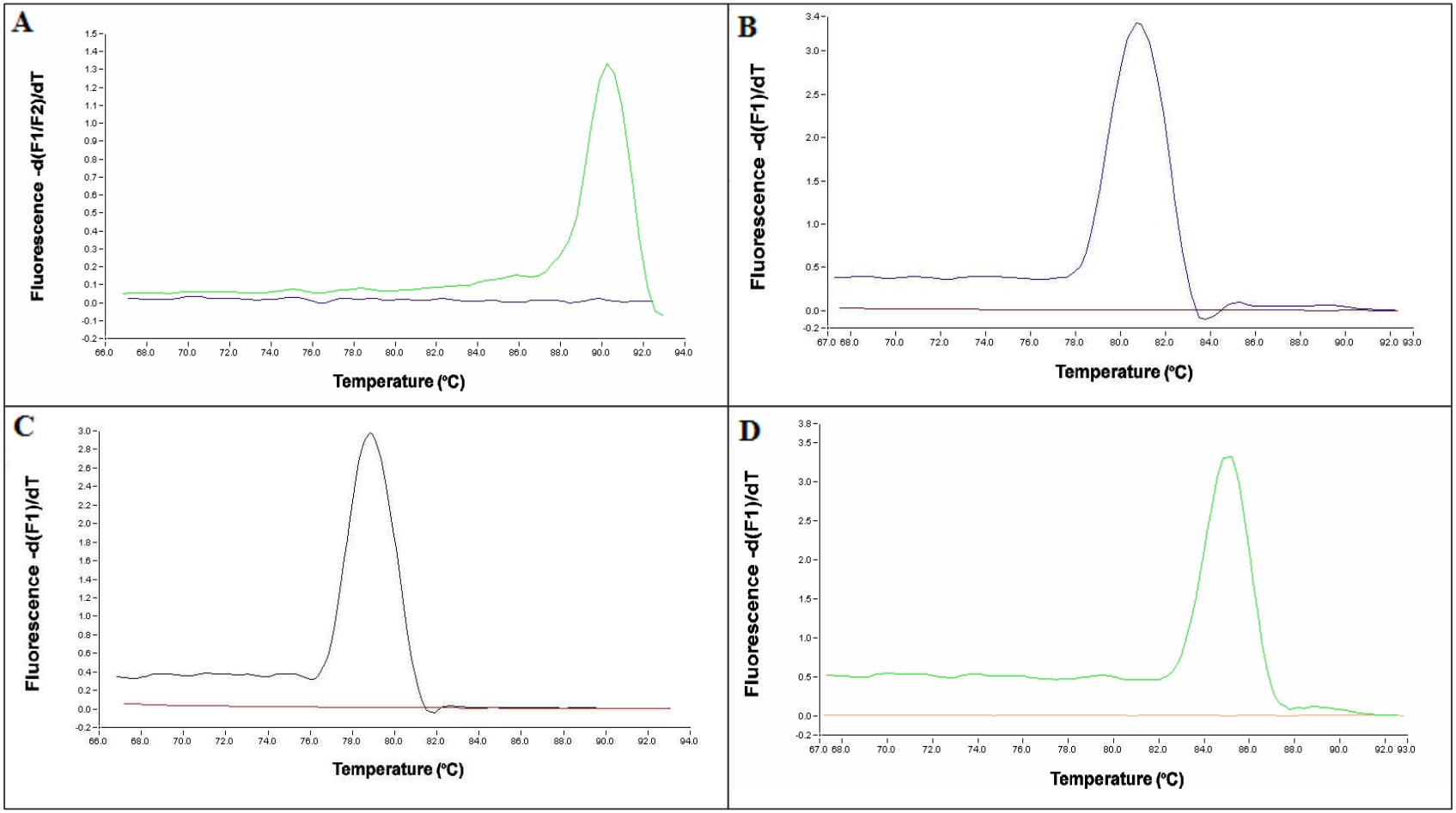

Fig. 3.5 Confirmation of real-time PCR specificity for target genes. Amplification of target genes **(A)** 16S rRNA, **(B)** *alkM*, **(C)** *alkR*, **(D)** *rubA*, **(E)** *lipA*, **(F)** *lipB*, **(G)** *xcpR*, and **(H)** *estB*, as determined by melting curve analysis. Melting peaks were determined by plotting the continuous negative derivative of fluorescence emitted by each sample as PCR products were melted. The no-cDNA template control sample for each reaction does not show fluorescence, confirming the absence of primer dimers.

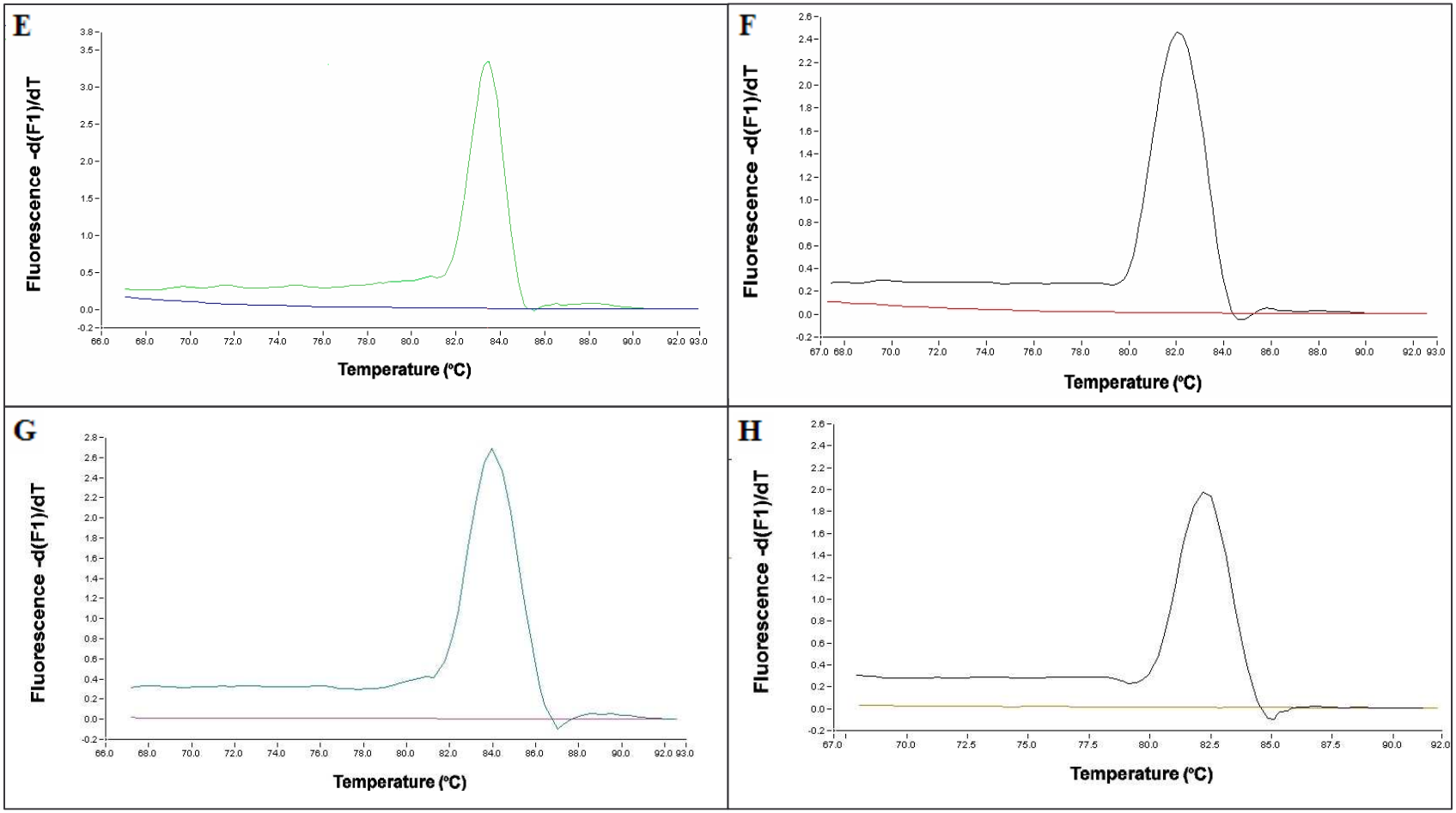

Fig. 3.5 …Continued

3.8 GENERATION OF RELATIVE STANDARD CURVES

The standard curve produces a linear relationship between C_p and initial amounts of cDNA. Standard curves were generated by quantifying a serially diluted cDNA standard in duplicate in each real-time PCR run (Fig. 3.6 and APPENDIX V). Real-time PCR efficiencies were calculated from the gradients generated by the LightCycler Software, Version 3.5. The corresponding PCR efficiency (*E*) of one cycle in the exponential phase was calculated using the equation: Efficiency (*E*) = $10^{-1/\text{slope}}$ - 1. PCR efficiency of the investigated transcripts are presented in Table 3.5. A high degree of efficiency ranging from 1.76 to 2.24 was achieved. E_{lipA} could not be determined as a suitable standard curve could not be generated due to very low expression levels of *lipA*. E_{alkR} yielded an efficiency of 2.24, exceeding the maximum permissible efficiency of 2 (*E* = 100 %), indicating an inappropriately optimized assay and/or poor specificity of primer pairs. Correlation coefficient squared (r^2) of 0.98 or greater indicates a stable and reliable assay (Nolan *et al*., 2006). All generated standard curves illustrated high linearity with r^2 values of 1.00 over three orders of magnitude (APPENDIX V).

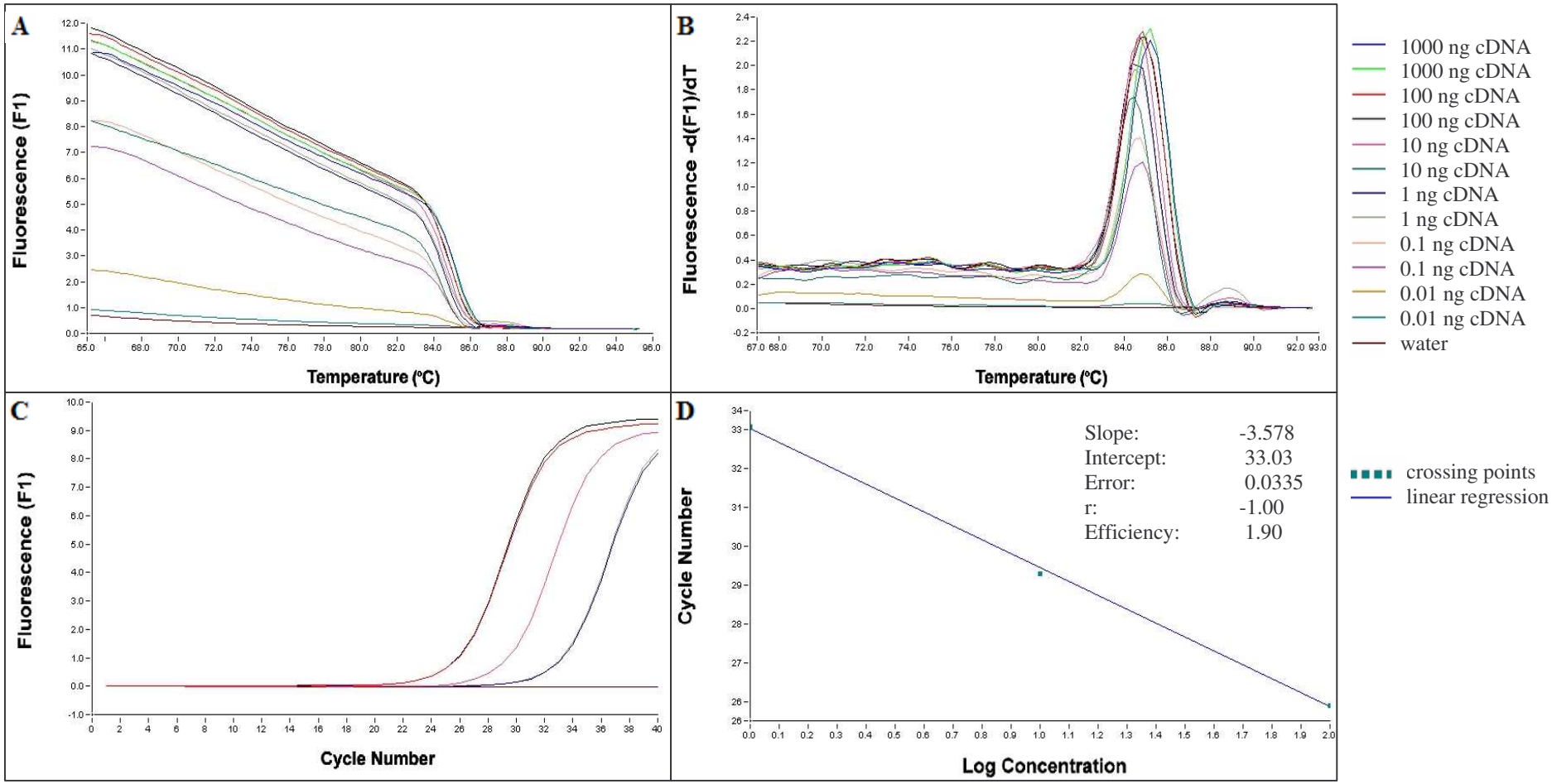

Fig. 3.6 Representative standard curve assay of *rubA*. **(A)** Melting curve analysis. **(B)** Melting peak analysis. **(C)** Amplification curve. **(D)** Standard curve constructed on the basis of sample dilution factors and the corresponding C_p values. PCR efficiency was estimated through the linear regression of the dilution curve with a correlation coefficient squared (r^2) of 1.00. The error values are the mean squared errors calculated by the LightCycler Software. Gradient and efficiency were -3.578 and 1.90, respectively.

Table 3.5 Real-time PCR efficiencies and standard curve gradients of target genes

Target gene	Efficiency (*E*)	Gradient
16S rRNA	1.83	-3.798
alkM	1.92	-3.524
***alk*R**	2.24	-2.867
rubA	1.90	-3.578
estB	1.89	-3.630
lipB	1.76	-4.092
xcpR	1.86	-3.692

3.9 STATISTICAL ANALYSIS OF REAL-TIME PCR DATA AND RELATIVE QUANTIFICATION OF GENE EXPRESSION

Quantification of target gene expression levels was investigated using the following sample sizes: $n = 7$ for LT_1, $n = 7$ for LT_1A, and $n = 8$ for V_2. Sample size of $n = 7$ for both LT_1 and LT_1A is in consequence of the omission of LT_1 - day 5 and LT_1A - day 10 samples due to poor cDNA quality.

Target gene analysis involved the quantification of gene expression, generation of an expression profile, descriptive statistics and melting curve analysis. Gene expression was quantified relatively based on the relative expression of the target gene versus a reference gene, using the Pfaffl model with the aid of Relative Expression Software Tool - XL (REST-XL) - Version 2. REST-XL uses the Pairwise Fixed Reallocation Randomization Test to calculate significance of the obtained result and also indicates whether the

reference gene used is suitable for normalization. The relative expression ratio was computed on the basis of the actual *E* value generated from the standard curve slopes, and not the static *E* value of 2.

Crossing point (C_p) values used in the quantification procedure are shown in (APPENDIX VI). The C_p values that were generated by samples that produced primer dimers and/or multiple products were regarded as invalid. For the generation of an expression profile, C_p data was converted to the linear form 2^{-Cp} (APPENDIX VI), and plotted against sampling time. The extent of C_p variation can be difficult to evaluate, as a result of its exponential scale. Therefore, descriptive statistics such as the sample means, minimal (Min) and maximal (Max) values, standard deviation (SD), and coefficient of variance expressed as a percentage (CV%), of the derived C_p values were computed for each investigated gene to determine intra-sample variation (Tables 3.6). Since SD is derived from C_p values of the investigated target genes, a SD value of 1 signifies a starting template variation by the factor 2 (Pfaffl *et al*., 2004).

Table 3.6 Descriptive statistics and variation data output for target genes of LT_1, LT_1A, and V_2 samples

Factor	16S rRNA	*rubA*	*alkM*	*alkR*	*lipA*	*lipB*	*xcpR*	*estB*
LT_1								
n	7	7	7	7	7	7	7	7
Sample means	12.27	25.46	32.14	39.48	-	40.94	34.58	-
Min	10.32	23.02	29.7	35.46	-	37.08	31.98	-
Max	13.56	28.55	35.57	44.50	-	46.30	37.90	-
SD	1.27	3.55	4.06	10.11	-	10.27	3.63	-
CV(%)	10.31	13.92	12.65	25.60	-	25.10	10.49	-
LT_1A								
n	7	7	7	7	7	7	7	7
Sample means	10.85	26.36	33.62	39.86	-	43.65	36.28	-
Min	8.575	24.04	32.05	36.54	-	40.08	34.94	-
Max	12.86	28.08	35.04	46.00	-	46.66	40.67	-
SD	2.33	2.24	1.39	10.18	-	7.56	4.23	-
CV(%)	21.52	8.49	4.14	25.55	-	17.31	11.66	-
V_2								
n	8	8	8	8	8	8	8	8
Sample means	12.29	29.09	*	*	-	39.76	*	31.81
Min	9.542	23.84	*	*	-	37.70	*	29.34
Max	16.86	34.50	*	*	-	41.23	*	33.58
SD	6.61	10.48	*	*	-	1.41	*	2.38
CV(%)	53.81	36.02	*	*	-	3.55	*	7.47

- Invalid C_p values due to nonspecific binding

* Invalid C_p values due to multiple product formation

3.9.1 Analysis of 16S rRNA gene expression

3.9.1.1 Expression profile of 16S rRNA gene

The gene expression profile was determined by comparing 2^{-Cp} values in response to sampling time. The 16S rRNA gene was not stably expressed in all three isolates at determined sampling times for the duration of the incubation period with SD values of 1.27, 2.33 and 6.61 for LT_1, LT_1A, and V_2 isolates, respectively (Tables 3.6). The 16S rRNA gene was most stably expressed in LT_1 samples and showed the lowest degree of intra-sample variation based on SD and CV% of C_p (Table 3.6). No apparent gene expression trend was observed (Fig. 3.7).

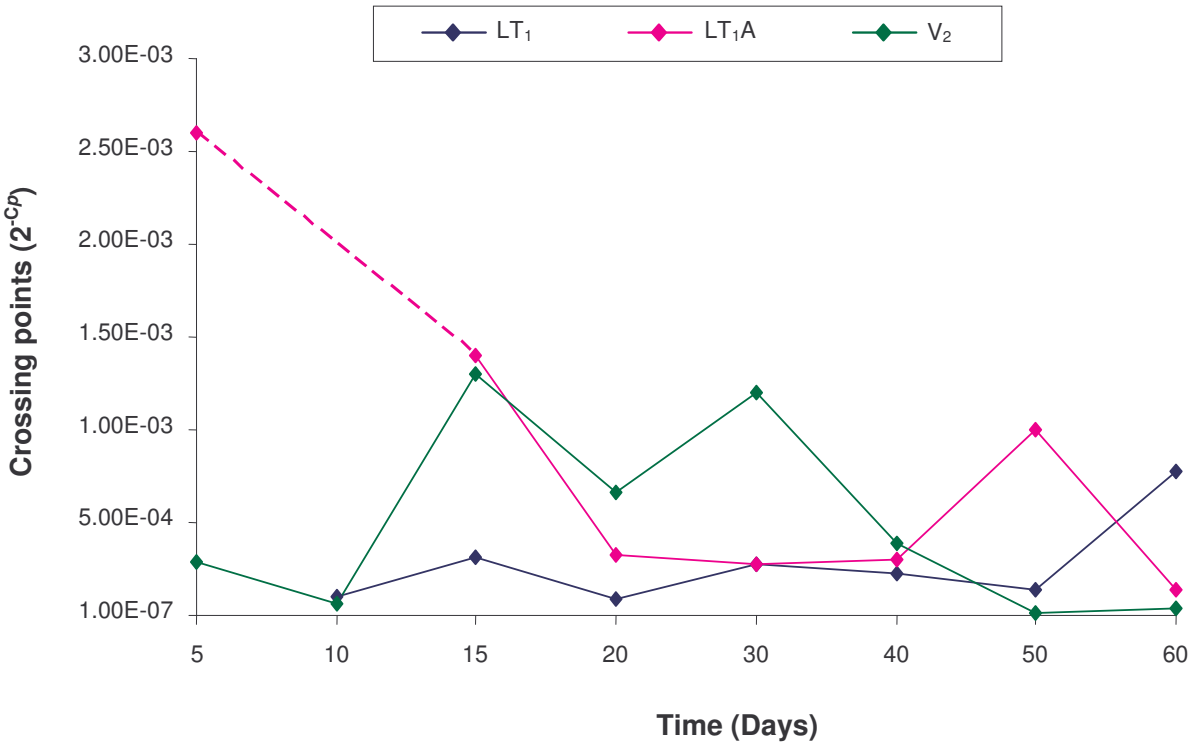

Fig. 3.7 Expression profile of 16S rRNA gene of *A. calcoaceticus* isolates LT_1, LT_1A, and V_2.

3.9.1.2 Randomization test results for 16S rRNA gene (not normalized by a reference gene)

In relation to 16S rRNA gene of LT_1 samples, 16S rRNA gene was up-regulated by the factor 2.36 in LT_1A isolates and down-regulated by the factor 1.013 in V_2 isolates. Expression of the 16S rRNA gene of LT_1A and V_2 was not significantly different from 16S rRNA of LT_1 with *p* values of 0.9835 and 0.072, respectively. Hence, 16S rRNA presented a suitable reference gene for normalization during relative quantification, demonstrating an accepted level of gene expression variability.

3.9.1.3 Melting peak analysis of 16S rRNA gene

Melting peak analysis performed revealed single, sharply defined peaks for all LT_1, LT_1A, and V_2 samples that were investigated. A representative melting peak analysis of 16S rRNA gene showing the amplification of LT_1 samples is illustrated in Fig. 3.7. A single amplification product of projected T_m was achieved (Table 3.4). No primer dimerisation or non-specific binding was observed in the investigated samples of the three isolates for the applied number of cycles.

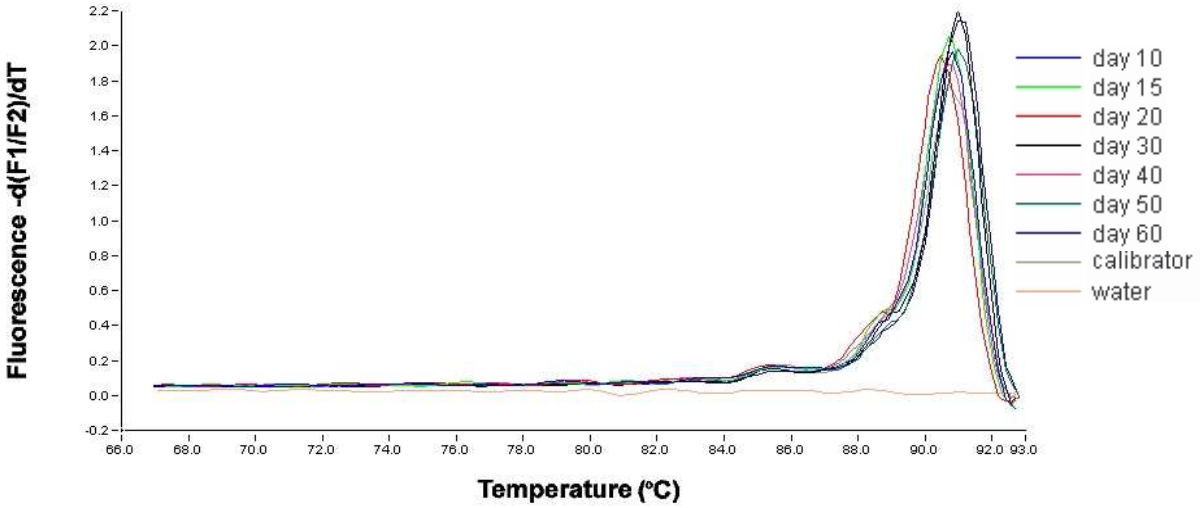

Fig. 3.8 Representative melting peak analysis of 16S rRNA gene of LT_1 samples.

3.9.2 Analysis of *rubA* expression

3.9.2.1 Expression profile of *rubA*

The *rubA* gene was expressed in all three isolates. LT_1 and V_2 samples exhibited maximum *rubA* expression during the initial stages of incubation with expression levels declining as incubation time progressed (Fig. 3.9). An unexpected increase in *rubA* expression was observed for LT_1 at day 60. However, due to the study culminating at day 60, no further observations or assumptions could be made regarding *rubA* expression subsequent to day 60.

The *rubA* gene of LT_1A samples illustrated a contrasting expression trend in relation to LT_1 and V_2 samples with expression levels peaking at day 30, midway through the study (Fig. 3.9). Standard deviation (SD) of 3.55, 2.24, and 10.48 and CV% of 10.31, 8.49, and

36.02 for LT_1, LT_1A, and V_2, respectively (Table 3.6), indicated a high degree of intra-sample variation in C_p. LT_1A showed the lowest intra-sample variation among the three isolates.

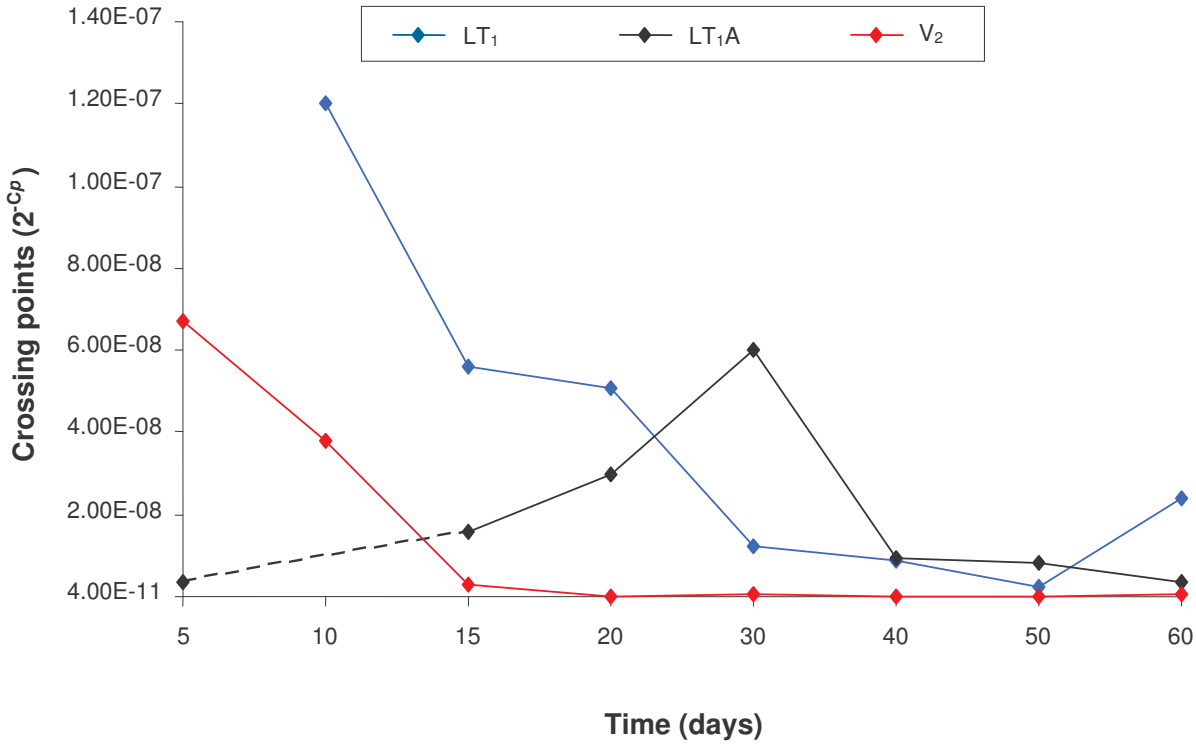

Fig. 3.9 Expression profile of *rubA* of *A. calcoaceticus* isolates LT_1, LT_1A, and V_2.

3.9.2.2 Randomization test results for *rubA* (normalized by reference gene)

In comparison to the expression levels of *rubA* of LT_1, *rubA* of LT_1A and V_2 was down-regulated by the factor 4.206 and 10.115, respectively. Despite the down regulation, expression levels for *rubA* of LT_1A and V_2 were not significantly different from *rubA* of LT_1 with *p* values of 0.0865 and 0.066, respectively.

3.9.2.3 Melting peak analysis of *rubA*

Melting peak analysis of *rubA* for LT_1, LT_1A and V_2 samples revealed a single product of T_m 85.0366°C (Table 3.4). A representative melting peak analysis of *rubA* showing the amplification of LT_1A samples is illustrated in Fig. 3.10. No primer dimerisation was observed in the negative control for the applied number of cycles, highlighting the specificity of primers for the target sequence. Non-specific binding was not observed during *rubA* amplification of LT_1, LT_1A and V_2 samples.

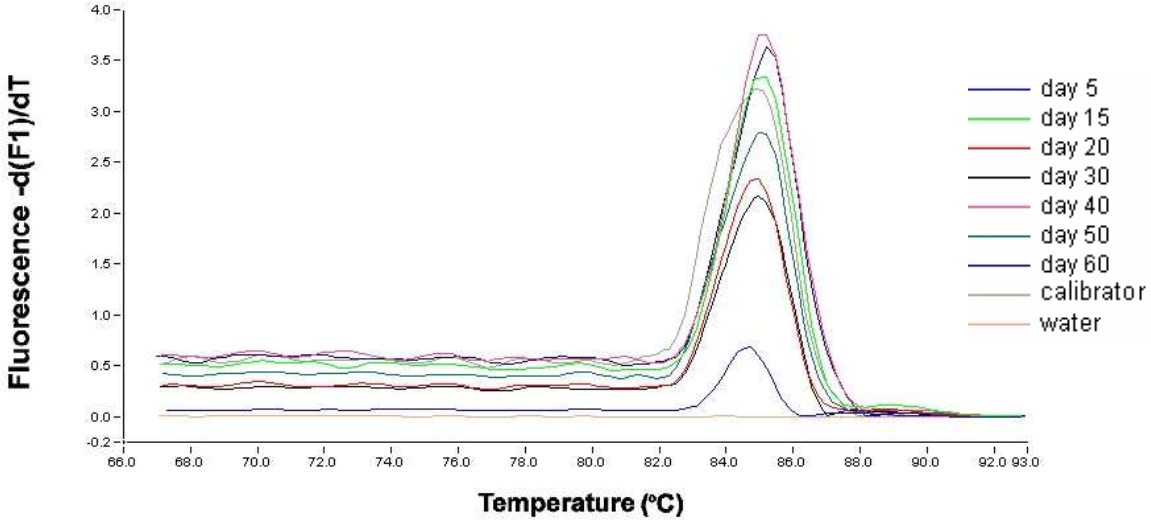

Fig. 3.10 Representative melting peak analysis of *rubA* of LT_1A samples.

3.9.3 Analysis of *alkM* expression

3.9.3.1 Expression profile of *alkM*

The *alkM* gene expression levels of LT_1 were highest at day 10 and gradually declined as incubation time advanced. However, there was a sudden increase in *alkM* expression at day 60 (Fig. 3.11). The expression trend observed for *alkM* of LT_1 samples was comparable to that demonstrated by *rubA* (Fig. 3.9). For *alkM* of LT_1A, expression levels were lower during the initial days of incubation, gradually increasing towards day 40 after which expression levels declined again (Fig. 3.11).

Despite variation in *alkM* expression levels, LT_1A samples displayed a low degree of intra-sample variation in C_p with SD and CV% of 1.39 and 4.14, respectively. LT_1 samples, however, showed a higher degree of intra-sample variation in C_p with SD and CV% of 4.06 and 12.65, respectively (Table 3.6). An expression profile could not be generated for *alkM* of V_2 due to multiple product formation and invalidity of C_p values as a consequence thereof.

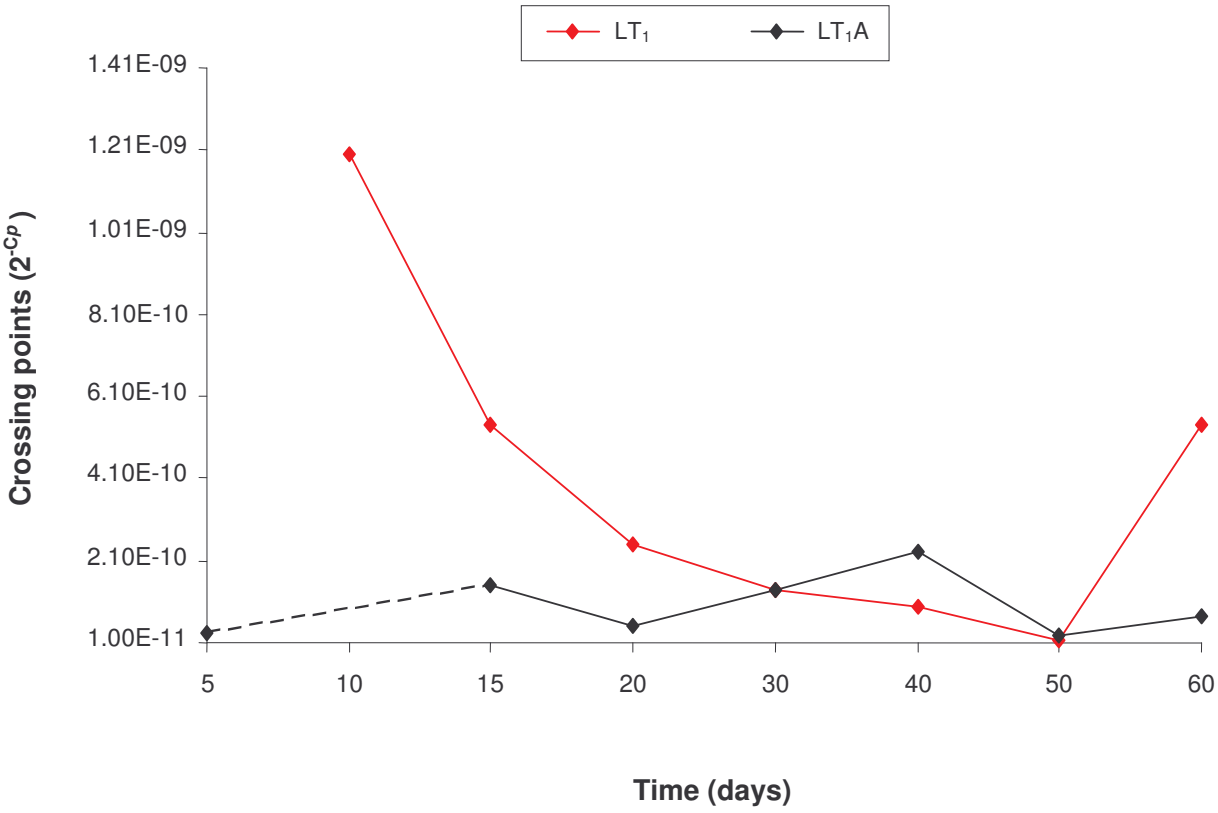

Fig. 3.11 Expression profile of *alkM* of *A. calcoaceticus* isolates LT_1 and LT_1A.

3.9.3.2 Randomization test results for *alkM* (normalized by reference gene)

Target gene *alkM* of LT_1A was down-regulated in comparison to *alkM* of LT_1 by the factor 6.221. The *alkM* gene of LT_1A was found to be significantly different from *alkM* of LT_1 with a *p* value of 0.0425. Expression levels of *alkM* for V_2 samples could not be quantified as a result of multiple product formation.

3.9.3.3 Melting curve and melting peak analysis of *alkM*

Melting curve and melting peak analysis of *alkM* of LT_1 and LT_1A (Fig. 3.11 A and B), revealed the formation of a single amplification product (*alkM1*) of the projected melting temperature (T_m = 80.3645°C) throughout the incubation period. However, for *alkM* of V_2 samples, the formation of a distinctive second product (*alkM2*) exhibiting a much higher T_m exceeding 92°C was evident between 20 and 50 days of incubation (Fig. 3.13 A and B). Amplification of *alkM1* and *alkM2* genes of V_2 samples was repeated and results were highly reproducible.

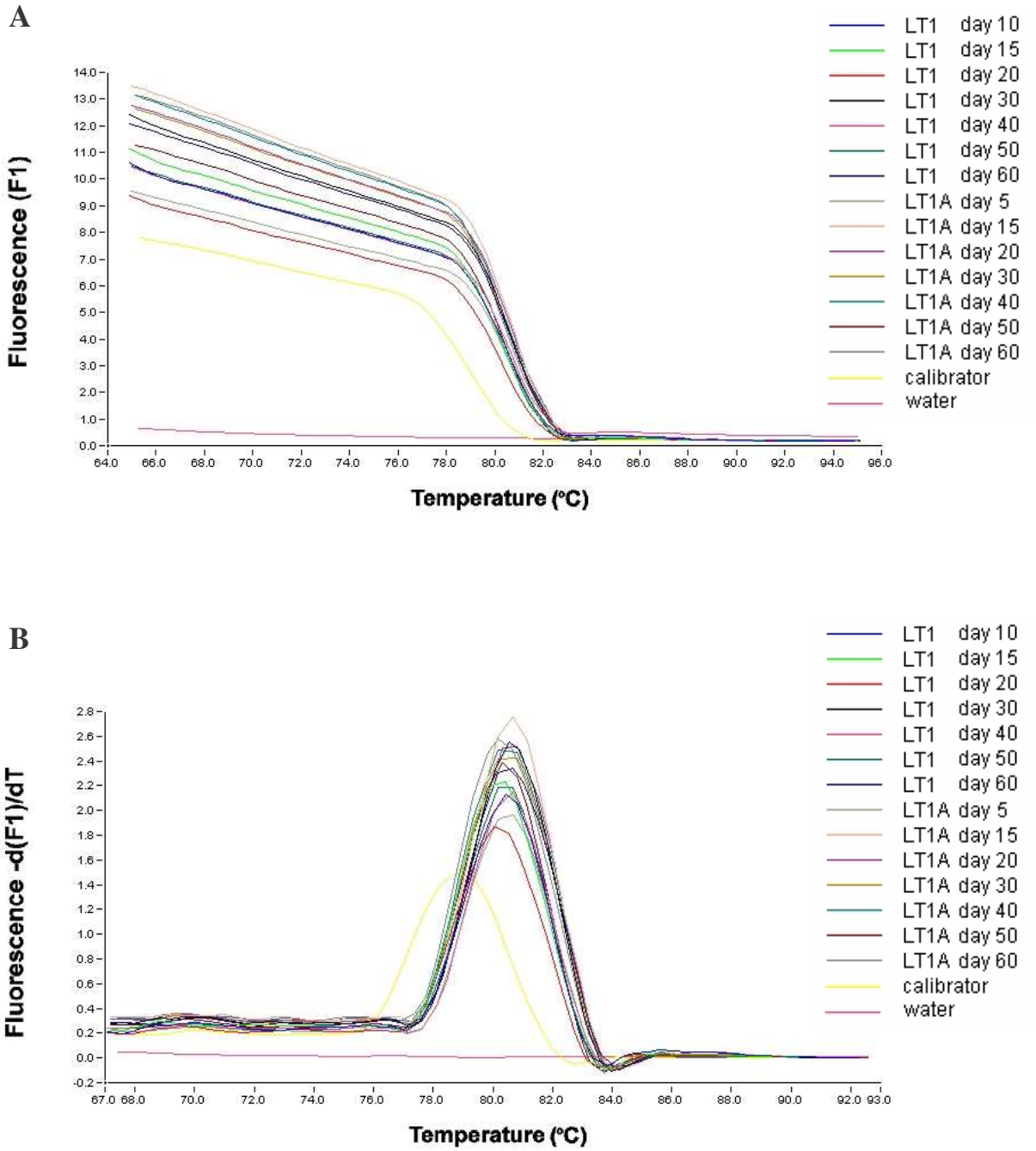

Fig. 3.12 Melting curve and melting peak analysis of *alkM* of LT_1 and LT_1A samples. **(A)** Melting curve analysis determined by fluorescence (F1), and **(B)**, melting peak analysis determined by plotting the negative derivative of fluorescence [-d(F1)/dT] of *alkM*.

A

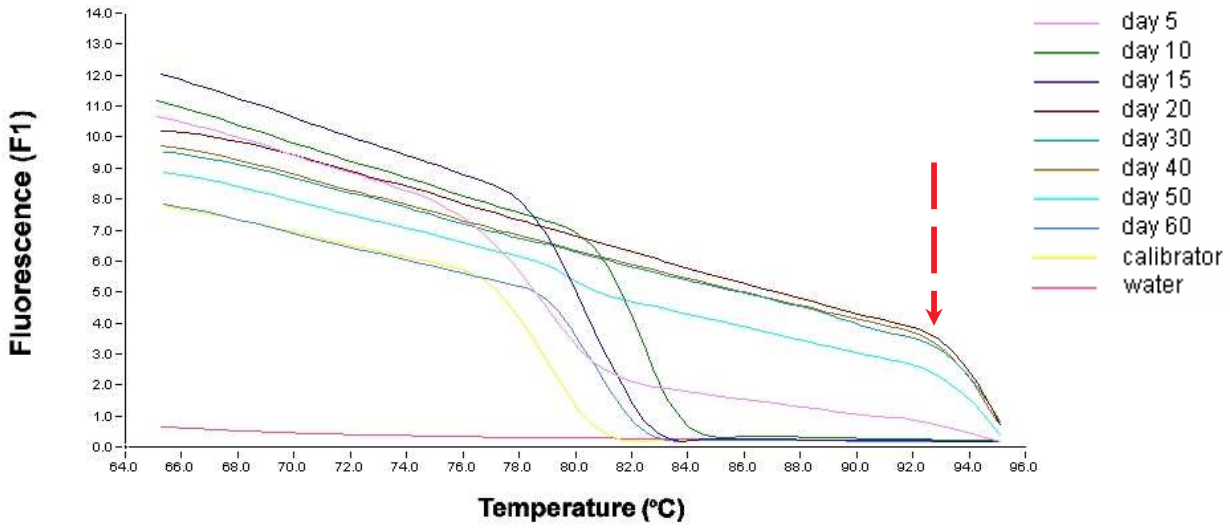

B

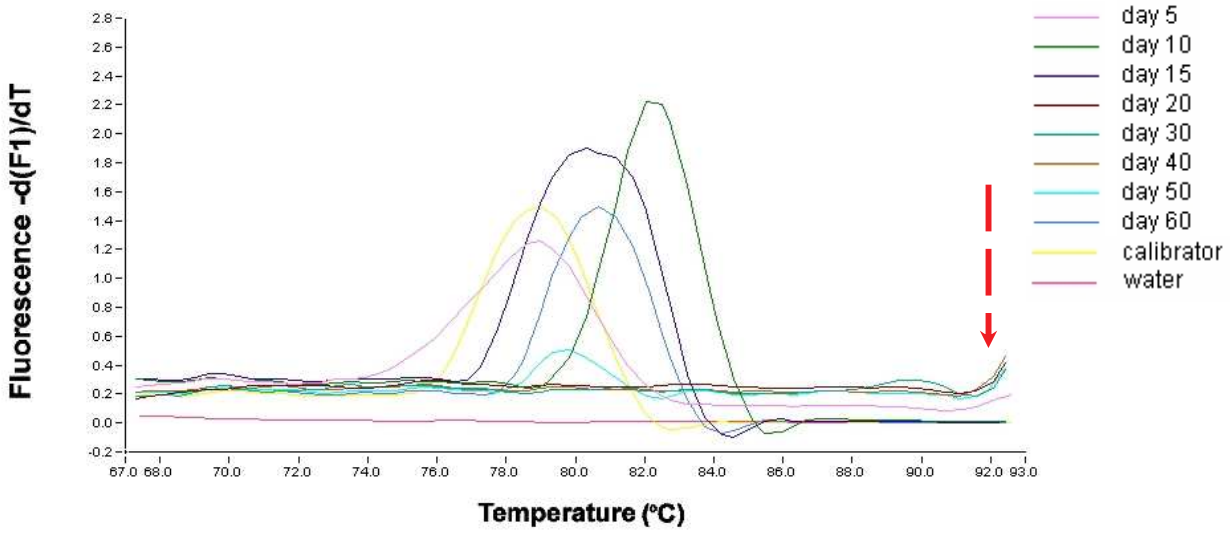

Fig. 3.13 Melting curve and melting peak analysis of *alkM* of V_2 samples. (A) Melting curve analysis determined by fluorescence (F1), and **(B)**, melting peak analysis determined by plotting the negative derivative of fluorescence [-d(F1)/dT] of *alkM*. Formation of an additional amplification product (*alkM2*) is indicated by the red coloured arrow.

3.9.3.4 Validation of *alkM1* and *alkM2* amplicons by agarose gel electrophoresis

Electrophoresis of *alkM1* amplicons of LT_1A on 2% (wt/vol) agarose gel confirmed the presence of the anticipated product of 189 bp from day 5 to day 60 (Fig. 3.13 A). No product or primer dimers were detected in the negative control, reiterating the specificity of primer pairs.

Electrophoresed *alkM1* and *alkM2* amplicons of V_2 samples (Fig. 3.14 B), revealed the expected product (*alkM1*) of 189 bp for the day 15 sample only. An additional product of 336 bp accompanied by ancillary bands, was evident from day 20 to day 50. No amplification products were detected for days 5, 10, and 60, albeit, melting peak analysis of *alkM* of V_2 samples indicated positive peak formations for the aforementioned sampling days (Fig. 3.13 B). Peak formations resulted from amplifications occurring very late in the real-time PCR reaction with non-defined C_p values of > 46.00 in a 50 cycle amplification segment (APPENDIX VI). These findings are suggestive of a false-positive result and such peaks are deemed invalid.

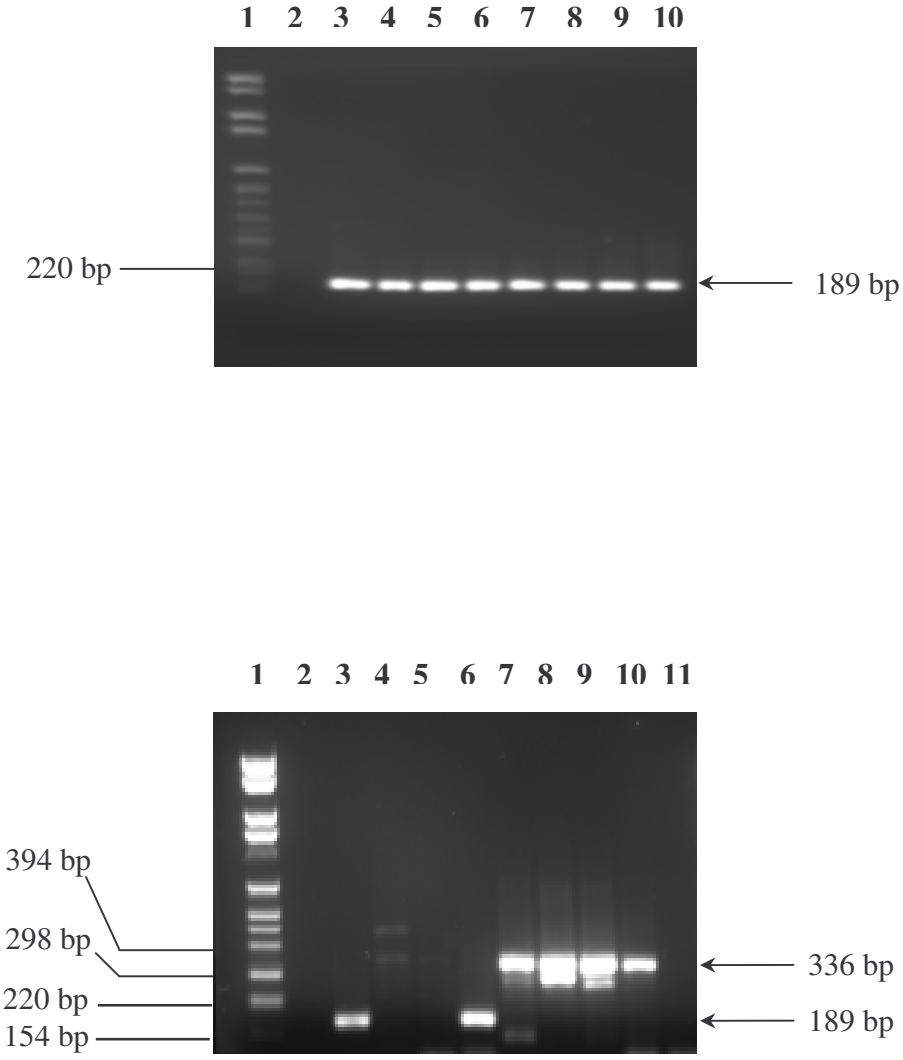

Fig. 3.14 Validation of *alkM* amplicons by 2% (wt/vol) agarose gel electrophoresis. **(A)** Electrophoresed *alkM1* amplicons of LT_1A. **Lanes 1**, Molecular weight marker IV (Roche Diagnostics); **2**, negative control (no cDNA); **3**, positive control (calibrator); **4 - 1o**, day 5 to day 60, respectively. **(B)** Electrophoresed *alkM1* and *alkM2* gene amplicons of V_2 samples. **Lanes 1**, Molecular weight marker IV (Roche Diagnostics); **2**, negative control (no cDNA); **3**, positive control (calibrator); **4 - 11**, days 5 to 60, respectively.

3.9.3.5 Sequencing and alignment of *alkM1* and *alkM2* amplicons

The *alkM* amplification products of the V_2 - day 15 sample, V_2 - day 20 sample and calibrator (LT_1 pooled cDNA) were sequenced by Inqaba Biotech (South Africa). Sequences of *alkM1* of V_2 - day 15 sample and calibrator cDNA (LT_1) were and aligned. Partial sequence alignment (Fig. 3.15) showed 100% homogeneity of the two sequences. The *alkM* gene of LT_1 samples is therefore analogous to *alkM1* of V_2. Sequencing of *alkM2* of V_2 - day 20 sample proved to be unsuccessful.

```
V2-15   1    ATTCACGTCTTGTGAAGAGTTTTATTCCACTGCAATATGCTGCAAATGTTTATGCATGTT
             ||||||||||||||||||||||||||||||||||||||||||||||||||||||||||||
LT1     1    ATTCACGTCTTGTGAAGAGTTTTATTCCACTGCAATATGCTGCAAATGTTTATGCATGTT

V2-15   61   ATTTAACAAGCCGTAAAACCACGTCATTCATTGATAAAATTTTGCTCGGTGTTTCGATG
             ||||||||||||||||||||||||||||||||||||||||||||||||||||||||||||
LT1     61   ATTTAACAAGCCGTAAAACCACGTCATTCATTGATAAAATTTTGCTCGGTGTTTCGATG
```

Fig. 3.15 Partial sequence alignment of *alkM1* amplicons.

3.9.4 Analysis of *alkR* expression

3.9.4.1 Expression profile of *alkR*

Maximum *alkR* expression levels for LT_1 samples were documented at the onset of the study period. Expression levels declined constantly as incubation time progressed. On the contrary, *alkR* expression levels for LT_1A samples increased steadily with incubation time, exhibiting maximum expression at day 50 before declining at day 60 (Fig. 3.16). A profile of *alkR* expression of V_2 samples could not be illustrated due to multiple product formation and invalid C_p values. LT_1 and LT_1A samples showed equivalently high levels of intra-sample variation with SD values of 10.11 and 10.18, respectively (Table 3.6).

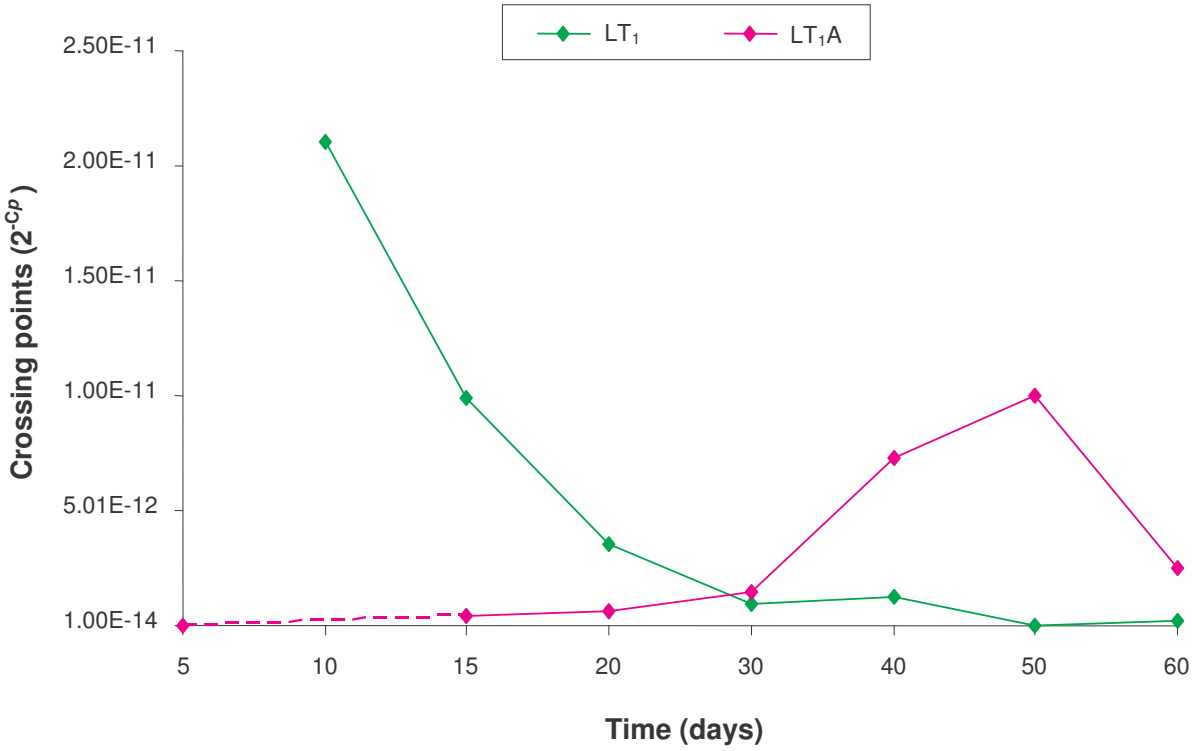

Fig. 3.16 Expression profile of *alkR* of *A. calcoaceticus* isolates LT_1 and LT_1A.

3.9.4.2 Randomization test results for *alkR* (normalized by reference gene)

The *alkR* gene of LT_1A was down-regulated in comparison to *alkR* of LT_1 by the factor 3.203. The *alkR* gene of LT_1A is not significantly different from *alkR* of LT_1 with a *p* value of 0.5095. Gene expression levels of *alkR* of V_2 could not be quantified on account of multiple product formation and C_p values generated thereof are considered invalid.

3.9.4.3 Melting peak analysis of *alkR*

Melting peak analysis of *alkR* of LT_1 and LT_1A (Fig. 3.17A), verified the presence of a single amplification product of expected melting temperature (T_m = 79.3354°C) at each sampling time. However, for *alkR* of V_2 samples, the presence of a second product exhibiting a higher T_m was evident (Fig. 3.17 B). The expected amplification product (*alkR1*) was only observed at days 30, 50, and 60. However, there was shift in T_m of approximately 2^oC for day 30 and day 60 samples. Despite the disparity in T_m, the amplification product size was identical to that of day 50. Day 5, 10, and 15 samples showed the formation of an additional product (*alkR2*) with T_m exceeding 84^oC. No *alkR* amplification occurred for day 20 and day 40 samples. The *alkR1* gene of V_2 is analogous to *alkR* of LT_1 and LT_1A on the basis of T_m and amplification product size.

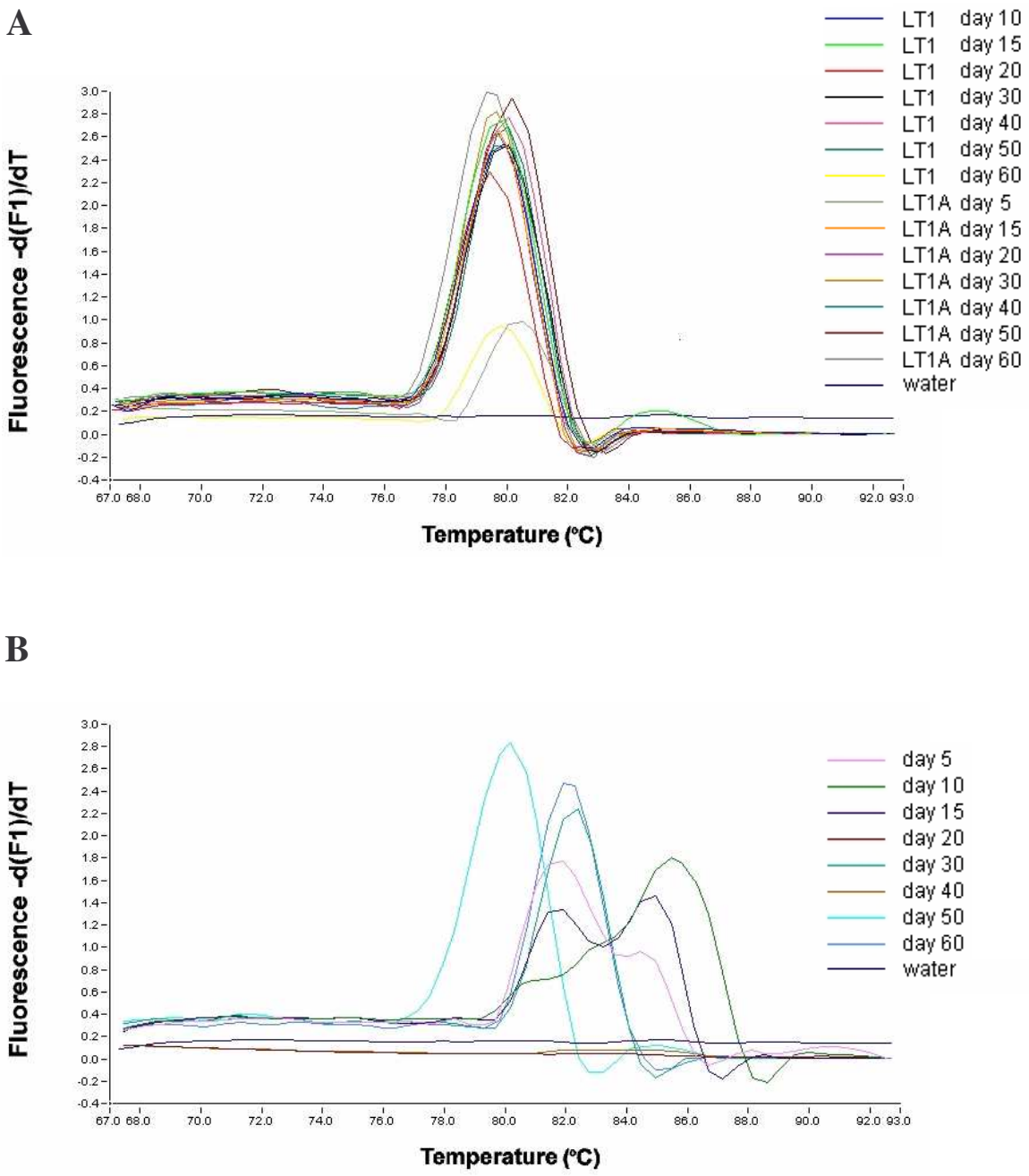

Fig. 3.17 Melting peak analysis of *alkR*. **(A)** Melting peaks of *alkR* of LT_1 and LT_1A samples and **(B)** V_2, determined by plotting the negative derivative of fluorescence [-d(F1)/dT].

3.9.5 Analysis of *estB* expression

3.9.5.1 Expression profile of *estB*

The expression trend observed for *estB* of V_2 samples showed increasing activity from day 5 to day 10, with maximum expression at day 10. Expression levels declined noticeably after day 10 and remained fairly constant thereafter. No *estB* expression profile could be generated for LT_1 and LT_1A samples due to invalid C_p values generated from primer dimerisation and nonspecific binding. Intra-sample variation with SD and CV% of 2.38 and 7.47 indicated a moderate regulation of *estB* amongst V_2 samples.

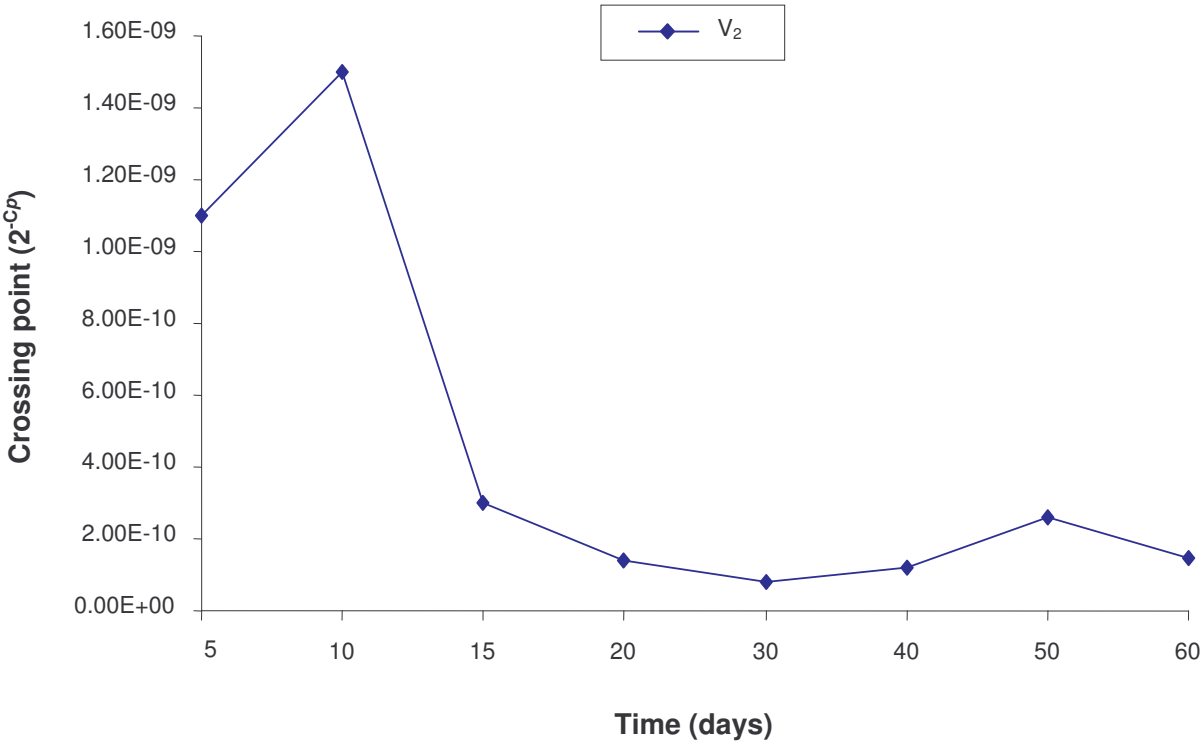

Fig. 3.18 Expression profile of *estB* of *A. calcoaceticus* isolate V_2.

3.9.5.2 Melting peak analysis of *estB*

Melting peak analysis of *estB* of LT_1 and LT_1A indicated primer dimerisation and nonspecific binding (Fig. 3.19 A). Positive peak formations at the desired T_m were observed for samples LT_1 - days 10, 20, 50, and samples LT_1A - days 30 and 60. However, such peaks are a consequence of amplification occurring very late in the PCR with C_p values > 51.00 in a 55 cycle amplification segment (APPENDIX VI). Very high C_p values and melting peaks resulting thereof are considered invalid and are indicative of false-positive results. A lack of target-specific amplification of *estB* in LT_1 and LT_1A samples, suggest either the absence of *estB* expression or extremely low levels of *estB* expression.

In contrast, *estB* activity was detected in all V_2 samples (Fig. 3.19 B). All melting peaks were narrow, well defined and occurred at the projected T_m of 82.8515°C. Peaks were valid as they resulted from low C_p values (APPENDIX VI).

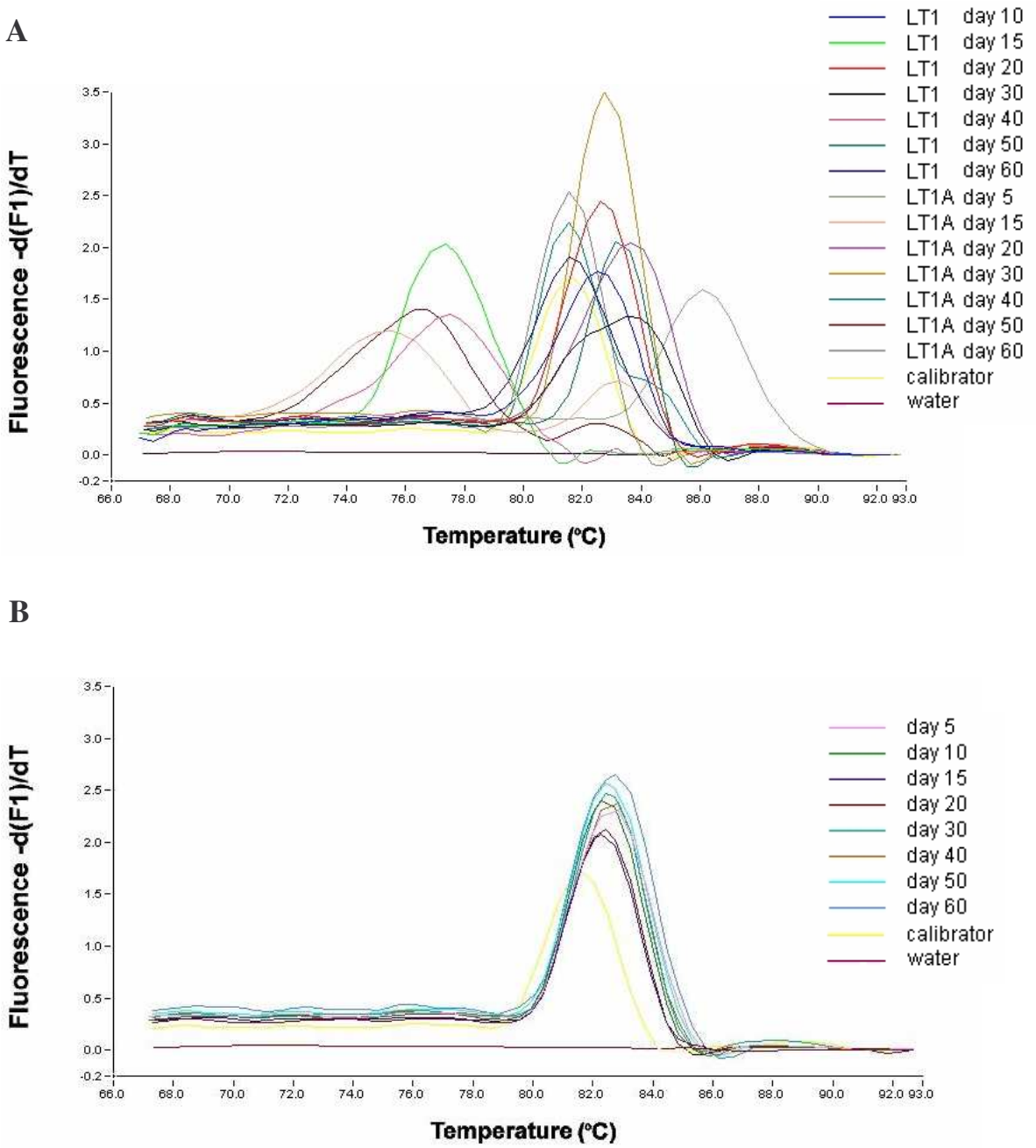

Fig. 3.19 Melting peak analysis of *estB*. **(A)** Melting peak of *estB* of LT_1 and LT_1A samples and **(B)** V_2 samples, determined by plotting the negative derivative of fluorescence [-d(F1)/dT].

3.9.6 Analysis of *lipA* expression

3.9.6.1 Expression profile of *lipA*

An expression profile of *lipA* could not be created for LT_1, LT_1A, and V_2 samples. Several LT_1 and LT_1A samples generated a non-defined C_p value of > 51.00 (APPENDIX VI). C_p values generated for V_2 samples resulted from amplification of primer dimers and could not be used in the generation of the expression profile. Intra-sample variation could also not be determined, as SD and CV% are dependent on C_p. Based on their available C_p values, very low *lipA* activity was detected in of LT_1 and LT_1A samples and no obvious expression trend was observed (APPENDIX VI).

3.9.6.2 Melting peak analysis of *lipA*

Melting peak analysis LT_1 and LT_1A revealed the desired amplification product (T_m = 83.41°C) as well as primer dimerisation and non-specific binding (Fig. 3.20 A). Peaks occurring for samples LT_1 - day 50 and LT_1A - days 5, 20, 50, and 60 have resulted from C_p values of > 51.00 and are representative of false-positive results. Melting peak analysis of V_2 samples confirmed the absence of target-specific amplification; hence, *lipA* was not expressed in V_2 samples (Fig. 3.20 B).

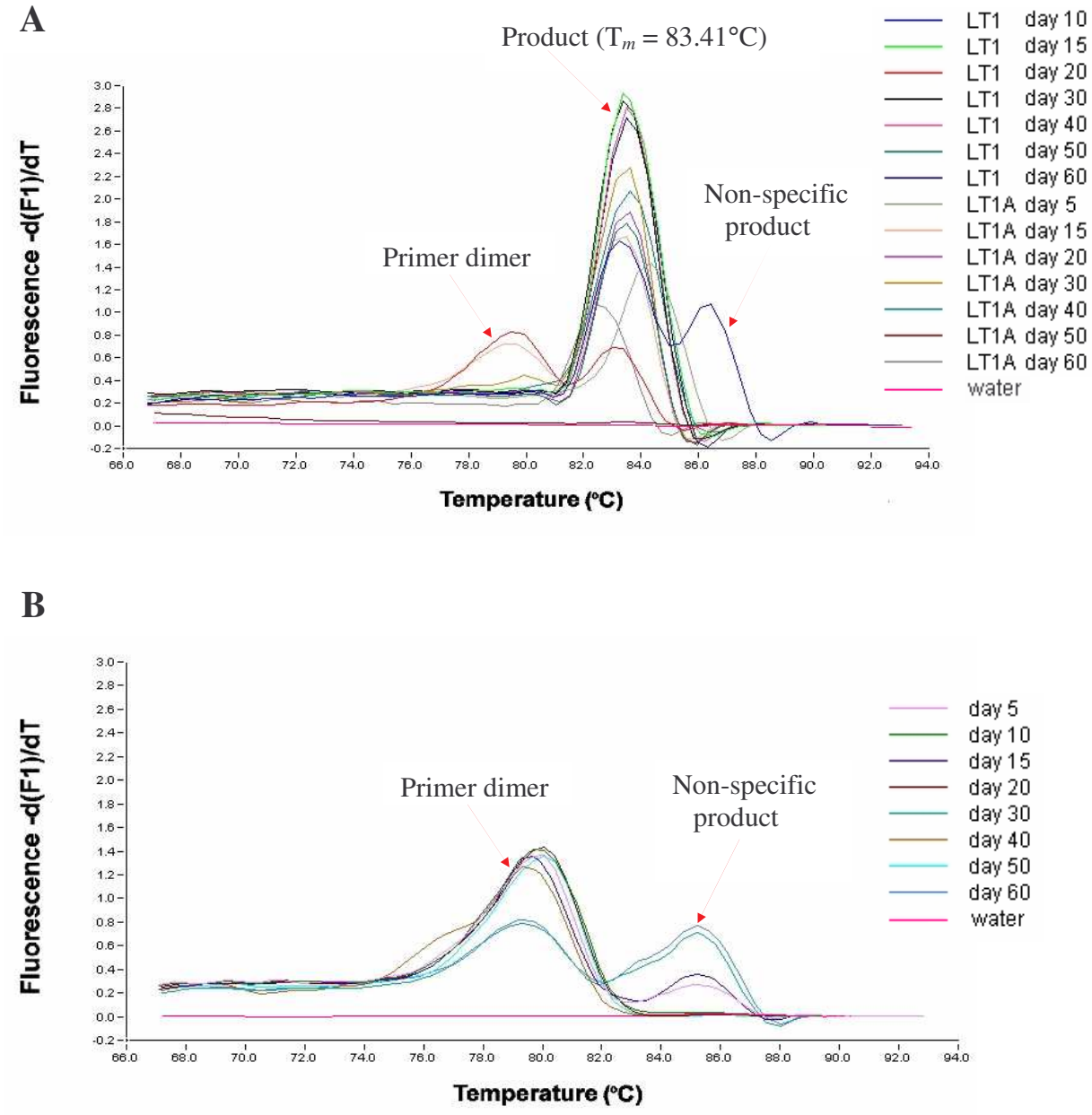

Fig. 3.20 Melting peak analysis of *lipA*. **(A)** Melting peaks of *lipA* of LT_1 and LT_1A samples and **(B)** V_2 samples, determined by plotting the negative derivative of fluorescence [-d(F1)/dT].

3.9.7 Analysis of *lipB* expression

3.9.7.1 Expression profile of *lipB*

The *lipB* gene was expressed in LT_1, LT_1A, and V_2 at all sampling times. Low expression levels of *lipB*, depicted by the high C_p values (APPENDIX VI) were observed among all three isolates. Expression levels increased with incubation time exhibiting maximum expression at day 20 for LT_1 and LT_1A samples and at day 15 for V_2 samples (Fig. 3.21). Thereafter, expression levels declined fairly constantly in V_2 samples, but fluctuated in LT_1 and LT_1A samples as incubation time proceeded. Expression trend observed LT_1 and LT_1A samples were comparable. Expression of *lipB* amongst V_2 samples was moderately constant exhibiting low SD and CV% values of 1.41 and 3.55 respectively, with *lipB* of LT_1 and LT_1A samples showing greater intra-sample variation (Table 3.6).

3.9.7.2 Randomization test results for *lipB* (normalized by reference gene)

In comparison to *lipB* of LT_1, *lipB* of LT_1A was down-regulated by a factor of 10.922 and *lipB* of V_2 was up-regulated by the factor 1.976. The *lipB* gene of LT_1A was significantly different to *lip*B of LT_1 with a *p* value of 0.0495 and *lip*B of V_2 was not significantly different to *lip*B of LT_1 with a *p* value of 0.436.

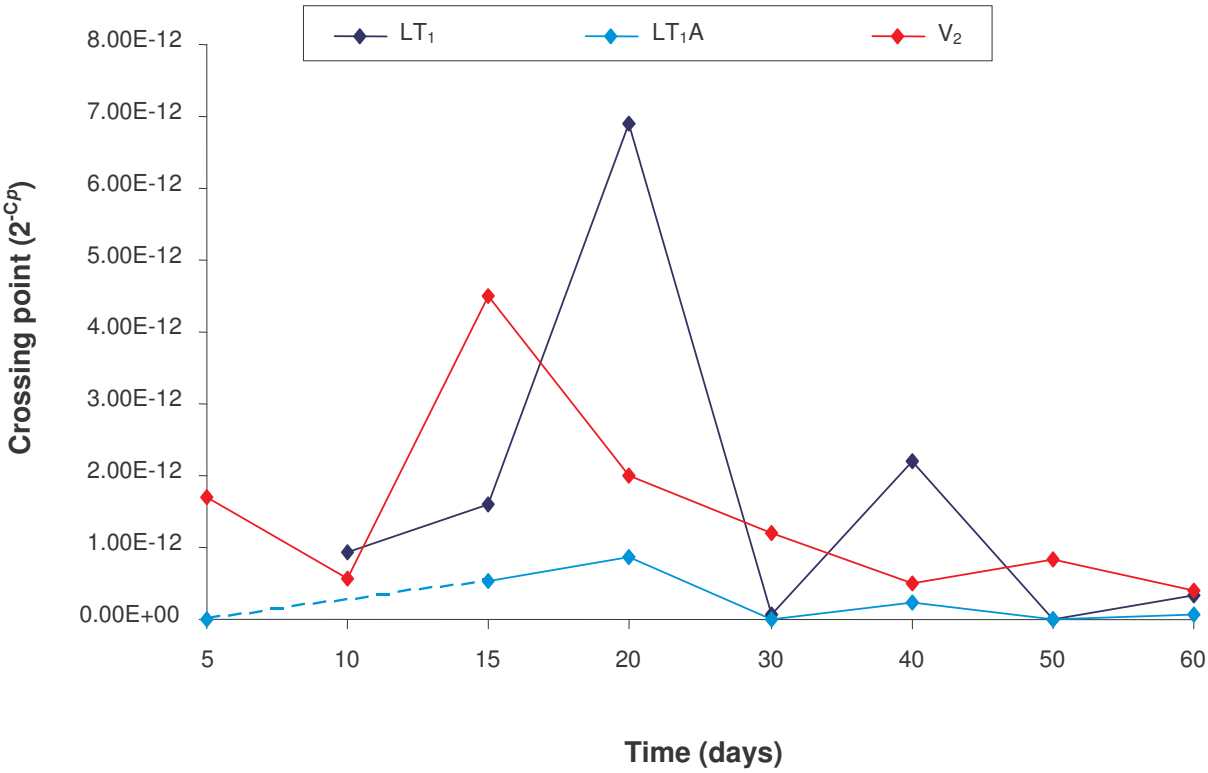

Fig. 3.21 Expression profile of *lipB* of *A. calcoaceticus* isolates LT_1, LT_1A and V_2.

3.9.7.3 Melting peak analysis of *lipB*

A melting peak analysis of *lip*B for LT_1, LT_1A, and V_2 isolates shows the presence of the anticipated amplification product (T_m = 82.3369°C). The *lipB* gene was expressed in all three isolates at every sampling time (Fig. 3.22 A - C). Several peaks were poorly defined exhibiting broader wavelengths, signifying low expression levels.

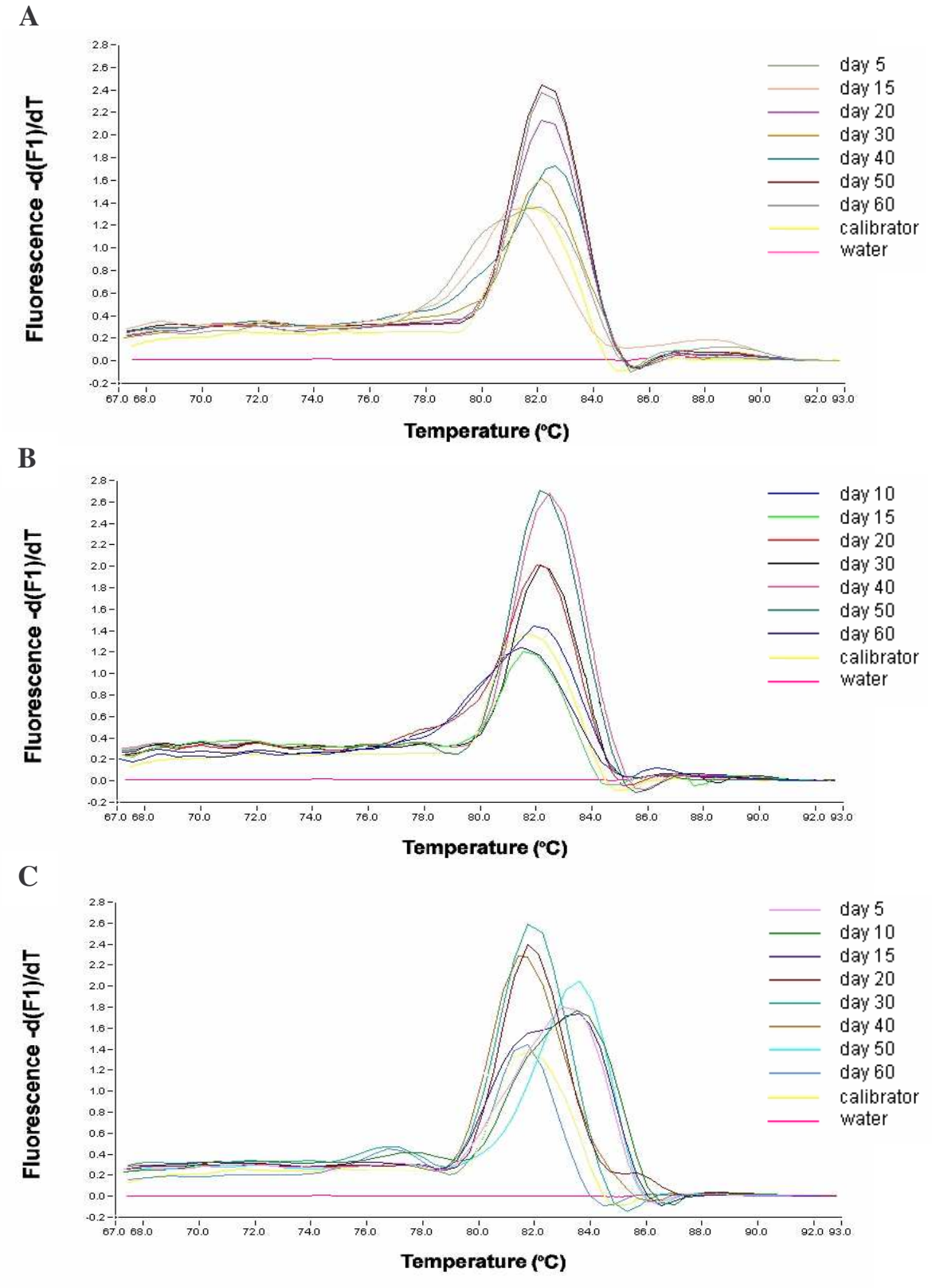

Fig. 3.22 Melting peak analysis of *lipB*. **(A)** Melting peaks of *lipB* of LT_1 **(B)** LT_1A and **(C)** V_2 samples.

3.9.8 Analysis of *xcpR* expression

3.9.8.1 Expression profile of *xcpR*

Expression of *xcpR* of LT_1 samples decreased progressively from day 10 to day 50. In contrast, expression levels of *xcpR* of LT_1A samples increased gradually from day 5, exhibited maximum expression levels at day 40, before subsiding at day 50. Both LT_1 and LT_1A showed an increase in *xcpR* expression levels at day 60 (Fig. 3.23). A comparably high degree of intra-sample variation in *xcpR* expression was observed for LT_1 and LT_1A samples with SD of 3.63 and 4.23, respectively, and CV% of 10.49 and 11.66, respectively (Table 3.6). The expression levels of *xcpR* of V_2 samples could not be illustrated due to multiple product formation.

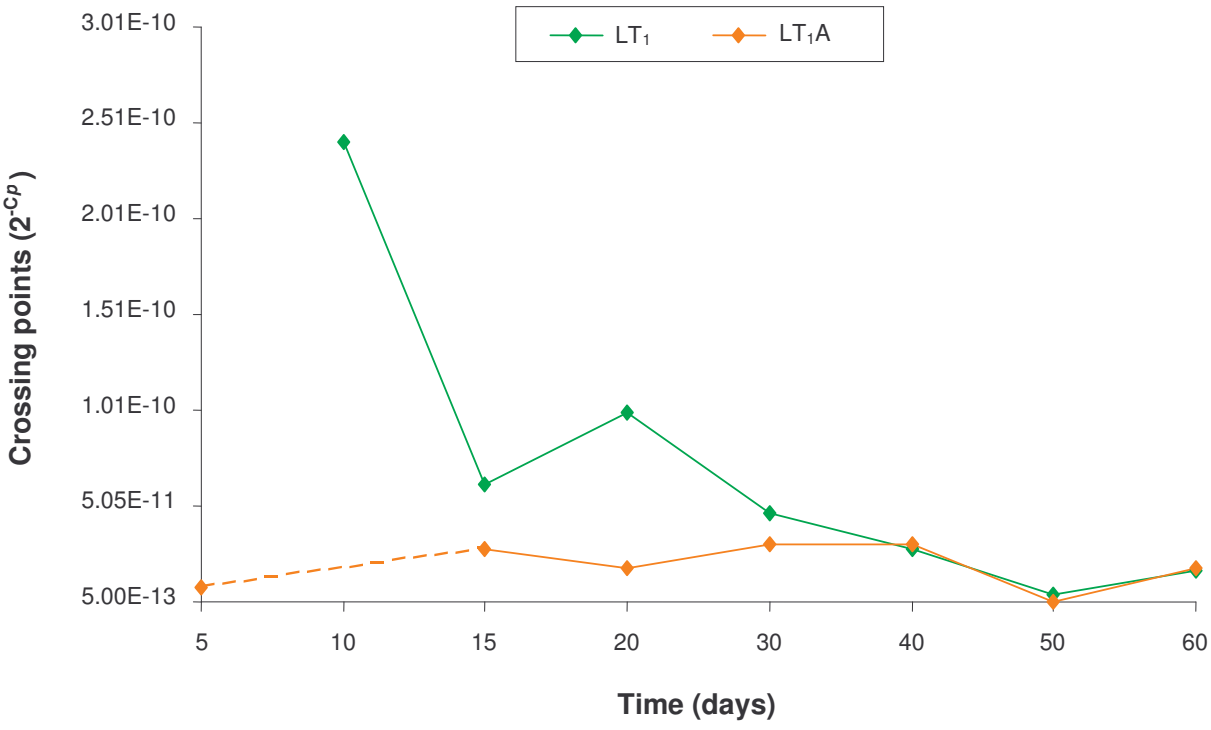

Fig. 3.23 Expression profile of *xcpR* of *A. calcoaceticus* isolates LT_1 and LT_1A.

3.9.8.2 Randomization test results for *xcpR* (normalized by reference gene)

The *xcpR* gene of LT_1A was down-regulated in comparison to *xcp*R gene of LT_1 by the factor 6.767. The *xcpR* gene of LT_1A was not significantly different from *xcpR* of LT_1 with a *p* value of 0.051. Levels of *xcpR* expression of V_2 samples could not be quantified as a result of multiple product formation.

3.9.8.3 Melting peak analysis of *xcpR*

Melting peak analysis of *xcpR* of LT_1 and LT_1A (Fig. 3.24 A), revealed the formation of a single amplification product of expected T_m of 84.0949°C for the duration of the study. However, the presence of additional amplification products, illustrated by three defined peaks, exhibiting higher T_ms were observed for *xcpR* of V_2 samples (Fig. 3.24 B). The amplification of *xcpR* of V_2 samples was repeated for confirmation of results. The results obtained for V_2 samples were highly reproducible yielding multiple products with identical melting temperatures (Fig. 3.24 C).

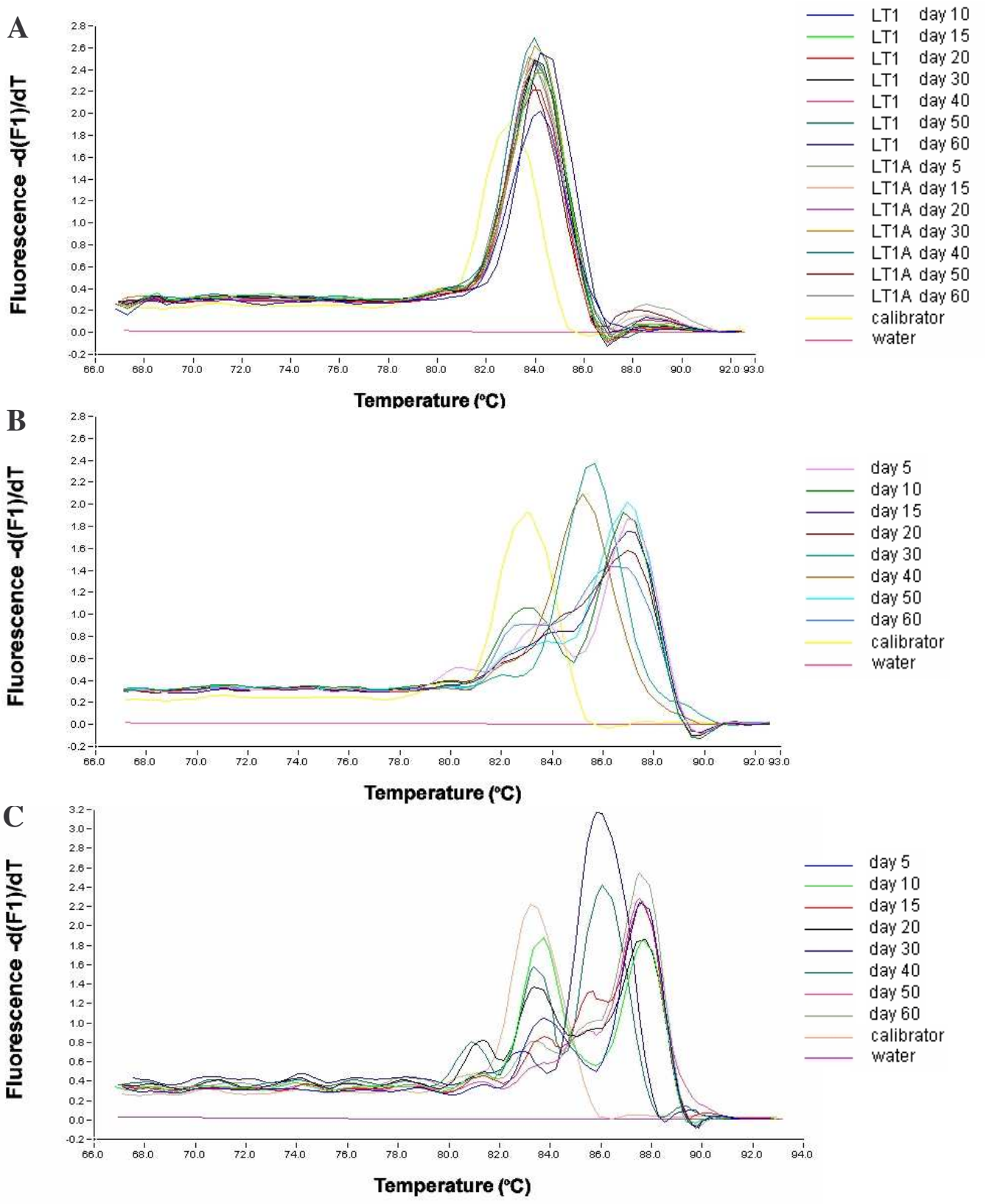

Fig. 3.24 Melting peak analysis of *xcpR*. **(A)** Melting peaks of *xcpR* of LT_1 and LT_1A samples, **(B)** V_2 samples and **(C)** reproduced melting peaks of V_2 samples.

3.8.9.4 Validation of *xcpR* amplicons by agarose gel electrophoresis

Real-time PCR amplification products of *xcpR* of V_2 samples were documented by gel electrophoresis on 2% (wt/vol) agarose, and ethidium bromide staining (Fig. 3.25). The absence of a band in the no-template control indicates the absence of primer dimers, and confirms specificity of the *xcpR* primer pair. The presence of two distinct products was observed. The expected 192 bp product (*xcpR1*) was observed in all samples. The presence of a larger fragment of approximately 500 bp (*xcpR2*) was observed in all samples except on day 30 and day 40.

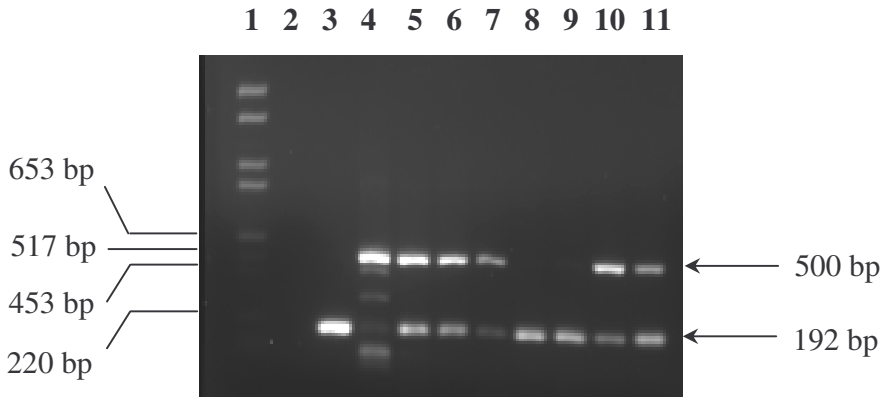

Fig. 3.25 Electrophoresed *xcpR* amplicons of V_2 samples. **Lanes 1** - molecular weight marker VI (Roche Diagnostics); **2** - negative control (no cDNA template); **3** - positive control (calibrator); **4 to 11** - *xcpR* amplicons of 5 days to 60 days samples, respectively.

4. DISCUSSION

Industrialization in the 20th century has resulted in the expulsion of a plethora of deleterious substances into the environment. Substantial amounts of petroleum hydrocarbons are present in water and soil as a result of spills from oil tankers, oil-drilling sites, petroleum refineries and storage facilities, gas stations, factories and leaking pipelines (Marín *et al.,* 1995).

Acinetobacter is the predominant bacterial genus isolated from petroleum-contaminated habitats and has been extensively used in *n*-alkane degradation studies (Asperger and Kleber, 1991). Although the degradation of *n*-alkanes remains a widespread trait among bacteria, there is a dearth of information regarding the regulation of genes encoding alkane utilization (Ratajczak *et al*., 1998).

The present study focused on the diesel degrading capabilities of three *A. calcoaceticus* isolates, LT_1, LT_1A, and V_2, and investigated the genes involved during *n*-alkane degradation. LT_1 and LT_1A were isolated from diesel contaminated soil in a previous study (Singh and Lin, 2008) and were found to be efficient in degrading medium-chain length hydrocarbons, such as diesel. V_2 was previously isolated from car engine oil contaminated soil and emerged as an efficient degrader of long-chain length hydrocarbons (Mandri and Lin, 2007).

During the incubation on diesel, isolates LT_1, LT_1A, and V_2, were each capable of utilizing the carbon source, as was assessed by gravimetric analysis. Gravimetric analysis

was only able to determine the quantitative differences, and not the qualitative differences, in the amount of diesel remaining at predetermined sampling times. Degradation was determined as a percentage of degraded diesel in the investigated samples in relation to the abiotic control sample. The abiotic control sample showed 9.40% diesel reduction after 60 days of incubation (APPENDIX III). This reduction can be attributed to abiotic losses due to the volatile nature of diesel.

Diesel was notably degraded by each of the three isolates during the first 5 days of incubation, where 58.6%, 51.7%, and 48.3% of diesel had been utilized by LT_1, LT_1A, and V_2, respectively (Fig. 3.1; APPENDIX III). These results support the findings of a previous study (Plohl *et al*., 2002) which showed that rapid degradation of medium-chain length alkanes occurred during the first 5 days of incubation. Such levels of degradation may be attributed to the exponential growth phase of the bacterial cells. At the end of the 60 day incubation period, a maximum degradation of 86.2%, 82.8%, and 89.7% of diesel was achieved for LT_1, LT_1A, and V_2, respectively (Fig. 3.1; APPENDIX III). All three isolates displayed comparable efficiency in the overall utilization of diesel as a sole carbon and energy source.

Previous studies conducted on *Acinetobacter* sp. strain ADP1 confirmed that at least five essential genes, namely *rubA, rubB*, *alkM*, *alkR*, and *xcpR*, are required for *n*-alkane utilization (Ratajczak *et al*., 1998). The comprehensive characterization, expression patterns, and quantification of expression, of the aforementioned genes as well as *lipA*, *lipB*, and *estB*, were elucidated in LT_1, LT_1A, and V_2 isolates grown on diesel. A real-

time PCR assay was optimized and validated for each investigated target gene to quantify the level mRNA expression at stipulated sampling times. The required steps implemented for the quantification of target gene expression by real-time PCR constituted both pre-analytical and analytical procedures such as RNA isolation, cDNA synthesis, data acquisition, efficiency determination, normalization, and data analysis. Each of the above mentioned steps were crucial for the accuracy and success of the real-time quantitative PCR assays.

The purity and integrity of the extracted RNA is fundamental for the accurate quantification of mRNA expression levels. In this study, RNA yield was determined spectrophotometrically with an $OD_{260/280}$ ratio. A ratio greater than 1.8 is considered a suitable indicator of good RNA quality (Manchester, 1996; Sambrook *et al*., 1989). LT_1 - day 5 sample, and LT_1A - day 10 samples, generated ratios of 1.30 and 1.50, respectively (Table 3.2), and are indicative of poor RNA quality.

A standardized amount of 1 µg RNA was reverse transcribed into cDNA as the efficiency of reverse transcription is dependent on the total starting concentration of RNA (Stahlberg *et al*., 2004). Validation of cDNA by agarose gel electrophoresis showed that a substandard level of cDNA was present in LT_1 - day 5 sample, and no cDNA was present in LT_1A - day 10 sample (Fig. 3.2). Poor cDNA quality is a corollary of poor RNA quality. LT_1 - day 5 and LT_1A - day 10 samples, were consequently omitted from the study. Incorporating the aforementioned samples in this study would have significantly hampered downstream processes and resulted in the generation of inaccurate gene

expression profiles. It is therefore mandatory to quantify and validate the concentrations and quality of the nucleic acids being investigated, prior to quantitative gene expression studies (Sharkey *et al*., 2004).

Analysis of data generated from quantitative real-time PCR experiments may be accomplished by either absolute or relative quantification. Since this study aimed to quantify changes in mRNA expression levels of target genes across multiple samples to establish expression trends amongst the isolates, it did not necessitate the determination of the exact transcript copy number. For this study, relative quantification provided an adequate quantitative strategy and was employed to describe the changes in expression of the target genes relative to a reference gene.

To ensure the accuracy of relative quantitative real-time PCR, the specific PCR conditions, as well as an appropriate internal control must be established. A reliable internal control could show negligible variation, whereas expression levels of a gene of interest may fluctuate significantly for the duration of an experiment (Dean *et al*., 2002). Thus, selection of a suitable internal control is imperative for the accurate quantification of gene expression, as normalization will compensate for differences in the mRNA purity and concentration of the investigated samples (Gilsbach *et al*., 2006)

However, unlike in eukaryotic cells, bacterial cells lack stably expressed housekeeping genes. Hence, the accurate quantification of RNA is often hindered by the absence of reliable standardization (Fey *et al*., 2004). In this study, the 16S rRNA gene was selected

as the housekeeping (reference) gene. Based on the standard deviation (SD) and percentage coefficient of variance (CV%) of crossing points (C_p), 16S rRNA expression levels varied across the different sampling times and amongst the isolates (Table 3.6; Fig 3.7). Such variation is probable as the expression of rRNA is firmly dependant on the physiological status of the bacteria (Gourse *et al.,* 1996). Despite the disparity in expression levels, the 16S rRNA gene, used in this study, proved to be a suitable reference gene for normalization, displaying an accepted level of gene expression variability with p values > 0.05 (section 3.9.1.2) A p value of > 0.05 is indicative of insignificant variability (Pfaffl *et al*., 2002).

Ideally, the use at least three housekeeping genes as internal standards is suggested, as normalization based on the use of a single gene may prove to be relatively erroneous (Thellin *et al.*, 1999; Vandesompele *et al*., 2002). Potential prokaryote housekeeping genes for normalization in quantification strategies are continuously being investigated. Housekeeping genes that are currently in use include sigma factor-encoding *rpoD* and *rpoS*, pyrroline-5-carboxylate reductase (*proC*), penicillin-binding protein 2 (*pbp-2*), malonyl CoA: acyl carrier protein [ACP] transacylase (*fabD*), and *ampC* encoding chromosomal beta-lactamase (Vandesompele *et al*., 2002).

The standard curves constructed for this study were relative standard curves. Relative standard curves were used exclusively to determine the efficiency of the real-time PCR and not to calculate target gene expression. Standard curves were constructed for all target genes (APPENDIX V) except *lipA* as a result of primer dimers occurring during

the amplification of the lower concentrations of the cDNA dilution series. The standard curve gradients ranged from -2.867 to -4.092 over three orders of magnitude (Table 3.5; APPENDIX V). All standard curves showed a high degree of linearity with correlation coefficient squared (r^2) values of 1 (APPENDIX V). Correlation coefficient squared values (r^2) of 0.98 or above are indicative of a stable and reliable assay (Nolan *et al*., 2006).

Real-time PCR efficiencies (*E*) were calculated from the standard curve gradients (Table 3.5). The real-time PCR efficiency should be as close to 100% (E = 2) as possible, corresponding to a doubling of the target amplicon at each cycle (Yuan *et al*., 2006). An assay with E = 100% is defined by a standard curve with a gradient of -3.32 (Yun *et al*., 2006). A high degree of efficiency ranging from 88% (E = 1.76) to 112% (E = 2.24) was achieved in the present study. A suitable standard curve for *lipA* could not be produced as a corollary of very low *lipA* expression levels. As a result, E_{lipA} could not be determined. E_{alkR} yielded an efficiency of 112% (E = 2.24), indicating an inappropriately optimized assay and/or poor specificity of primer pairs. Although E of 112% is not ideal, it still fell within an acceptable efficiency range of E = 100 ± 20% (Yun *et al*., 2006). The primer pair used for *alkR* amplification was the second set of primers that was designed for this study. The first pair of *alkR* primers that was tested failed to generate the target gene amplicon and only resulted in the formation of primer dimers. The difficulty that was experienced in the designing of an appropriate assay and primer pairs for *alk*R amplification could be circumvented by the use of gene-specific hybridization probes.

No association could be made between *E* and C_p values as higher C_p values did not necessarily translate in lower *E* values. This finding is in accordance with the results of Karlen *et al.* (2007) and Čikoš *et al*. (2007) who did not find a dependency of *E* value on C_p value and suggested that amplicon and primer sequences were the foremost contributors to influence amplification efficiency.

Previous studies have shown that rubredoxins (*rubA*) and rubredoxin reductase (r*ub*B) are indispensable in *n*-alkane degradation as *rubA*, *rubB*, and *alkM* constitute a three component alkane hydroxylase system in *A. calcoaceticus* (Geißdörfer *et al*., 1999; Ratajczak *et al*., 1998; van Beilen *et al*., 2002). In this study, rubredoxin reductase (r*ub*B) activity was not detected in any of the isolates despite rigorous optimizing strategies and redesigning of primers. Plausible reasons for the inability to detect *rub*B activity could be attributed to either very low expression levels, or poor primer design. An alternative approach to investigating *rubB* expression levels would be to utilize gene-specific hybridization probes instead of SYBR green dsDNA-binding dye. Hybridization probes are target-specific chemistries that append an additional level of specificity thereby ensuring that specificity does not only reside in the primers. Therefore, any nonspecific amplification and primer dimers that may occur will not generate a signal and would be disregarded by the fluorescence detector (Bustin and Nolan, 2004a).

Rubredoxin (*rubA*) activity was detected in all investigated samples of LT_1, LT_1A, and V_2 isolates. LT_1 and V_2 samples exhibited similar *rubA* expression trends whereas *rubA* of LT_1A samples illustrated a contrasting expression trend in relation to LT_1 and V_2

samples (Fig. 3.9). Although *rubA* expression was down-regulated in LT_1A, and V_2 samples in relation to LT_1, the differences in expression levels were not significant with $p > 0.05$ (section 3.9.1.2). An unexpected increase in *rubA* expression was observed for LT_1 at day 60. Due to the study culminating at day 60, no further observations or assumptions pertaining to *n*-alkane degradation could be made regarding *rubA* expression subsequent to day 60. However, 16S rRNA expression levels of LT_1 samples also increased considerably at day 60 and may be associated with *rubA* expression at day 60, thus, indicating the possible involvement of *rubA* in other cellular functions.

Genes *rubA* and *rubB* are constitutively expressed and are involved in a variety of other electron transfer reactions necessary for cellular functioning. Therefore, levels of *rubA* and *rubB* expression may not be dependent on the presence of an alkane substrate (Fu and Maier, 1994; Gomes *et al*., 1997). The cloning, sequencing, and functional analysis in previous studies has revealed that rubredoxins and rubredoxin reductase are interchangeable among the alkane hydroxylase systems of both Gram-negative and Gram-positive organisms. This is possible due to the highly conserved structural features that are essential for electron transfer (van Beilen *et al*., 2002).

Involvement of *estB* in *n*-alkane utilization has been investigated as *estB* occurs in an operon with components of the alkane hydroxlase system, *rubA* and *rubB*, in *Acinetobacter* sp. strain ADP1 (Geißdörfer *et al*., 1999). Although *rubA*, *rubB*, and *estB* constitute an operon, it was established that *estB* is not regulated by alkanes and there was no indication of a functional relationship between the three genes. However, *estB*

was found to encode a functional esterase (Geißdörfer *et al*., 1999). In this study, no association could be ascertained between the expression of *rubA* and *estB*, and is in accordance with the findings by Geißdörfer *et al*. (1999). The *rubA* gene was expressed in all LT_1, LT_1A, and V_2 samples, whereas expression of *estB* was predominantly observed in V_2 samples. The mispriming and non-defined C_p values generated during *estB* amplification in LT_1 and LT_1A samples are suggestive of either non-expression or extremely low expression of *estB*.

During the diesel degradation phase of this study, flasks containing V_2 inocula were found to possess an opaque, waxy material that was observed in the hydrocarbon and hydrocarbon-culture medium fraction for the duration of the incubation. This phenomenon was not observed in flasks containing LT_1 and LT_1A inocula. After and including 10 days of incubation, however, the diesel in the V_2 sample flasks no longer appeared as a confluent layer over the culture medium phase, but rather as minuscule droplets enfolded within the opaque substance. This occurrence is characteristic of bioemulsification as observed in previous studies on *A. calcoaceticus* RAG-1, which produced a bioemulsifier known as emulsan (Gutnick *et al*., 1991). Emulsan reduces the surface tension of diesel resulting in the surface of the diesel droplets to break upon contact with the hydrophobic layer (Gutnick *et al*., 1991). Once the diesel droplets are further broken down into microdroplets of 100 µm or less, they become surrounded by bacterial cells and are consumed as a carbon source. The bioemulsifier coating eventually causes the microdroplets to become repulsive. Consequently, the microdroplets are

dispersed into the medium without the adhering bacterial cells (Baldi *et al*., 1999). The bioemulsifier that was produced in this study by the V_2 isolate was not characterized.

Studies on the bioemulsification activities of *A. calcoaceticus* RAG-1 showed that emulsan initially accumulates as a minicapsule on the surface of the cell (Goldman *et al*., 1982; Pines *et al*., 1983; Shabtai and Gutnick, 1985). As the cells approach the stationary phase, emulsan is released into the medium as an active emulsifier. The involvement of an esterase has been advocated in the release of emulsan from the cell surface (Shabtai and Gutnick, 1985).

The expression profile of *estB* of V_2 samples showed increasing levels of expression from day 5 to day 10 with maximum expression at day 10 (Fig. 3.18). Expression levels declined considerably after day 10 and remained fairly constant until the end of the 60 day incubation period. Bacterial growth, determined by spectrophotometry (Table 3.1), of V_2 - day 5 sample and V_2 - day 10 sample are indicative of a late exponential phase and early stationary phase, respectively. These findings are suggestive that the involvement of *estB* in the release of the bioemulsifier may be plausible. The basis of this postulation is that (i) *estB* was predominantly expressed in V_2 samples that coincidentally also appeared to produce the bioemulsifier and (ii) maximum *estB* expression was recorded at the onset of the stationary phase. However, to confirm as to whether *estB* does encode the esterase that is responsible for the release the bioemulsifier, further studies are warranted.

Several bacterial species are capable of utilizing *n*-alkanes by virtue of alkane hydroxylases (van Beilen *et al*., 2006). The alkane hydroxylase gene (*alkM*) of LT_1A was significantly down-regulated in comparison to *alkM* of LT_1 with a *p* value of 0.0425. LT_1A samples also displayed a low degree of intra-sample variation in C_p with SD and CV% of 1.39 and 4.14, respectively (Table 3.6), indicating that the regulation of *alkM* expression was fairly constant in LT_1A samples throughout the study period. Maximum *alkM* expression in LT_1A samples was observed at 40 days of incubation (Fig. 3.11). Maximum expression of *alkM* in LT_1A samples during the stationary phase may have been induced by a specific by-product of alkane oxidation. Different by-products of alkane oxidation have the ability to induce alkane hydroxylases. The alkane hydroxylases of different bacterial species are induced by different by-products of alkane oxidation (Marín *et al*., 2003). Down-regulation of *alkM* in LT_1A samples may also be suggestive of the involvement of an additional alkane hydroxlase. LT_1 samples showed a higher degree of intra-sample variation (Table 3.6), with maximum *alkM* expression during the initial stages of incubation (Fig. 3.11). The high *alkM* expression levels from day 5 to day 10, corresponds to the high levels of diesel degradation achieved by LT_1 on those respective days (Fig 3.1). Expression levels of *alkM* of V_2 samples could not be quantified due to the formation of multiple amplification products.

During the amplification of *alkM* of V_2 samples, the *alkM* primer pair concurrently amplified the anticipated *alkM* gene (*alkM1*) as well an additional product; presumed to be another alkane hydroxlase that was tentatively designated *alkM2*. Formation of additional products could also be attributed to co-amplification of two or more genes as a

result of sequence similarity, or the amplification of either degraded RNA or contaminating genomic DNA (gDNA). However, the size of the additional amplification product was 336 bp (Fig. 3.14 B) and is too large to have resulted from the amplification of degraded RNA (Nolan *et al*., 2006), and contaminating gDNA was removed by DNase treatment during the RNA extraction procedure (section 2.5). Although an amplification product was formed for *alkM2*, the amplification conditions were not optimal for *alkM2*. Therefore the multiple band formation at days 20 to 50 is a consequence of sub-optimal amplification conditions and poor primer specificity, and will be eliminated with proper optimization.

The presence of multiple alkane hydroxylases in a single bacterial strain is not an atypical occurrence. Multiple alkane hydroxylases enable alkane degraders to grow on a broad range of alkane substrates, where each alkane hydroxylase may exhibit unique properties, and have different induction patterns (van Beilen *et al*., 2003). Commercial strain *Acinetobacter* sp. M-1 is a long-chain alkane degrader and is known to contain two alkane hydroxylases, *alkMa* and *alkMb*, that are differentially induced in response to *n*-alkane chain length. Alkane hydroxylases, *alkMb* oxidizes C_{16} to C_{22} *n*-alkanes, with *alkMa* showing a higher activity with C_{22} or larger alkanes (Tani *et al.,* 2001). Studies conducted on alkane degrader *Pseudomonas aeruginosa* also confirmed the presence of two alkane hydroxlase genes, *alkB1* and *alkB2* (Marín *et al*., 2003). However, although both genes were induced by C_{10} to C_{22}/C_{24} alkanes, they were preferentially expressed at different stages in the bacterial growth phase. Differential expression was not based on alkane chain length but rather on the levels of oxygen. The *alkB2* expression was highest

during the early exponential phase where oxygen was abundant, while *alkB1* was induced during the late exponential/stationary phase where oxygen supply was limited (Marín *et al*., 2003).

Accordingly, the presence of two or more alkane hydroxylases in the V_2 isolate is very conceivable. Since V_2 is efficient in degrading both medium-chain (Fig 3.1) and long-chain length *n*-alkanes (Mandri and Lin, 2007), the differential alkane hydroxlase (*alk*M1 and *alk*M2) expression could have been regulated by the carbon chain length of its substrate. The premise that the differential alkane hydroxlase expression in V_2 is based on oxygen levels, as in the case of *P. aeruginosa* (Marín *et al*., 2003), may also be plausible as *alkM1* and *alkM2* were expressed at different stages in the growth phase with *alkM1* being expressed at the late exponential/early stationary phase and *alkM2* expression evident throughout the late stationary phase.

Amongst the V_2 samples, the *alkM1* gene was only expressed at 15 days of incubation, while *alkM2* was expressed during 20 days to 50 days of incubation. The *alkM2* gene may share some sequence similarity to *alkM1* and the annealing of the *alkM* primers to the *alkM2* could possibly be a consequence thereof. Partial gene sequence analysis and alignment of the *alkM1* gene of V_2 - day 15 sample and the pooled cDNA of LT_1 samples showed 100% homogeneity between the two sequences (Fig. 3.15). On the basis of gene sequence homogeneity (Fig. 3.15), amplicon size (Fig. 3.14 A and B), and identical T_m (Fig. 3.12; Fig. 3.13) it can be ascertained that *alkM* of LT_1 samples is analogous to *alkM1* of V_2. Sequencing of *alkM2* of V_2 - day 20 sample proved to be unsuccessful. The

alkM primer pair used in the sequencing *alkM2* gene was designed and optimized for the amplification of the alkane hydroxylase, *alkM*. While some sequence similarity may exist between *alkM* and *alkM2*, the specificity of *alkM* primers, and the amplification and cycling conditions were not optimal for *alkM2* amplification. Further investigation into the sequence of *alkM2* would require the incorporation of *alkM2* gene fragment into a cloning vector before sequencing.

Validation of *alkM* amplicons of V_2 samples by 2% (wt/vol) agarose gel electrophoresis revealed that no amplification products were observed prior to day 15, and at day 60 (Fig. 3.14 B), signifying the absence of alkane hydroxylase activity at the aforementioned sampling times. However, despite the absence of *alkM1* or *alkM2* expression, maximum diesel utilization was recorded prior to day 15 (Fig. 3.1). The involvement of alkane hydroxylase cytochrome P-450 in some *Acinetobacter* strains capable of utilizing both medium- and long-chain length *n*-alkanes has been documented (Asperger *et al*., 1981), and might provide an alternative system for the oxidation of alkanes. Since neither *alkM1* nor *alkM2* activity was detected prior to 15 days of incubation, the participation of a third alkane hydroxlase, such as cytochrome P-450, may be possible. The activity of the bioemulsifier may have also contributed to the high levels of diesel degradation prior to day 15. According to this study, V_2 may regulate its alkane hydroxylase activity in response to either the substrate chain length or oxygen content by alternating the alkane hydroxylase component, *alkM1* and *alkM2*, while the rubredoxin component (*rubA*) of the alkane hydroxlase complex remains constitutively expressed.

In this study, the *alkR* gene of LT_1A samples was down-regulated in comparison to *alkR* of LT_1 samples; however the regulation was not significant with a *p* value of 0.5095. In compliance with *alkM* expression, expression levels of *alkR* of V_2 samples could not be quantified on account of invalid C_p values generated from multiple product formation. Although LT_1A and LT_1 samples displayed comparable levels *alkR* expression with equally high levels of intra-sample variation (Table 3.6), the onset of expression differed. The *alk*R gene expression of LT_1 samples declined as incubation time progressed, and *alkR* expression of LT_1A samples increased with incubation time. The overall *alkR* expression of both LT_1, and LT_1A samples was comparatively low in relation to the alkane hydroxylase complex genes, *alkM* and *rubA* (APPENDIX VI). This inference is in accordance with preceding studies that found *alkR* to be expressed at very low levels during alkane degradation despite its indispensability in the degradation process (Ratajczak *et al*., 1998).

Melting peak analysis of *alkR* of LT_1 and LT_1A (Fig. 3.17A), confirmed the amplification of a single product of envisaged melting temperature (T_m = 79.3354^oC) at each sampling time. However, for the amplification of *alkR* of V_2 samples, the presence of a second product exhibiting a higher T_m was evident (Fig. 3.17 B).

A. calcoaceticus sp. M-1 that contained the two alkane hydroxylases *alkMa* and *alkMb* was also found to possess two transcription regulators *alkRa* and *alkRb* (Tani *et al.,* 2001). Each alkane hydroxylase was regulated by either *alkRa* or *alkRb*. The *alkRa* and *alkRb* induction responded to the alkane chain lengths recognized by the corresponding

hydroxylase (Tani *et al*., 2001). Likewise, since two *alkM* products were amplified in the V_2 isolate in this study, the possibility of two *alkR* amplification products is not implausible.

The expected amplification product (*alkR1*) was only observed at days 30, 50, and 60. A shift in T_m of approximately 2^oC was observed for day 30 and day 60 samples (Fig. 3.17 B). Given that T_m is dependent on the guanine plus cytosine (G+C) content (Espy *et al*., 2006), and disparity in T_m could have possibly resulted from the amplification of an *alkR* isozyme at day 30 and day 60. Isozymes represent a variant of the same enzyme as a result of differences in the amino acid sequence, but serves to perform the same function (Hunter and Merkert, 1957). Despite the discrepancy in T_m, the amplification product size was the equivalent to that of the day 50 sample. Day 5, 10, and 15 samples showed the amplification of an additional product (*alkR2*) with T_m exceeding 84^oC. No amplification products were observed for day 20 and day 40 samples. The *alkR1* gene of V_2 is comparable to *alkR* of LT_1 and LT_1A on the basis of T_m and amplification product size. Therefore *alkR2*, expressed from day 5 to day 15, and *alkR1*, expressed after day 15, possibly serves as a transcription regulator for *alkM1* and *alkM2*, respectively.

The *xcpR* gene, that encodes a subunit of the general secretory pathway, is required for alkane degradation in *Acinetobacter* sp. strain ADP1 (Parche *et al*., 1997). The general secretory pathway is also common to *P. aeruginosa* and has been implicated degradation of alkanes (Hardegger *et al*., 1994). The expression of *xcpR* in conjunction with *rubA* and *rubB* in *A. calcoaceticus* is known to be constitutive (Ratajczak *et al*., 1998).

The *xcpR* gene of LT_1A was down-regulated in comparison to *xcpR* of LT_1, but not significantly, with a *p* value of 0.051. Maximum *xcpR* expression levels for LT_1 samples was observed during in initial days of incubation on diesel whereas *xcpR* expression levels for LT_1A samples was at its highest at 40 days of incubation (Fig. 3.22). Levels of *xcpR* expression of V_2 samples could not be quantified as a consequence of invalid C_p values that were generated from multiple product formation.

Melting peak analysis of *xcpR* of LT_1 and LT_1A revealed the formation of a single amplification product of the anticipated T_m of 84.0949°C throughout the 60 day incubation period (Fig. 3.24 A). However, melting peak analysis of *xcpR* of V_2 samples indicated the presence of additional amplification products, illustrated by three defined peaks, exhibiting higher T_ms (Fig. 3.24 B). The results obtained for V_2 samples were highly reproducible yielding multiple products with identical melting temperatures (Fig. 3.24 C).

Validation of *xcpR* amplicons of V_2 samples by 2% (wt/vol) agarose gel electrophoresis authenticated the presence of two distinct amplification products, albeit, three melting peaks were observed. Although day 30 and day 40 samples displayed an amplification product that exceeded the projected T_m by approximately 2°C (Fig. 3.24 B), the amplification product size was the expected 192 bp (Fig. 3.25). As described for *alkR*, disparity in T_m could have possibly resulted from the amplification of an isozyme at day 30 and day 40 sample. The expected 192 bp product (*xcpR1*) was observed in all V_2

samples. In addition, the presence of a larger amplification fragment of approximately 500 bp (*xcpR2*) was observed in all samples except on day 30 and day 40 (Fig. 3.25).

The *xcpR* gene encodes a type IV pilus-related system that may not only be required for the secretion of proteins but may represent a more universal transport system for a variety of macromolecules. It may also facilitate the alleviation of membrane stress incurred by bacterial cells during alkane degradation (Parche *et al*., 1997). The metabolism of *n*-alkanes in the V_2 isolate appears to be very complex. Its broad substrate range, diversity and functions of the enzymes involved in alkane degradation, and its contrasting regulation of both constitutive and differential gene expression may be reminiscent of the fact that two and perhaps more *xcpR* genes are required to provide an adequate transport system during alkane degradation.

Lipase activity, which was observed in strains isolated from petroleum-polluted environments, has been correlated with hydrocarbon degradation (Marín *et al*., 1995; Schindler *et al*., 1975). This occurrence, however, is regarded as contradictory since hydrocarbons do not serve as lipase substrates and their degradation does not require lipase activity. Furthermore, some alkanes, such as hexadecane, have been shown to repress lipase expression (Kok *et al*., 1996).

In this study, very low expression levels of *lipA* was detected in LT_1 and LT_1A samples. Several samples generated mispriming (Fig. 3.20 A) and non-defined C_p values (APPENDIX VI) as a consequence of low expression. Expression of *lipA* was absent in

all V_2 samples. Low expression of *lipA* in LT_1 and LT_1A samples, and moreover, lack of expression in V_2 is an indication of its non-involvement in the degradation of diesel.

Previous studies conducted by Kok *et al.* (1995) confirmed that *A. calcoaceticus* BD413 produced notably high levels of extracellular lipase when grown on long-chain alkanes. In a different study, an inactivation of *xcpR* in *A. calcoaceticus* ADP1 chromosome hindered the secretion of esterase and lipase that resulted in the lack of growth on long-chain length alkanes (Parche *et al*., 1997). The findings of the present study may be suggestive that induction of *lipA* expression may be substrate dependent and is required for long-chain and not for medium-chain alkane degradation in *A. calcoaceticus*. Furthermore, no association in the expression trend of *xcpR*, *lipA* and *lipB* could be ascertained. Research conducted by Kok *et al.* (1996), indicated that during growth of *A. calcoaceticus* on alkanes, *lipA* expression was induced at the onset of the stationary growth phase. Although the expression *lipA* was not found to be induced at the onset of the stationary growth phase in this study, the induction of *lipB* was evident.

The *lipB* gene, which was expressed in all investigated samples, exhibited maximum expression at 20 days of incubation for LT_1 and LT_1A, and at 15 days for V_2 (Fig. 3.20). The *lipB* gene encodes a lipase chaperone LipB that prevents the complete folding of the LipA polypeptide before it traverses the outer cell membrane (Frenken *et al*., 1993). The lipase chaperone also serves protective function. Not only does it protect the immature LipA from degradation by proteases, it also prevents the formation of active lipase before secretion is complete, thereby protecting the cell membrane from the activities of the

functional lipase. LipB is therefore not only essential for lipase production, but also vital to a lipase-producing cell (Kok *et al.*, 1995).

Genes *lipA* and *lipB* constitute a bicistronic operon that indicates a synchronized regulation of their expression (Kok *et al.*, 1995). However in this study, the expression trends of *lipA* and *lipB* were incongruent, and expression of *lipB* was still evident in the absence of *lipA* expression amongst V_2 samples. Therefore, it can be inferred that the expression of *lipA* and *lipB* may not be associated with diesel degradation. Hence, the explanation for lipase production by *Acinetobacter* sp. in the presence of alkanes remains intangible and further investigation is required.

The combination of mechanistic, physiological and genetic investigation that constituted this study aimed to provide a greater understanding of the regulation of gene expression during diesel degradation in *A. calcoaceticus* isolates. Although all three isolates were comparably efficient in degrading diesel (Fig. 3.1), each isolate employed a unique approach to facilitate the degradation process.

A general expression trend for the investigated target genes *rubA*, *alkM*, *alkR*, *lipB*, and *xcpR* was conserved in LT_1 and LT_1A; however, the patterns of induction of the target genes were contrasting in each isolate. With the exception of *lipB*, LT_1 displayed maximum gene expression during the initial days of incubation with gene activity subsiding towards the end of incubation period. This expression trend is in direct correlation with the bacterial growth phase where maximum expression occurred during

the exponential phase and declined during the stationary phase. LT_1A demonstrated an overall down-regulation of target gene expression in relation to LT_1 and V_2, with maximum target gene expression levels observed during the stationary phase of growth. Despite the down-regulation of target genes and specifically the significantly down-regulated *alkM* gene in LT_1A, the isolate degraded a comparable amount of diesel in relation to LT_1. This occurrence may be suggestive that the relatively lower levels of target gene expression in LT_1A may have been adequate for degradation of the diesel substrate and that an additional factor may have aided in degradation. It may be possible that LT_1A employed an alternate alkane oxidation pathway or mechanism of adhesion to diesel in relation to that of LT_1. The degradation of diesel by the V_2 isolate engaged the contributions of a bioemulsifier and the controlled induction of two alkane hydroxylases. Despite the apparent diversity of the diesel degradation strategies employed by the isolates, LT_1, LT_1A and V_2 ultimately displayed similar diesel degrading capabilities by achieving comparable levels of diesel degradation.

5. CONCLUSION

The present study provided an overview of the presence, absence, and regulation of catabolic genes involved in the degradation of diesel. The findings of this study are suggestive that the course of alkane degradation is not uniform in *A. calcoaceticus* isolates LT_1, LT_1A, and V_2, albeit all three isolates ultimately achieved comparable levels of diesel degradation. It is apparent that different members of the genus *Acinetobacter*, that are well recognized for their virtuosity in degrading alkanes, may employ a variety of alkane-degrading mechanisms such as alternative pathways for alkane oxidation, implementation of different methods of adhesion to diesel, and emulsification. Alkane oxidation in V_2 appears to be complex due to its diverse substrate range, and its controlled regulation of multiple alkane hydroxylases and alkane hydroxylase transcription regulators in contrast to the constitutive expression of the rubredoxin component of the alkane hydroxylase complex.

Research on the diversity of alkane hydroxylase genes, their induction patterns, substrate specificity, properties of host organisms, and enzyme kinetics, will significantly contribute towards optimizing the biodegradative capabilities of hydrocarbon-degrading microorganisms.

6. REFERENCES

Abdel-El-Haleem, D. 2003. *Acinetobacter:* environmental and biotechnological applications. *African Journal of Biotechnology*. **2:** 71-74.

Abed, M. M. R., N. M. D. Safi, J. Koster, D. de Beer, Y. El-Nahhal, J. Rullkotter, F. Garcia-Pichel. 2002. Microbial diversity of a heavily polluted microbial mat and its community changes following degradation of petroleum compounds. *Applied and Environmental Microbiology*. **68:** 1674-1683.

Alfreider, A., C. Vogt, and W. Babel. 2003. Expression of chlorocatechol 1,2-dioxygenase and chlorocatechol 2,3-dioxygenase genes in chlorobenzene-contaminated subsurface samples. *Applied and Environmental Microbiology*. **69:** 1372-1376.

Altschul, S. F., W. Gish, W. Miller, E. W. Meyers, and D. J. Lipman. 1990. Basic local alignment search tool. *Journal of Molecular Biology*. **215:** 403-410.

Alula, M., M. Diack, R. Gruber, G. Kirsch, J. C. Wilhelm, and D. Cagniant. 1989. Efficiency of sequential elution solvent chromatography-extrography technique for the characterization of hydroliquefaction and pyrolysis products. *Fuel*. **10:** 1330-1335.

Amann, R., B. M. Fuchs, and S. Behrens. 2001. The identification of microorganisms by fluorescence *in situ* hybridization. *Current Opinions in Biotechnology*. **12:** 231-236.

Asperger, O., and H. P. Kleber. 1991. Metabolism of alkanes by *Acinetobacter*, *In* K. J. Towner, E. Bergogne-Berezin, and C. A. Fewson (Eds), The biology of *Acinetobacter*. pp. 323-350. Plenum Press, New York, NewYork.

Atlas, R. M. 1981. Microbial degradation of petroleum hydrocarbons: an environmental perspective. *Microbiology Reviews*. **45:** 180-209.

Atlas, R. M. 1991. Microbial hydrocarbon degradation – bioremediation of oil spills. *Journal of Chemical Technology and Biotechnology*. **52:** 149-156.

Atlas, R. M., and R. Bartha. 1992. Hydrocarbon biodegradation and oil spill bioremediation. *Advances in Microbial Ecology.* **12:** 287-338.

Atlas, R. M., and C. E. Cerniglia. 1995. Bioremediation of petroleum pollutants: diversity and environmental aspects of hydrocarbon biodegradation. *BioScience.* **45:** 332-338.

Baldi, F., N. Ivošević, A. Minacci, M. Pepi, R. Fani, V. Svetličić, and V. Žutić. 1999. Adhesion of *Acinetobacter venetianus* to diesel fuel droplets studied with in situ electrochemical and molecular probes. *Applied and Environmental Microbiology*. **65:** 2041-2048.

Banat, I. M., N. Samarah, M. Murad, R. Horne, and S. Banerjee. 1991. Biosurfactant production and use in oil tank clean-up. *World Journal of Microbiology and Biotechnology*. **7:** 80-88.

Barbe, V., D. Vallenet, N. Fonknechten, A. Kreimeyer, S. Oztas, L. Labarre, S. Cruveiller, C. Robert, S. Duprat, P. Wincker, L. N. Ornston, J. Weissenbach, P. Marlière, G. N. Cohen, and C. Médigue. 2004. Unique features revealed by the genome sequence of *Acinetobacter* sp. ADP1, a versatile and naturally transformation competent bacterium. *Nucleic Acids Research.* **32:** 5766-5779.

Bastiaens, L., D. Springael, P. Wattiau, H. Harms, R. Dewachter, H. Verachtert, and L. Diels. 2000. Isolation of adherent polycyclic aromatic hydrocarbon (PAH)-degrading bacteria using PAH-sorbing carriers. *Applied and Environmental Microbiology*. **66:** 1834-1843.

Belsky, I., D. L. Gutnick, and E. Rosenberg. 1979. Emulsifier of *Arthrobacter* RAG-1: determination of emulsifier bound fatty acids. FEBS Letters. **101:** 175-178.

Bengtsson, M., H. J. Karlsson, G. Westman, and M. Kubista. 2003. A new minor groove binding asymmetric cyanine reporter dye for real-time PCR. *Nucleic Acids Research*. **31:** e45.

Bhattacharya, D., P. M. Sarma, S. Krishnan, S. Mishra, and B. Lal. 2002. Evaluation of genetic diversity among *Pseudomonas citronellolis* strains isolated from oily sludge-contaminated sites. *Applied and Environmental Microbiology*. **69:** 1435-1441.

Boonchan, S., M. L. Britz, and G. A. Stanley. 2000. Degradation and mineralization of high-molecular-weight polycyclic aromatic hydrocarbons by defined fungal-bacterial cocultures. *Applied and Environmental Microbiology*. **66:** 1007-1019.

Breuil, C., D. B. Shinkler, J. S. Sijher, and D. J. Kushner. 1978. Stimulation of lipase production during growth on alkanes. *Journal of Bacteriology.* **133:** 601-606.

Bushnell, L. D., and H. F. Haas. 1941. The utilization of certain hydrocarbons by microorganisms. *Journal of Bacteriology*. **41:** 653-673.

Bustin, S. A. 2002. Quantification of mRNA using real-time RT-PCR. Trends and problems. *Journal of Molecular Endocrinology*. **29 (1):** 23-39.

Bustin, S. A., V. Benes, T. Nolan, and **M. W. Pfaffl.** 2005. Quantitative real-time RT-PCR – a perspective. *Journal of Molecular Endocrinology*. **34:** 597-601.

Bustin, S. A., and T. Nolan. 2004a. Pitfalls of quantitative real-time reverse-transcription polymerase chain reaction. *Journal of Biomolecular Techniques*. **15(3):** 155-166.

Bustin, S. A., and T. Nolan. 2004b. Template handling, preparation, and quantification. pp. 87-120. *In* Bustin, S. A. (Ed.), The real-time PCR encyclopaedia A-Z of quantitative PCR. Published by International University Line, La Jolla, California.

Cerniglia, C. E. 1992. Biodegradation of polycyclic aromatic hydrocarbons, pp. 351-368. *In* Rosenberg, E. (Ed.), Microorganisms to combat pollution. Kluwer Academic Publishers, Dordrecht, The Netherlands.

Chakrabarty, A. M. 1973. Genetic fusion of incompatible plasmids in *Pseudomonas*. *Proceedings of the National Academy of Sciences USA*. **70**: 1641-1644.

Čikoš, Š, A. Bukovská, and J. Koppel. 2007. Relative quantification of mRNA: comparison of methods currently used for real-time PCR data analysis. *BMC Molecular Biology*. **8:** 113.

Collin, P. H. 2001. Dictionary of ecology and the environment, fourth ed. Peter Collin Publishing, London.

Colores, G. M., R. E. Macur, D. M. Ward, and W. P. Inskeep. 2000. Molecular analysis of surfactant-driven microbial population shifts in hydrocarbon contaminated soil. *Applied and Environmental Microbiology*. **66:** 2959-2964.

Cunningham, C. J., and J. C. Philp. 2000. Comparison of bioaugmentation and biostimulation in *ex situ* treatment of diesel contaminated soil. *Land Contamination and Reclamation*. **8:** 261-269.

Dean, J. D., P. H. Goodwin, and T. Hsiang. 2002. Comparison of relative RT-PCR and northern blot analyses to measure expression of β-1, 3-glucanase in *Nicotiana benthamiana* infected with *Colletotrichum destructivum*. *Plant Molecular Biology Reporter* **20:** 347-356.

de Bont, J. A. M. 1998. Solvent-tolerant bacteria in biocatalysis. *Trends in Biotechnology.* **16:** 493-499

Espy, M. J., J. R. Uhl, L. M. Sloan, S. P. Buckwalter, M. F. Jones, E. A. Vetter, J. D. C. Yao, N. L. Wengenack, J. E. Rosenblatt, F. R. Cockerill III, and T. F. Smith.

2006. Real-time PCR in clinical microbiology: Applications for routine laboratory testing. *Clinical Microbiology Reviews.* **19:** 165-256.

Fey, A., S. Eichler, S. Flavier, R. Christen, M. G. Höfle and C. A. Guzmán. 2004. Establishment of a real-time PCR-based approach for accurate quantification of bacterial RNA targets in water, using *Salmonella* as a model organism. *Applied and Environmental Microbiology*. **70:** 3618-3623.

Finnerty, W. R. 1977. The biochemistry of microbial alkane oxidation: new insights and perspectives. *Trends in Biochemical Sciences.* **2:** 73-75.

Finnerty, W. R. 1988. Lipids of *Acinetobacter*, pp. 184-188. *In* Applewhite, A. H. (Ed.), Proceedings of the World Conference on Biotechnology for the Fats and Oil Industry. American Oil Chemical Society, Champaign, Illinois.

Finnerty, W. R. 1990. Assay methods for long-chain alkane oxidation in *Acinetobacter*. *Methods in Enzymology*. **188:** 10-14.

Fleige, S., and M. W. Pfaffl. 2006. RNA integrity and the effect on the real-time qRT-PCR performance. *Molecular Aspects of Medicine.* **27:** 126-139.

Fox, B. G., J. Shanklin, A. Jingyuan, T. M. Loehr, and J. Sanders-Loehr. 1994. Resonance Raman evidence for an Fe-O-Fe center in stearoyl-ACP desaturase. Primary sequence identity with other diiron-oxo proteins. *Biochemistry.* **33:** 12776-12786.

Frenken, L. G. J., A. Degroot, J. Tommassen, and C. T. Verrips. 1993. Role of the *lipB* gene product in the folding of the secreted lipase of *Pseudomonas glumae*. *Molecular Microbiology*. **9:** 591-599

Fu, C., and R. J. Maier. 1994. Organization of the hydrogenase gene cluster from *Bradyrhizobium japonicum*: sequences and analysis of five more hydrogenase-related genes. *Gene*. **145:** 91-96.

Geißdörfer, W., R. G. Kok, A. Ratajczak, K. J. Hellingwerf, and W. Hillen. 1999. The genes *rubA* and *rubB* for alkane degradation in *Acinetobacter* sp. strain ADP1 are in an operon with *estB*, encoding an esterase, and *oxyR*. *Journal of Bacteriology*. **181:** 4292-4298.

Ghazali, F.M., R. N. Z. A. Rahman, A. B. Salleh, M. Basri. 2004. Biodegradation of hydrocarbons in soil by microbial consortium. *International Biodeterioration and Biodegradation*. **54:** 61- 67.

Gibson, U. E., C. A. Heid, and P. M. Williams. 1996. A novel method for real time quantitative RT-PCR. *Genome Research*. **6:** 995-1001.

Gilsbach, R., M. Kouta, H. Bönisch, and M. Brüss. 2006. Comparison of in vitro and in vivo reference genes for internal standardization of real-time PCR data. *BioTechniques* **40:** 173-177.

Goldman, S., Y. Shabtai, C. Rubinovitz, E. Rosenberg, and D. L. Gutnick. 1982**.** Emulsan in *Acinetobacter calcoaceticus* RAG-1: distribution of cell-free and cell-

associated cross-reacting material. *Applied and Environmental Microbiology.* **44:** 165-170.

Gomes, C. M., G. Silva, S. Oliveira, J. LeGall, M. Y. Liu, A. V. Xavier, C. Rodrigues-Pousada, and M. Teixeira. 1997. Studies on the redox centers of the terminal oxidase from *Desulfovibrio gigas* and evidence for its interaction with rubredoxin. *Journal of Biological Chemistry.* **272:** 22502-22508.

Gourse, R. L., T. Gaal, M. S. Bartlett, J. A. Appleman, and W. Ross. 1996. rRNA transcription and growth rate-dependent regulation of ribosome synthesis in *Escherichia coli*. *Annual Review of Microbiology*. **50:** 645-677.

Gralton, E. M., A. L. Campbell, and E. L. Neidle. 1997. Directed introduction of DNA cleavage sites to produce a high-resolution genetic and physical map of the *Acinetobacter* sp. strain ADP1 (BD413UE) chromosome. *Microbiology.* **143:** 1345-1357.

Gutnick, D. L., R. Allon, C. Levy, R. Petter, and W. Minas. 1991. Applications of *Acinetobacter* as an industrial microorganism. *In* Towner, K. J. (Ed.). The biology of *Acinetobacter*, Plenum Press, New York, New York.

Hanson, K., G. Vikram, C. Kale, and A. J. Desai. 1994. The possible involvement of cell surface and outer membrane proteins of *Acinetobacter* sp. A3 in crude oil degradation. *FEMS Microbiology Letters*. **122:** 275-280.

Hardegger, M., A. K. Koch, U. A. Ochsner, A. Fiechter, and J. Reiser. 1994. Cloning and heterologous expression of a gene encoding an alkane-induced extracellular protein

involved in alkane assimilation from *Pseudomonas aeruginosa*. *Applied and Environmental Microbiology.* **60:** 3679-3687.

Heid, C. A., J. Stevens, K. J. Livak, and P. M. Williams. 1996. Real-time quantitative PCR. *Genome Research.* **6:** 986-994.

Heipieper, H. J., F. J. Weber, J. Sikkema, H. Keweloh, and J. A. M. de Bont. 1994. Mechanisms of resistance of whole cells to toxic organic solvents. *Trends in Biotechnology*. **12:** 406-416.

Higuchi, R., C. Fockler, G. Dollinger, and R. Watson. 1993. Kinetic PCR analysis: Real-time monitoring of DNA amplification reactions. *Biotechnology*. **11:** 1026-1030.

Hobbs, M., and J. S. Mattick. 1993. Common components in the assembly of type 4 fimbriae, DNA transfer systems, filamentous phage and protein secretion apparatus: a general system for the formation of surface-associated protein complexes. *Molecular Microbiology*. **10:** 233-243.

Hunter, R. L. And C. L. Merkert. 1957. Histochemical demonstration of enzymes separated by zone electrophoresis in starch gels. *Science*. **125:** 1294-1295.

Imbeaud, S., E. Graudens, V. Boulanger, X. Barlet, P. Zaborski, E. Eveno, O. Mueller, A. Schroeder, C. Auffray. 2005. Toward standardization of RNA quality assessment using user-independent classifiers of microcapillary electrophoresis traces. *Nucleic Acids Research*. **33:** e56.

Irwin, R. J. 1997. Environmental contaminants encyclopaedia. Diesel oil number 4 entry. National Park Services. [Online] http://www.nature.nps.gov. pp 1-57. December 2007.

Ishige, T., A. Tani, K. Takabe, K. Kawasaki, Y. Sakai, and N. Kato. 2002. Wax ester production from *n*-alkanes by *Acinetobacter* sp. strain M-1: Ultrastructure of cellular inclusions and role of acyl coenzyme A reductase. *Applied and Environmental Microbiology.* **68 (3):** 1192-1195.

Jansen, K., B. Nordén, M. Kubista. 1993. Sequence dependence of 4´,6-diamidino-2-phenylindole (DAPI)-DNA interactions. *Journal of American Chemical Society.* **115:** 10527-10530.

Johnson, K., S. Anderson, and C. S. Jacobson. 1996. Phenotypic and genotypic characterization of phenanthrene-degrading fluorescent *Pseudomonas* biovars. *Applied and Environmental Microbiology*. **62:** 3818-3825.

Karlen, Y., A. McNair, S. Perseguers, C. Mazza, and N. Mermod. 2007. Statistical significance of quantitative PCR. *BMC Bioinformatics*. **8:** 131.

Kok, R. G., C. B. Nudel, R. H. Gonzalez, I. M. Nugteren-Roodzant, K. J. Hellingwerf. 1996. Physiological factors affecting production of extracellular lipase (LipA) in *Acinetobacter calcoaceticus* BD413: fatty acid repression of *lip*A expression and degradation of LipA. *Journal of Bacteriology*. **178:** 6025-6035.

Kok, R. G., J. J. Van Thor, I. M. Nugteren-Roodzant, B. Vosman, and K. J. Hellingwerf. 1995. Characterization of lipase-deficient mutants of *Acinetobacter calcoaceticus* BD413: Identification of a periplasmic lipase chaperone essential for the production of extracellular lipase. *Journal of Bacteriology*. **177:** 3295-3307.

Kubista, M., J. M Andrade, M. Bengtsson, A. Forootan, J. Jonák, K. Lind, R. Sindelka, R. Sjöback, B. Sjögreen, L. Strömbom, A. Ståhlberg, and N. Zoric. 2006. The real-time polymerase chain reaction. *Molecular Aspects of Medicine*. **27:** 95-125.

Laurie, A. D., and G. Lloyd-Jones. 2000. Quantification of *phnAc* and *nahAc* in contaminated New Zealand soils by competitive PCR. *Applied and Environmental Microbiology*. **66:** 1814-1817.

Leahy, J. G., and R. R. Colwell. 1990. Microbial degradation of hydrocarbons in the environment. *Microbiological Reviews*. **54:** 305-315.

Lee, H. J., J. Basran, and N. S. Scrutton. 1998. Electron transfer from flavin to iron in the *Pseudomonas oleovorans* rubredoxin reductase-rubredoxin electron transfer complex. *Biochemistry*. **37:** 15513-15522.

Livak, K. J. 1997. ABI Prism 7700 Sequence Detection System, User Bulletin 2. PE Applied Biosystems, Foster City, CA.

Livak, K. J., and T. D. Schmittgen. 2001. Analysis of relative gene expression data using real-time quantitative and $2^{[-\Delta\Delta CT]}$ Method. *Methods*. **25:** 402-408.

Liu, W., and D. A. Saint. 2002. A new quantitative method of real time reverse transcription polymerase chain reaction assay based on simulation of polymerase chain reaction kinetics. *Analytical Biochemistry*. **302:** 52-59.

Maeng, J. H., Y. Sakai, Y. Tani, and N. Kato. 1996. Isolation and characterization of a novel oxygenase that catalyzes the first step of *n*-alkane oxidation in *Acinetobacter* sp. strain M-1. *Journal of Bacteriology*. **178:** 3695-3700.

Mackay, I. M. 2004. Real-time PCR in the microbiology laboratory. *Clinical Microbiology and Infectious Diseases*. **10:** 190-212.

Mackay, I. M., K. E. Arden, and A. Nitsche. 2002. Real-time PCR in virology. *Nucleic Acids Research.* **30:** 1292-1305.

Manchester, K. L.1996. Use of UV methods for measurement of protein and nucleic acid concentrations. *Biotechniques.* **20:** 968-970.

Mandri, T., and J. Lin. 2007. Isolation and characterization of engine oil degrading indigenous microorganisms in KwaZulu-Natal, South Africa. *African Journal of Biotechnology.* **6:** 23-27.

Marchesi, J. R., T. Sato, A. J. Weightman, T. A. Martin, J. C. Fry, S. H. Hiom, and W. G. Wade. 1998. Design and evaluation of useful bacterium-specific PCR primers that amplify genes coding for bacterial 16S rRNA. *Applied and Environmental Microbiology* **64:** 795-799.

Margesin, R., A. Zimmerbauer, and F. Schinner. 2000. Monitoring of bioremediation by soil biological activities. *Chemosphere.* **40:** 339-346.

Marín, M., A. Pedregosa, S. Ríos, M. L. Ortiz, and F. Laborda. 1995. Biodegradation of diesel and heating oil by *Acinetobacter calcoaceticus* MM5: Its possible applications on bioremediation. *International Biodeterioration and Biodegradation*. 269-285.

Marín, M., L. Yuste, and F. Rojo. 2003. Differential expression of the components of the two alkane hydroxylases from *Pseudomonas aeruginosa. Journal of Bacteriology*. **185:** 3232-3237.

Markovetz, A. J. 1971. Subterminal oxidation of aliphatic hydrocarbons by microorganisms. *Critical Reviews in Microbiology.* **1:** 225-238.

Marquez-Rocha, F. J., V. Hernandez-Rodriguez, and M. T. Lamela. 2001. Biodegradation of diesel oil in soil by a microbial consortium. *Water, Air, and Soil Pollution*. **128:** 313-320.

Mattick, J. S. 2002. Type IV pili and twitching motility. *Annual Review of Microbiology*. **56:** 289-314.

May, S. W., and A. G. Katoposis. 1990. Hydrocarbon monooxygenase system of *Pseudomonas oleovorans*. *Methods in Enzymology*. **188:** 3-9.

Molina-Barahona, L., R. Rodrìguez-Vázquez, M. Hernández-Velasco, C. Vega-Jarquìn, O. Zapata-Pérez, A. Mendoza-Cantú, and A. Albores. 2004. Diesel removal

from contaminated soils by biostimulation and supplementation with crop residues. *Applied Soil Ecology*. **27:** 165-175.

Nakar, D., and D. L. Gutnick. 2001. Analysis of the *wee* gene cluster responsible for the biosynthesis of the polymeric bioemulsifier from the oil-degrading strain *Acinetobacter lwoffii* RAG-1. *Microbiology*. **147:**1937-1946.

Nolan, T., R. E. Hands, and S. A. Bustin. 2006. Quantification of mRNA using real-time RT-PCR. *Nature Protocols*. **1:** 1559-1582.

Okuda, H. 1991. Esterases. *In* Kuby S. A (Ed.), A study of enzymes. pp. 563-577. CRC Press, Boca Raton, Florida.

Parche, S., W. Geißdörfer, and W. Hillen. 1997. Identification and characterization of *xcpR* encoding a subunit of the general secretory pathway necessary for dodecane degradation in *Acinetobacter calcoaceticus* ADP1. *Journal of Bacteriology.* **179:** 4631-4634.

Park, M. O. 2005. New pathway for long-chain *n*-alkane synthesis via l-alcohol in *Vibrio furnissii* M1. *Journal of Bacteriology*. **187:** 1426-1429.

Paul, J. H., and W. H. Jeffrey. 1985. Evidence for separate adhesion mechanisms for hydrophilic and hydrophobic surfaces in *Vibrio proteolytica*. *Applied and Environmental Microbiology*. **50:** 431-437.

Pfaffl, M. W. 2001. A new mathematical model for relative quantification in real-time RT-PCR. *Nucleic Acids Research.* **29:** 2002-2007.

Pfaffl, **M. W.** 2004. Quantification strategies in real-time PCR. *In* Bustin, S. A. (Ed.), The real-time PCR encyclopaedia A-Z of quantitative PCR. pp. 1-20. International University Line, La Jolla, California.

Pfaffl, M. W. 2005. Nucleic acids: mRNA identification and quantification. *In* Worsfold, P. J., Gallagher, P. K. (Eds.), Nucleic Acids, Encyclopedia of Analytical Science, second edition. pp. 417-426. Academic Press, ISBN 0-12-764100-9.

Pfaffl, **M. W., and M. Hageleit.** 2001. Validities of mRNA quantification using recombinant RNA and recombinant DNA external calibration curves in real-time RT-PCR. *Biotechnology letters*. **23:** 275-282.

Pfaffl, M. W., G. W. Horgan, and L. Dempfle. 2002. Relative Expression Software Tool (REST-XL) for group-wise comparison and statistical analysis of relative expression results in real-time PCR. *Nucleic Acids Research.* **30:** e36.

Pfaffl, M. W., A. Tichopad, C. Prgomet, and T. P. Neuvians. 2004. Determination of stable housekeeping genes, differentially regulated target genes and sample integrity: BestKeeper - Excel-based tool using pair-wise correlations. *Biotechnology Letters* **26:** 509-515.

Plohl K, H. Leskovšek, M. Bricelj. 2002. Biological degradation of motor oil in water. *Acta Chimica Slovenica.* **49:** 279-289.

Prince, R. C. 1997. Bioremediation of marine oil spills. Trends in Biotechnology. **15:** 158-160.

Pines, O., E. A. Bayer, and D. L. Gutnick. 1983. Localization of emulsan-like polymers associated with the cell surface of *Acinetobacter calcoaceticus*. *Journal of Bacteriology*. **154:** 893-905.

Pugsley, A. P. 1993. The complete general secretory pathway in Gram-negative bacteria. *Microbiological Reviews*. **57:** 50-108.

Rasmussen, R. P. 2001. Quantification on the LightCycler. *In* Meuer, S., C. Wittwer, K. Nakagawara. (Eds.). Rapid cycle real-time PCR, methods and applications. pp. 21-34. Springer Press. Heidelberg.

Ratajczak, A., W. Geißdörfer, and W. Hillen. 1998. Expression of alkane hydroxylase from A*cinetobacter* sp. strain ADP1 is induced by a broad range of *n*-alkanes and requires the transcriptional activator AlkR. *Journal of Bacteriology*. **180:** 5822-5827.

Rehm, H., and I. Reiff. 1981. Mechanism and occurrence of microbial oxidation of long-chain alkanes. *Advances in Biochemical Engineering*. **19:** 175-215.

Rosenberg, E., A. Zuckerberg, C. Rubinovitz, and D. L. Gutnick. 1979. Emulsifier of *Arthrobacter* RAG-1: isolation and emulsifying properties. *Applied and Environmental Microbiology.* **37:** 402-408.

Rosenberg, M., E. A. Bayer, L. Delarea, and E. Rosenberg. 1982. Role of thin fimbriae in adherence and growth of *Acinetobacter calcoaceticus* RAG-1 on hexadecane. *Applied and Environmental Microbiology*. **44:** 929-937.

Rusansky, S., R. Avigad, S. Michaeli, and D. L. Gutnick. 1987. Involvement of a plasmid in growth on and dispersion of crude oil by *Acinetobacter calcoaceticus* RA57. *Applied and Environmental Microbiology*. **53:** 1918-1923.

Samanta, K. S, O. V. Singh, and R. K. Jain. 2002. Polycyclic aromatic hydrocarbons: environmental pollution and bioremediation. *Trends in Biotechnology*. **20:** 243-248.

Sambrook, J., E. F. Fritsch, and T. Maniatis. 1989. Molecular cloning: a laboratory manual, second ed. Cold Spring Harbor Laboratory Press, Cold Spring Harbor, New York.

Sarkar, D., M. Ferguson, R. Datta, and S. Birnbaum. 2005. Bioremediation of petroleum hydrocarbons in contaminated soils: comparison of biosolids addition, carbon supplementation, and monitored natural attenuation. *Environmental Pollution*. **136:** 187-195.

Schindler, D. B., B. F. Scott, and D. B. Carlisle. 1975. Effect of crude oil on populations of bacteria and algae in artificial ponds subject to winter weather and ice formation. *Verhandlungen Internationale Vereinigung fur Theoretische und Angewandte Limnologie* **19:** 2138-2144.

Schoor, O., T. Weinschenk, J. Hennenlotter, S. Corvin, A. Stenzl, H. G. Rammensee, and S. Stevanovic. 2003. Moderate degradation does not preclude microarray analysis of small amounts of RNA. *BioTechniques.* **35:** 1192-1201.

Shabtai, Y., and D. L. Gutnick. 1985. Exocellular esterase and emulsan release from the cell surface of *Acinetobacter calcoaceticus*. *Journal of Bacteriology*. **161:** 1176-1181.

Sharkey, F. H., I. M. Banat, and R. Marchant. 2004. Detection and quantification of gene expression in environmental bacteriology. *Applied and Environmental Microbiology.* **70:** 3795-3806.

Sikkema, J., J. A. M. de Bont, and B. Poolman. 1995. Mechanisms of membrane toxicity of hydrocarbons. *Microbiological Reviews*. **59:** 201-222.

Singer, M. E., and W. R. Finnerty. 1985. Fatty aldehyde dehydrogenases in *Acinetobacter* sp. strain HO1-N: role in hexadecane and hexadecanol metabolism. *Journal of Bacteriology*. **164:** 1011-1016.

Singh, C., and J. Lin. 2008. Isolation and characterization of diesel oil degrading indigenous microorganisms in Kwazulu-Natal, South Africa. *African Journal of Biotechnology*. **7:** 1927-1932.

Söhngen, N. L. 1913. Benzin, petroleum, paraffinöl und paraffin als kohlenstoff - und Energiequelle für Mikroben. *Zentr Bacteriol Parasitenk* Abt II. **37:** 595-609.

Sorkhoh, **N. A., R. H. Al-Hasan, M. Khanafer, and S. S. Radwan.** 1995. Establishment of oil-degrading bacteria associated with cyanobacteria in oil-polluted soil. *Journal of Applied Bacteriology.* **78:** 194-199.

Souaze, F., A. Ntodou-Thome, C. Y. Tran, W. Rostene, and P. Forgez. 1996. Quantitative RT-PCR: limits and accuracy. *BioTechniques.* **21:** 280-285.

Speight, G. J. 2002. Handbook of petroleum product analysis. pp. 1-127. *John Wiley and Sons*, Inc., Hoboken, New Jersey.

Stahlberg, A., J. Hakansson, X. Xian, H. Semb, and M. Kubista. 2004. Properties of the reverse transcription reaction in mRNA quantification. *Clinical Chemistry*. **50:** 509-515.

Swannell, R. P. J., K. Lee, and M. McDonagh. 1996. Field Evaluations of marine oil spill bioremediation. *Microbiological Reviews*. **60:** 342-365.

Tani, A., T. Ishige, Y. Sakai, and N. Kato. 2001. Gene structures and regulation of the alkane hydroxylase complex in *Acinetobacter* sp. strain M-1. *Journal of Bacteriology*. **183:** 1819-1823.

Tani, A, T. Ishige, Y. Sakai, and N. Kato. 2002. Two acyl-CoA dehydrogenases of *Acinetobacter* sp. strain M-1 that uses very long-chain *n*-alkanes. *Journal of Bioscience and Bioengineering*. **94:** 326-329.

Tani, A., Y. Sakai, T. Ishige, and N. Kato. 2000. Thermostable $NADP^+$-dependent medium-chain alcohol dehydrogenase from *Acinetobacter* sp. strain M-l: purification and characterization and gene expression in *Escherichia coli. Applied and Environmental Microbiology*. **66:** 523l-5235.

Teo, I. A., J. W. Choi, J. Morlese, G. Taylor, and S. Shaunak. 2002. LightCycler qPCR optimization for low copy number target DNA. *Journal of Immunological Methods* **270:** 119-133.

Thellin, O., W. Zorzi, B. Lakaye, B. De Borman, B. Coumans, G. Hennen, T. Grisar, A. Igout, and E. Heinen. 1999. Housekeeping genes as internal standards: use and limits. *Journal of Biotechnology.* **75:** 291-295.

Thornley, M. J., K. J. I. Thorne, and A. M. Glauert. 1974. Detachment and chemical characterization of the regularly arranged subunits from the surface of an *Acinetobacter*. *Journal of Bacteriology*. **118:** 654-662.

Tommassen, J., A. Filloux, M. Bally, M. Murgier, and A. Lazdunski. 1992. Protein secretion in *Pseudomonas aeruginosa*. *FEMS Microbiology Reviews.* **103:** 73-90.

Tookey, D., and J. Abbott. 1991. Clean-up of soft sediments, phase 2 trials at Steart flats. WSL report CR 3643. National Environmental Technology Center, AEA Technology, Culham, Abingdon, United Kingdom.

U.S. Congress Office of Technology Assessment. 1991. Bioremediation of marine oil spills - background paper. OTA-BP-0-70. U.S. Government Printing Office, Washington, D.C.

Valasek, M. A., and J. J. Repa. 2005. The power of real-time PCR. *Advances in Physiology Education.* **29:** 151-159.

van Beilen , J. B., and E. G. Funhoff. 2007. Alkane hydroxylases involved in microbial alkane degradation. *Applied Microbiology and Biotechnology*. **74:** 13-21.

van Beilen, J. B., E. G. Funhoff, A. van Loon, A. Just, L. Kaysser, M. Bouza, R. Holtackers, M. Röthlisberger, Z. Li, and B. Witholt. 2006. Cytochrome P450 alkane

hydroxylases of the CYP153 family are common in alkane-degrading eubacteria lacking integral membrane alkane hydroxylases. *Applied and Environmental Microbiology*. **72:** 59-65.

van Beilen, J. B., J. Kingma, and B. Witholt. 1994a. Substrate specificity of the alkane hydroxylase system of *Pseudomonas oleovorans* GPo1. *Enzyme and Microbial Technology.* **16:** 904-911.

van Beilen, J. B., Z. Li, W. A. Duetz, T. H. M. Smits, and B. Witholt. 2003. Diversity of alkane hydroxylase systems in the environment. *Oil and Gas Science and Technology*. **58:** 427-440.

van Beilen, J. B., M. Neuwenschwander, T. H. M. Smits, C. Roth, S. B. Balada, and B. Witholt. 2002. Rubredoxins involved in alkane oxidation. *Journal of Bacteriology.* **184:** 1722-1732.

van Beilen, J. B., M. G. Wubbolts, and B. Witholt. 1994b. Genetics of alkane oxidation by *Pseudomonas oleovorans*. *Biodegradation.* **5:** 161-174.

Vandesompele, J., K. De Preter, F. Pattyn, B. Poppe, N. Van Roy, A. De Paepe, and F. Speleman. 2002. Accurate normalization of real-time quantitative RT-PCR data by geometric averaging of multiple internal control genes. *Genome Biology*. **3:** 0034.1-0034.11. http://genomebiology.com/2002/3/7/research/0034. January 2007

Van Hamme, J. D., A. Singh, and O. P. Ward. 2003. Recent advances in petroleum microbiology. *Microbiology and Molecular Biology Reviews*. **60:** 503-549.

Whyte, L. G., T. H. M. Smits, D. Labbé, B. Witholtm, C. W. Greer, and J. B. van Beilen. 2002. Gene cloning and characterization of multiple alkane hydroxylase systems in *Rhodococcus* Strains Q15 and NRRL B-16531 *Applied and Environmental Microbiology*. **68:** 5933-5942.

Wilderman, P. J., A. I. Vasil, Z. Johnson, M. J. Wilson, H. E. Cunliffe, L. L. Lamont, and M. L. Vasil. 2001. Characterization of an endoprotease (PrpL) encoded by a PvdS-regulated gene in *Pseudomonas aeruginosa. Infection and Immunity.* **69:** 5385-5394.

Wilhelm, J., and A. Pingoud. 2003. Real-time polymerase chain reaction. *ChemBioChem*. **4:** 1120-1128.

Winer, J., C. K. Jung, I. Shackel, and P. M. Williams. 1999. Development and validation of real-time quantitative reverse transcriptase-polymerase chain reaction for monitoring gene expression in cardiac myocytes *in vitro*. *Analytical Biochemistry*. **270:** 41-49.

Witholt, B., M. J. de Smet, J. Kingma, J. B. van Beilen, M. Kok, R. G. Lageveen, and G. Eggink. 1990. Bioconversions of aliphatic compounds by *Pseudomonas oleovorans* in multiphase bioreactors: background and economic potential. *Trends in Biotechnology*. **8:** 46-52.

Wittwer, C. T., G. C. Fillmore, and D. R. Hillyard. 1989. Automated polymerase chain reaction in capillary tubes with hot air. *Nucleic Acids Research*. **17:** 4353-4357.

Wittwer, C. T., M. G. Herrmann, C. N. Gundry, and K. S. Elenitoba-Johnson. 2001. Real-time multiplex PCR assays. *Methods.* **25:** 430-442.

Wittwer, C. T., M. G. Herrmann, A. A. Moss, and R. P. Rasmussen. 1997. Continuous fluorescence monitoring of rapid cycle DNA amplification. *Biotechniques.* **22:** 130-138.

Wong, M. L., and J. F. Medrano. 2005. Real-time PCR for mRNA quantitation. *BioTechniques.* **39:** 75-85.

Wouters, J., B. Bergman, and S. Janson. 2003. Cloning and expression of a putative cyclodextrin glucosyltransferase from the symbiotically competent cyanobacterium *Nostoc* sp. PCC 9229. *FEMS Microbiology Letters.* **219:** 181-185.

Yuan, J. S., A. Reed, F. Chen, and C. N. Stewart Jr. 2006. Statistical analysis of real-time PCR data. *BMC Bioinformatics*. **7:** 85.

Yun, J. J., L. E. Heisler, I. I. L. Hwang, O. Wilkins, S. K. Lau, M. Hyrcza, B. Jayabalasingham, J. Jin, J. McLaurin, M. Tsao, and S. D. Der. 2006. Genomic DNA functions as a universal external standard in quantitative real-time PCR. *Nucleic Acids Research.* **34:** e85.

Zamorano, P. L, V. B. Mahesh, and D. W. Brann. 1996. Quantitative RT-PCR for neuroendocrine studies. A minireview. *Neuroendocrinology.* **63:** 397-407.

7. APPENDICES

APPENDIX I

Composition of media and reagents

Bushnell-Haas (BH) Broth

1.00 g K_2HPO_4

1.00 g KH_2PO_4

1.00 g NH_4NO_3

0.02 g $CaCl_2.2H_2O$

0.20 g $MgSO_4.7H_2O$

0.05 g $FeCl_3$

Bring to 1 litre with distilled water, pH 7

Luria Bertani (LB) Broth

10.0 g tryptone

5.00 g yeast extract

10.0 g NaCl

Bring to 1 litre with distilled water.

Phosphate Buffered Saline (PBS)

8.00 g NaCl

0.20 g KCl

1.44 g Na_2HPO_4

0.24 g KH_2PO_4

Bring to 1 litre with distilled water, pH 7.6

Tris Acetate EDTA (TAE) 50× buffer (pH 8.3)

242 g Tris base

57.1 ml Glacial acetic acid

100 ml 0.5M EDTA stock (pH 8.0)

Add Tris base and EDTA stock to 500ml of distilled water.

Add glacial acetic acid.

Bring to 1 litre with distilled water.

Gel loading buffer

0.25% bromophenol blue (0.125 g)

40% sucrose (20 g in 50 ml distilled water)

Filter sterilize through 0.22 μm pore size filter.

APPENDIX II

16S rRNA gene sequencing of isolates

```
Consensus   TAATGCTTAGGAATCTGCCTATTAGTGGGGGcACAACATTTCGAAAGGAATGCTAATACC   120
JL11        TAATGCTTAGGAATCTGCCTATTAGTGGGGG.ACAACATTTCGAAAGGAATGCTAATACC
LT1A        TAATGCTTAGGAATCTGCCTATTAGTGGGGG.ACAACATTTCGAAAGGAATGCTAATACC
LT1         TAATGCTTAGGAATCTGCCTATTAGTGGGGGCACAACATTTCGAAAGGAATGCTAATACC
V2          TAATGCTTAGGAATCTGCCTATTAGTGGGGG.ACAACATTTCGAAAGGAATGCTAATACC

Consensus   GCATACGTCCTACGGGAGAAAGCAGGGGATCTTCGGACCTTGCGCTAATAGATGAGCCTA   180
JL11        GCATACGTCCTACGGGAGAAAGCAGGGGATCTTCGGACCTTGCGCTAATAGATGAGCCTA
LT1A        GCATACGTCCTACGGGAGAAAGCAGGGGATCTTCGGACCTTGCGCTAATAGATGAGCCTA
LT1         GCATACGTCCTACGGGAGAAAGCAGGGGATCTTCGGACCTTGCGCTAATAGATGAGCCTA
V2          GCATACGTCCTACGGGAGAAAGCAGGGGATCTTCGGACCTTGCGCTAATAGATGAGCCTA

Consensus   AGTCGGATTAGCTAGTTGGTGGGGTAAAGGCCTACCAAGGCGACGATCTGTAGCGGGTCT   240
JL11        AGTCGGATTAGCTAGTTGGTGGGGTAAAGGCCTACCAAGGCGACGATCTGTAGCGGGTCT
LT1A        AGTCGGATTAGCTAGTTGGTGGGGTAAAGGCCTACCAAGGCGACGATCTGTAGCGGGTCT
LT1         AGTCGGATTAGCTAGTTGGTGGGGTAAAGGCCTACCAAGGCGACGATCTGTAGCGGGTCT
V2          AGTCGGATTAGCTAGTTGGTGGGGTAAAGGCCTACCAAGGCGACGATCTGTAGCGGGTCT

Consensus   GAGAGGATGATCCGCCACACTGGGACTGAGACACGGCCCAGACTCCTACGGGAGGCAGCA   300
JL11        GAGAGGATGATCCGCCACACTGGGACTGAGACACGGCCCAGACTCCTACGGGAGGCAGCA
LT1A        GAGAGGATGATCCGCCACACTGGGACTGAGACACGGCCCAGACTCCTACGGGAGGCAGCA
LT1         GAGAGGATGATCCGCCACACTGGGACTGAGACACGGCCCAGACTCCTACGGGAGGCAGCA
V2          GAGAGGATGATCCGCCACACTGGGACTGAGACACGGCCCAGACTCCTACGGGAGGCAGCA

Consensus   GTGGGGAATATTGGACAATGGGCGSAAGCCTGATCCAGCCATGCCGCGTGTGTGAAGAAG   360
JL11        GTGGGGAATATTGGACAATGGGCGCAAGCCTGATCCAGCCATGCCGCGTGTGTGAAGAAG
LT1A        GTGGGGAATATTGGACAATGGGCGCAAGCCTGATCCAGCCATGCCGCGTGTGTGAAGAAG
LT1         GTGGGGAATATTGGACAATGGGCGCAAGCCTGATCCAGCCATGCCGCGTGTGTGAAGAAG
V2          GTGGGGAATATTGGACAATGGGCGGAAGCCTGATCCAGCCATGCCGCGTGTGTGAAGAAG

Consensus   GCCTTATGGTTGTAAAGCACTTTAAGCGAGGAGGAGGCTACTTTAGTTAATACCTAGAGA   420
JL11        GCCTTATGGTTGTAAAGCACTTTAAGCGAGGAGGAGGCTACTTTAGTTAATACCTAGAGA
LT1A        GCCTTATGGTTGTAAAGCACTTTAAGCGAGGAGGAGGCTACTTTAGTTAATACCTAGAGA
LT1         GCCTTATGGTTGTAAAGCACTTTAAGCGAGGAGGAGGCTACTTTAGTTAATACCTAGAGA
V2          GCCTTATGGTTGTAAAGCACTTTAAGCGAGGAGGAGGCTACTTTAGTTAATACCTAGAGA

Consensus   TAGTGGACGTTACTCGCAGAATAAGCACCGGCTAACTCTGTGCCAGCAGCCGCGGTAATA   480
JL11        TAGTGGACGTTACTCGCAGAATAAGCACCGGCTAACTCTGTGCCAGCAGCCGCGGTAATA
LT1A        TAGTGGACGTTACTCGCAGAATAAGCACCGGCTAACTCTGTGCCAGCAGCCGCGGTAATA
LT1         TAGTGGACGTTACTCGCAGAATAAGCACCGGCTAACTCTGTGCCAGCAGCCGCGGTAATA
V2          TAGTGGACGTTACTCGCAGAATAAGCACCGGCTAACTCTGTGCCAGCAGCCGCGGTAATA

Consensus   CAGAGGGTGCAAGCGTTAATCGGATTTACTGGGCGTAAAGCGCGCGTAGGCGGCTAATTA   540
JL11        CAGAGGGTGCAAGCGTTAATCGGATTTACTGGGCGTAAAGCGCGCGTAGGCGGCTAATTA
LT1A        CAGAGGGTGCAAGCGTTAATCGGATTTACTGGGCGTAAAGCGCGCGTAGGCGGCTAATTA
LT1         CAGAGGGTGCAAGCGTTAATCGGATTTACTGGGCGTAAAGCGCGCGTAGGCGGCTAATTA
V2          CAGAGGGTGCAAGCGTTAATCGGATTTACTGGGCGTAAAGCGCGCGTAGGCGGCTAATTA

Consensus   AGTCAAATGTGAAATCCCCGAGCTTAACTTGGGAATTGCATTCGATACTGGTTAGCTAGA   600
JL11        AGTCAAATGTGAAATCCCCGAGCTTAACTTGGGAATTGCATTCGATACTGGTTAGCTAGA
LT1A        AGTCAAATGTGAAATCCCCGAGCTTAACTTGGGAATTGCATTCGATACTGGTTAGCTAGA
LT1         AGTCAAATGTGAAATCCCCGAGCTTAACTTGGGAATTGCATTCGATACTGGTTAGCTAGA
V2          AGTCAAATGTGAAATCCCCGAGCTTAACTTGGGAATTGCATTCGATACTGGTTAGCTAGA
```

Fig IIa Partial 16S rRNA gene sequence alignment of JL11, LT_1, LT_1A and, V_2.

```
Consensus   GTGTGGGAGAGGATGGTAGAATTCCAGGTGTAGCGGTGAAATGCGTAGAGATCTGGAGGA   660
JL11        GTGTGGGAGAGGATGGTAGAATTCCAGGTGTAGCGGTGAAATGCGTAGAGATCTGGAGGA
LT1A        GTGTGGGAGAGGATGGTAGAATTCCAGGTGTAGCGGTGAAATGCGTAGAGATCTGGAGGA
LT1         GTGTGGGAGAGGATGGTAGAATTCCAGGTGTAGCGGTGAAATGCGTAGAGATCTGGAGGA
V2          GTGTGGGAGAGGATGGTAGAATTCCAGGTGTAGCGGTGAAATGCGTAGAGATCTGGAGGA

Consensus   ATACCGATGGCGAAGGCAGCCATCTGGCCTAACACTGACGCTGAGGTGCGAAAGCATGGG   720
JL11        ATACCGATGGCGAAGGCAGCCATCTGGCCTAACACTGACGCTGAGGTGCGAAAGCATGGG
LT1A        ATACCGATGGCGAAGGCAGCCATCTGGCCTAACACTGACGCTGAGGTGCGAAAGCATGGG
LT1         ATACCGATGGCGAAGGCAGCCATCTGGCCTAACACTGACGCTGAGGTGCGAAAGCATGGG
V2          ATACCGATGGCGAAGGCAGCCATCTGGCCTAACACTGACGCTGAGGTGCGAAAGCATGGG

Consensus   GAGCAAACAgGATTAGATACCCTGGTAGTCCATGCCGTAAACGATGTCTACTAGCCGTTG   780
JL11        GAGCAAACAGGATTAGATACCCTGGTAGTCCATGCCGTAAACGATGTCTACTAGCCGTTG
LT1A        GAGCAAACAGGATTAGATACCCTGGTAGTCCATGCCGTAAACGATGTCTACTAGCCGTTG
LT1         GAGCAAACAGGATTAGATACCCTGGTAGTCCATGCCGTAAACGATGTCTACTAGCCGTTG
V2          GAGCAAACA.GATTAGATACCCTGGTAGTCCATGCCGTAAACGATGTCTACTAGCCGTTG

Consensus   GGGCCTTTGAGGCTTTAGTGGCGCAGCTAACGCGATAAGTAGACSSCYKgGGGAGTACGG   840
JL11        GGGCCTTTGAGGCTTTAGTGGCGCAGCTAACGCGATAAGTAGACCGCCTGGGGAGTACGG
LT1A        GGGCCTTTGAGGCTTTAGTGGCGCAGCTAACGCGATAAGTAGACGCCT..GGGAGTACGG
LT1         GGGCCTTTGAGGCTTTAGTGGCGCAGCTAACGCGATAAGTAGACGCCTG.GGGAGTACGG
V2          GGGCCTTTGAGGC
```

Fig IIa …Continued.

APPENDIX III

Table IIIa Computation of percentage diesel degradation

Sample	Mass of tube (g)	Mass of tube + diesel(g)	Mass of diesel (g)	% diesel remaining	% diesel degraded
LT_1					
Day 5	8.98	9.10	0.12	41.4	58.6
Day 10	8.93	9.03	0.10	34.5	65.5
Day 15	8.99	9.08	0.09	31.0	69.0
Day 20	9.07	9.13	0.06	20.7	79.3
Day 30	9.10	9.17	0.07	24.1	75.9
Day 40	8.91	8.99	0.08	27.6	72.3
Day 50	9.02	9.09	0.06	20.7	79.3
Day 60	9.07	9.11	0.04	13.8	86.2
LT_1A					
Day 5	8.89	9.03	0.14	48.3	51.7
Day 10	8.96	9.07	0.11	37.9	62.1
Day 15	9.09	9.18	0.09	31.0	69.0
Day 20	9.07	9.13	0.06	20.7	79.3
Day 30	8.99	9.07	0.08	27.6	72.3
Day 40	9.05	9.11	0.06	20.7	79.3
Day 50	9.10	9.02	0.08	27.6	72.3

Table IIIa Continued…

Day 60	8.91	8.96	0.05	17.2	82.8
V_2					
Day 5	9.07	9.22	0.15	51.7	48.3
Day 10	8.97	9.09	0.12	41.4	58.6
Day 15	9.05	9.10	0.05	17.2	82.8
Day 20	9.03	9.10	0.07	24.1	75.9
Day 30	9.04	9.10	0.06	20.7	79.3
Day 40	9.03	9.07	0.04	13.8	86.2
Day 50	9.04	9.09	0.05	17.2	82.8
Day 60	9.06	9.09	0.03	10.3	89.7
Control					
Day 0	9.07	9.39	0.32	100	0
Day 60	9.03	9.32	0.29	90.6	9.40

APPENDIX IV

Table IVa Reaction composition for cDNA synthesis

Isolate	Component volume per 20 µl reaction*	
	Nuclease-free water (µl)	RNA template (µl)
LT_1		
Day 10	12.6	2.40
Day 15	11.5	3.50
Day 20	10.4	4.60
Day 30	12.1	2.90
Day 40	12.8	2.20
Day 50	12.9	2.10
Day 60	12.9	2.10
LT_1A		
Day 5	11.3	3.70
Day 15	9.40	5.60
Day 20	12.5	2.50
Day 30	11.1	3.90
Day 40	13.2	1.80
Day 50	12.7	2.30
Day 60	12.3	2.70
V_2		
Day 5	0.40	14.6
Day 10	8.80	6.20
Day 15	11.6	3.40
Day 20	12.5	2.50
Day 30	13.3	1.70
Day 40	13.1	1.90
Day 50	13.7	1.30
Day 60	13.0	2.00

* Each 20 µl reaction contained 4 µl 5×iScript Reaction Mix and 1 µl iScript Reverse Transcriptase (BIORAD)

APPENDIX V

Relative standard curves

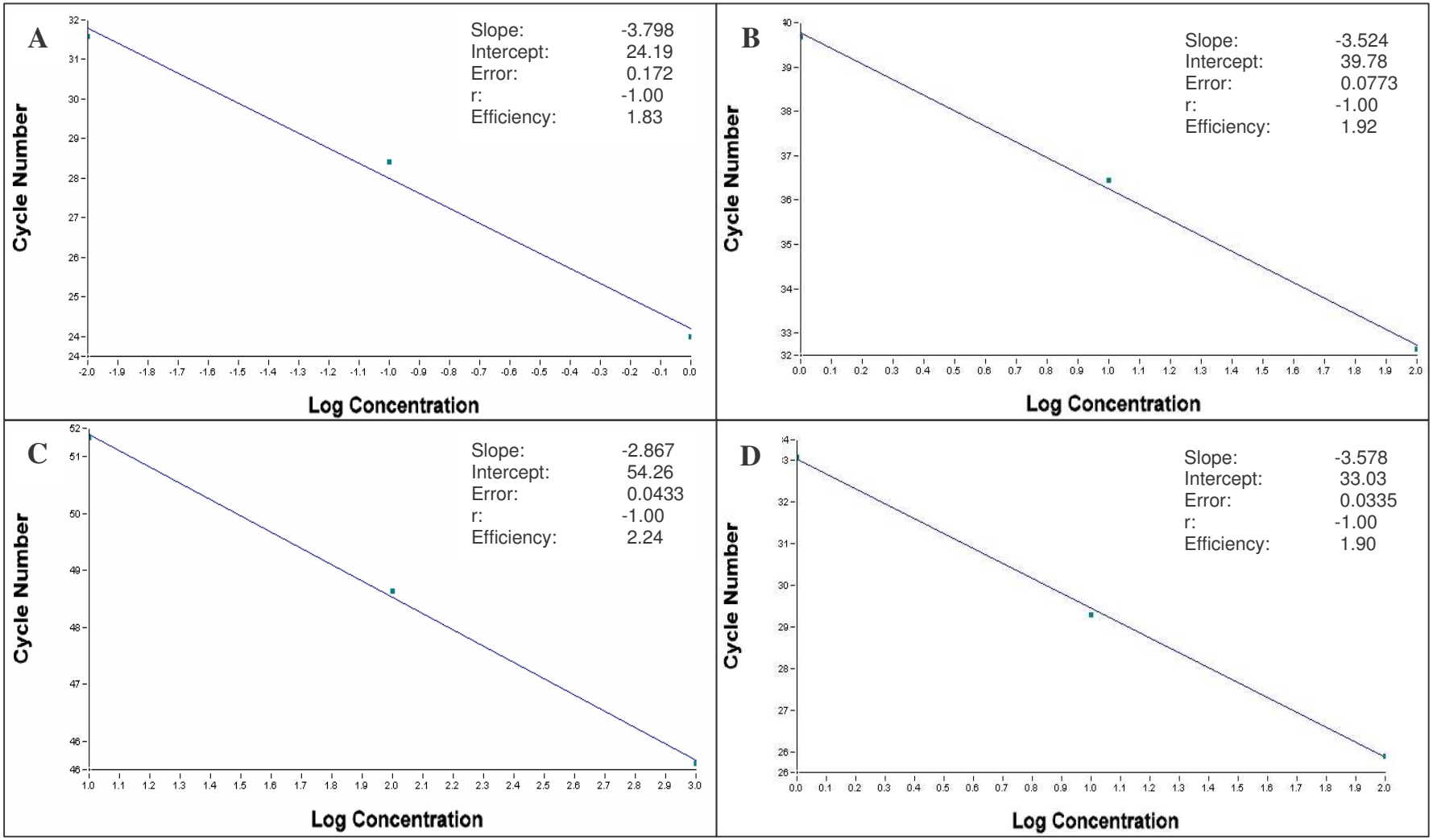

Fig. Va Relative standard curves. Standard curves of **(A)** 16s rRNA, **(B)** *alkM*, **(C)** *alkR*, **(D)** *rubA*, **(E)** *lipB*, **(F),** *xcpR*, and **(G)** *estB* were generated by the LightCycler Software, Version 3.5. Correlation coefficients (r) and amplification efficiencies (*E*) are shown.

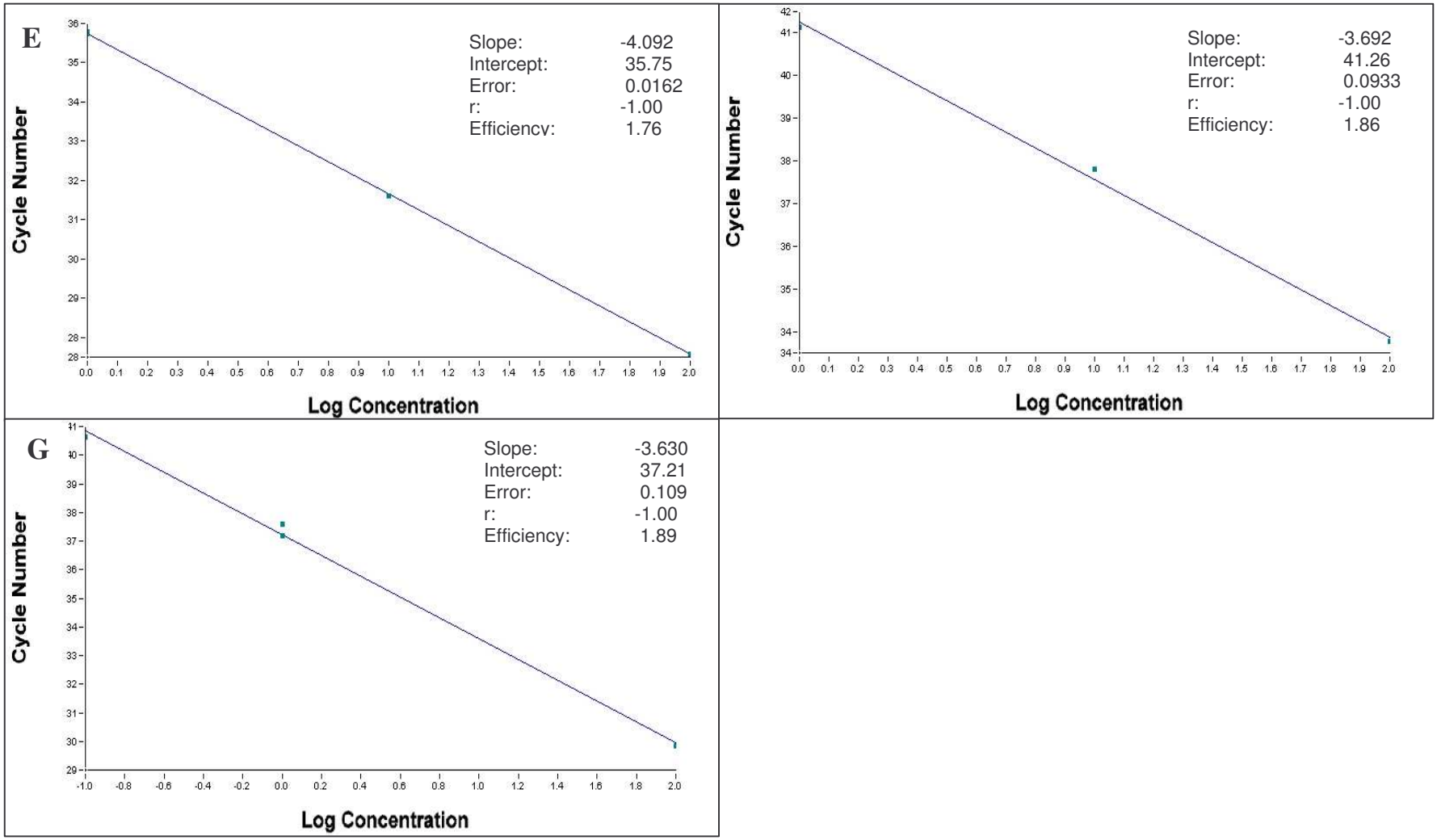

Fig. Va … Continued.

APPENDIX VI

Crossing point data

Table VIa Crossing point values for 16S rRNA gene

Sample	Crossing point (C_p)	2^{-Cp}
LT_1		
Day 10	13.22	1.0E-04
Day 15	11.67	3.1E-04
Day 20	13.56	8.3E-05
Day 30	11.85	2.7E-04
Day 40	12.16	2.2E-04
Day 50	13.09	1.4E-04
Day 60	10.32	7.8E-04
LT_1A		
Day 5	8.575	2.6E-03
Day 15	9.514	1.4E-03
Day 20	11.57	3.3E-04
Day 30	11.78	2.8E-04
Day 40	11.71	3.0E-04
Day 50	9.913	1.0E-03
Day 60	12.86	1.4E-04
V_2		
Day 5	11.77	2.9E-04
Day 10	13.85	6.8E-05
Day 15	9.542	1.3E-03
Day 20	10.56	6.6E-04
Day 30	9.771	1.2E-03
Day 40	11.31	3.9E-04
Day 50	16.86	8.4E-06
Day 60	14.56	4.1E-05

Table VIb Crossing point values for *rubA*

Sample	Crossing point (C_p)	2^{-Cp}
LT_1		
Day 10	23.02	1.2E-07
Day 15	24.08	5.6E-08
Day 20	24.22	5.1E-08
Day 30	26.32	1.2E-08
Day 40	26.73	9.0E-09
Day 50	28.55	2.6E-09
Day 60	25.31	2.4E-08
LT_1A		
Day 5	28.08	3.5E-09
Day 15	25.86	1.6E-08
Day 20	25.04	3.0E-08
Day 30	24.04	6.0E-08
Day 40	26.71	9.1E-09
Day 50	26.88	8.1E-09
Day 60	27.96	3.8E-09
V_2		
Day 5	23.84	6.7E-08
Day 10	24.64	3.8E-08
Day 15	28.31	3.0E-09
Day 20	32.41	1.8E-10
Day 30	30.35	7.3E-10
Day 40	31.50	3.3E-10
Day 50	34.50	4.1E-11
Day 60	30.16	8.3E-10

Table VIc Crossing point values for *alkM*

Sample	Crossing point (C_p)	2^{-Cp}
LT_1		
Day 10	29.70	1.2E-09
Day 15	30.80	5.4E-10
Day 20	31.89	2.5E-10
Day 30	32.73	1.4E-10
Day 40	33.30	9.5E-11
Day 50	35.75	1.7E-11
Day 60	30.78	5.4E-10
LT_1A		
Day 5	34.93	3.1E-11
Day 15	32.66	1.5E-10
Day 20	34.28	4.8E-11
Day 30	32.73	1.4E-10
Day 40	32.05	2.3E-10
Day 50	35.04	2.8E-11
Day 60	33.66	7.4E-11
V_2		
Day 5	>46.00	<1.4E-14
Day 10	>46.00	<1.4E-14
Day 15	37.03	7.1E-12
Day 20	>46.00[a]	<1.4E-14
Day 30	>46.00[a]	<1.4E-14
Day 40	45.29[a]	2.3E-14
Day 50	44.68[a]	3.6E-14
Day 60	>46.00	<1.4E-14

[a] invalid C_p values as a result of multiple product formation.

Table VId Crossing point values for *alkR*

Sample	Crossing point (C_p)	2^{-Cp}
LT_1		
Day 10	35.46	2.1E-11
Day 15	36.56	9.9E-12
Day 20	38.06	3.5E-12
Day 30	39.89	9.8E-13
Day 40	39.50	1.3E-12
Day 50	44.50	4.0E-14
Day 60	42.41	1.7E-13
LT_1A		
Day 5	46.00	1.4E-14
Day 15	41.19	4.0E-13
Day 20	40.47	6.6E-13
Day 30	39.28	1.5E-12
Day 40	37.00	7.3E-12
Day 50	36.54	1.0E-11
Day 60	38.55	2.5E-12
V_2		
Day 5	42.09	2.1E-13
Day 10	40.66	5.8E-13
Day 15	>46.00	<1.4E-14
Day 20	>46.00	<1.4E-14
Day 30	>46.00	<1.4E-14
Day 40	>46.00	<1.4E-14
Day 50	37.62	4.7E-12
Day 60	42.74	1.4E-13

Table VIe Crossing point values for *xcpR*

Sample	Crossing point (C_p)	2^{-Cp}
LT_1		
Day 10	31.98	2.4E-10
Day 15	33.90	6.2E-11
Day 20	33.22	9.9E-11
Day 30	34.32	4.7E-11
Day 40	35.04	2.8E-11
Day 50	37.90	4.0E-12
Day 60	35.74	1.7E-11
LT_1A		
Day 5	36.92	7.7E-12
Day 15	35.04	2.8E-11
Day 20	35.71	1.8E-11
Day 30	34.94	3.0E-11
Day 40	34.97	3.0E-11
Day 50	40.67	5.7E-13
Day 60	35.71	1.8E-11
V_2		
Day 5	34.32[a]	4.7E-11
Day 10	36.43[a]	1.1E-11
Day 15	39.99[a]	9.2E-13
Day 20	37.59[a]	4.8E-12
Day 30	40.10[a]	8.5E-13
Day 40	39.65[a]	1.2E-12
Day 50	39.79[a]	1.1E-12
Day 60	41.30[a]	3.7E-13

[a] invalid C_p generated from multiple product formation.

Table VIf Crossing point values for *estB*

Sample	Crossing point (C_p)	2^{-Cp}
LT_1		
Day 10	>51.00	<4.4E-16
Day 15	42.71[p]	1.4E-13
Day 20	>51.00	<4.4E-16
Day 30	>51.00	<4.4E-16
Day 40	43.48[p]	8.2E-14
Day 50	>51.00	<4.4E-16
Day 60	>51.00	<4.4E-16
LT_1A		
Day 5	>51.00	<4.4E-16
Day 15	43.00[p]	1.1E-13
Day 20	>51.00	<4.4E-16
Day 30	>51.00	<4.4E-16
Day 40	>51.00	<4.4E-16
Day 50	44.88[p]	3.1E-14
Day 60	>51.00	<4.4E-16
V_2		
Day 5	29.71	1.1E-09
Day 10	29.34	1.5E-09
Day 15	31.64	3.0E-10
Day 20	32.75	1.4E-10
Day 30	33.58	8.0E-11
Day 40	33.00	1.2E-10
Day 50	31.85	2.6E-10
Day 60	32.63	1.5E-10

[p] - invalid C_p values generated as a result of mispriming.

Table VIg Crossing point values for *lipA*

Sample	Crossing point (C_p)	2^{-Cp}
LT_1		
Day 10	42.74 [p]	1.4E-13
Day 15	40.80	5.2E-13
Day 20	41.06 [p]	4.4E-13
Day 30	39.67	1.1E-13
Day 40	43.61	7.5E-13
Day 50	>51.00	<4.4E-16
Day 60	44.18	5.0E-14
LT_1A		
Day 5	>51.00	<4.4E-16
Day 15	47.80 [p]	4.1E-15
Day 20	>51.00	<4.4E-16
Day 30	45.05	2.8E-14
Day 40	41.82	2.6E-13
Day 50	>51.00	<4.4E-16
Day 60	>51.00	<4.4E-16
V_2		
Day 5	29.71 [p]	1.1E-09
Day 10	29.34 [p]	1.5E-09
Day 15	31.64 [p]	3.0E-10
Day 20	32.75 [p]	1.4E-10
Day 30	33.58 [p]	8.0E-11
Day 40	33.00 [p]	1.2E-10
Day 50	31.85 [p]	2.6E-10
Day 60	32.63 [p]	1.5E-10

[p] - invalid C_p values generated as a result of mispriming.

Table VIh Crossing point values for *lipB*

Sample	Crossing point (C_p)	2^{-Cp}
LT_1		
Day 10	39.94	9.5E-13
Day 15	39.17	1.6E-12
Day 20	37.08	6.9E-12
Day 30	43.86	6.3E-14
Day 40	38.70	2.2E-12
Day 50	46.30	1.2E-14
Day 60	41.52	3.2E-13
LT_1A		
Day 5	45.91	1.5E-14
Day 15	40.74	5.5E-13
Day 20	40.08	8.6E-13
Day 30	46.19	1.3E-14
Day 40	41.84	2.5E-13
Day 50	46.66	9.0E-15
Day 60	44.12	5.2E-14
V_2		
Day 5	39.08	1.7E-12
Day 10	40.66	5.8E-13
Day 15	37.70	4.5E-12
Day 20	38.86	2.0E-12
Day 30	39.56	1.2E-12
Day 40	40.87	5.0E-13
Day 50	40.10	8.5E-13
Day 60	41.23	3.9E-13